

CRYSTAL STRUCTURE OF THE ANTICANCER DRUG  
CISPLATIN BOUND TO DUPLEX DNA

by

Patricia Michele Takahara

B.S., Chemistry  
University of California at Berkeley  
(December, 1990)

Submitted to the Department of Chemistry  
in Partial Fulfillment of  
the Requirements for the Degree of  
Doctor of Philosophy

at the

Massachusetts Institute of Technology

June, 1996

© 1996 Massachusetts Institute of Technology  
All rights reserved

Signature of Author.....

Department of Chemistry  
May 16, 1996

Certified by.....

Stephen J. Lippard  
Arthur Amos Noyes Professor of Chemistry  
Thesis Supervisor

Accepted by.....

Dietmar Seyferth  
Chairman, Departmental Committee on Graduate Students

Science

MASSACHUSETTS INSTITUTE  
OF TECHNOLOGY

JUN 12 1996



This doctoral thesis has been examined by a Committee of the Department of Chemistry as follows:

.....  
Alan Davison  
Professor of Chemistry  
Committee Chairman

.....  
Stephen J. Lippard  
Arthur Amos Noyes Chair and Professor of Chemistry  
Thesis Supervisor

.....  
Carl O. Pabo  
Professor of Biology  
Howard Hughes Medical Institute  
Department of Biology



## CRYSTAL STRUCTURE OF THE ANTICANCER DRUG CISPLATIN BOUND TO DUPLEX DNA

by

Patricia Michele Takahara

Submitted to the Department of Chemistry on May 16, 1996 in partial fulfillment of the requirements for the Degree of Doctor of Philosophy in Chemistry

### ABSTRACT

Cisplatin is a simple coordination compound used in chemotherapeutic regimens and is considered to be a cure for testicular cancer. The major targets of cisplatin in the cell are the N7 atoms of adjacent guanine residues on DNA. The structure of cisplatin bound to a single-stranded dinucleotide was solved in 1985. Subsequent gel electrophoresis studies of cisplatin bound to duplex DNA revealed that platinum coordination induces a bend in the double helix, but molecular details of the structure were unavailable until now.

The X-ray crystal structure of the major (GpG) adduct of cisplatin on a duplex DNA dodecamer has been solved to a resolution of 2.6 Å ( $R = 0.203$ ,  $R$ -free = 0.245). The crystals are triclinic, spacegroup P1, with unit cell constants  $a = 31.3$  Å,  $b = 35.5$  Å,  $c = 47.0$  Å,  $\alpha = 79.8^\circ$ ,  $\beta = 84.8^\circ$ ,  $\gamma = 82.8^\circ$ , and  $Z = 2$ . The two molecules in the asymmetric unit are related by a non-crystallographic two-fold axis, but no symmetry constraints were used during the refinement. The crystal structure reported here affords two independent views of a cisplatin-modified DNA duplex.

The DNA duplex in this crystal structure is bent by a  $26^\circ$  roll toward the major groove at the site of platinum coordination. The platinum atom binds to the N7 atoms of adjacent guanine residues, compacts the major groove, and widens and flattens the minor groove. The crystal structure shows that the platinum atom sits out of the planes of the guanine bases by  $\sim 1$  Å and is considerably strained.

The overall structure of the cisplatin-modified duplex is a unique junction of A-like and B-like helices with an overall bend of  $38^\circ$ - $55^\circ$ . This bent structure is accommodated by an interesting and novel packing arrangement in the crystal. One end of each duplex packs end-to-end like crystals of B-DNA while the other end of each duplex packs into the minor groove of an adjacent

molecule much like A-DNA crystal packing. The opened minor groove and the bend caused by platinum binding probably facilitates protein recognition of the adduct and potentiates the antitumor activity of the drug.

Certain cellular proteins containing a basic domain of about 80 amino acids, known as the high mobility group (HMG) domain, have been found to bind cisplatin-DNA adducts in a structure specific manner and affect cell survival. The details of the cisplatin/DNA structure will facilitate the rational design of new platinum antitumor drug candidates. The DNA adducts of the candidates should bind more strongly to HMG domains.

Thesis Supervisor: Stephen J. Lippard

Title: Arthur Amos Noyes Professor of Chemistry

## ACKNOWLEDGMENTS

I'd like to start by thanking Stephen J. Lippard for allowing me to join his lab and work on the cisplatin/DNA crystallography project. It has not always been easy but I have learned quite a lot from him and from his group. Many thanks also to the people who got me started on the cisplatin/DNA project: Steve Bellon, Dan Bancroft, Chris Frederick. Steve Bellon worked very hard on the project before I arrived and crystallized two sequences of cisplatin-modified DNA. He laid the groundwork for my project and made things much easier for me when I started. Dan helped me mount my first crystals and allowed me to use his cold room and equipment when I first started collecting data. Chris, a professor at the Dana-Farber Cancer Institute at Harvard Medical School, allowed me to work in her lab, use her equipment, and encouraged me along during the whole project. She essentially allowed me to become a member of her research group and provided me with valuable crystallography experience.

Others who also have been very supportive throughout the project are Carl Pabo (MIT, Department of Biology) and Greg Petsko (Brandeis University). Whenever I needed help, they took time out of their busy schedules to help me understand what I was doing. I'd also like to thank Pär Nordlund for talking over my data problems when we got together on various MMO synchrotron trips. Things definitely start to make more sense after a few cups of sake.

Many thanks also to Mark Rould for his patience and help with many aspects of the structure solution. He met with me many times, looked at my maps, looked at my statistics, helped me understand what I was doing during my refinements, and answered at least a million questions about X-PLOR.

Amy Rosenzweig also answered a million questions about O, CCP4, computers, and Lippard lab life during my time in graduate school. We struggled with UNIX, FORTRAN, and SSRL ants together. Those synchrotron trips were fun at first, but I think we've had enough. Amy, I hope you get lots of students so you never have to go again.

Ken Comess also helped with my project by providing cisplatin expertise, reading drafts of my papers, and providing some distraction for my husband. Ken, thanks for keeping Mark occupied once in a while by playing tennis, seeing violent movies, and drinking beer with him. Thank you also for allowing me the honor of riding in your Taurus.

Thanks also to Amy Anderson for being my nucleic acid crystallography buddy. It's hard to do a DNA or RNA structure when people all around you always seem to get crystals that look wonderful and diffract no

matter what you do. Good luck with your structures - stick with it and things will work out eventually.

There have been many people in the Lippard Lab who have helped me out and supported me during my time at MIT. First, thanks to Chad Davis for being a wonderful UROP. All that HPLC and all those setups took a lot of patience and must have been really boring (is that why you went to medical school?) and I appreciate the help you gave me. Thank you for Thursday@3! Maybe you should drop out of medical school and make cannolis at Veniero's for a living. Thanks to Joanne Yun for introducing me to golden crowns and for talking basketball with Mark. Jon Wilker and Linda Doerrer, my classmates, have been very supportive during our whole time in the group and made my first year at MIT less boring than I thought it would be. Special thanks to Dave Coufal for taking such good care of the computers, spending so much time learning about the system, and keeping everything updated. Thank you also to all the members of the Manchanda family (Rajesh, Stephanie, Karen, Betsy, Andy, and Shari) for making me an honorary member, letting me hang a stocking by your fireplace, and introducing me to Stella.

My decision to go to graduate school dates back to my undergraduate days at Berkeley and the inorganic and small molecule crystallography classes I took there. Caroline, thanks for helping me get through those classes and put up with Ginny. I still laugh every time I open up Stout and Jensen. Caroline, I admire your free spirit, your sense of humor, and your hair-styling technique. I hope you never change.

My family also deserves many thanks for all their encouragement and help during my time in graduate school. Thanks Mom, Dad, and Tako23, your e-mail always made me laugh. Thanks Deb-the-celeb for all the newspaper clippings, pictures, tapes, and Arkansas stories. I still want to meet Peter, though, so keep going with all that tee-vee-in'.

And finally, I'd like to thank Mark Hasegawa, my husband. Thank you Mark for all your help and for helping me stick with grad school when it got really frustrating. Thank you for taking a chance with your career to be with me. I could not have gotten through all this without you, and this thesis is dedicated to you.



## TABLE OF CONTENTS

Abstract.....	5
Acknowledgments.....	7
Table of Contents .....	9
List of Tables.....	10
List of Figures.....	11
Abbreviations and Physical Constants.....	15
Dedication.....	17
Chapter 1. Introduction.....	19
Chapter 2. Materials and Methods.....	35
Materials .....	36
Deoxyoligonucleotide Synthesis and Purification.....	36
Crystallization.....	37
Analysis of Platinum/DNA Ratios in the Crystals .....	42
X-ray Data Collection.....	43
Data Reduction and Structure Determination.....	54
Chapter 3. Results.....	63
Canonical DNA Structures .....	64
The Unit Cell .....	70
Packing .....	80
The Platinated DNA Duplex .....	94
Structure of Molecule A.....	104
Structure of Molecule B.....	126
Bending.....	128
Details of the Platinum Binding Site.....	129
Chapter 4. Discussion.....	135
Crystal Structure of Cisplatin-modified DNA.....	136
Comparison with the NMR Solution Structure.....	138
Stabilization of the Cisplatin Lesion by Further Bending.....	145
HMG Domain Protein Binding to Cisplatin-modified DNA.....	148
Other DNA-binding Proteins and Bent DNA .....	149
Interstrand Adducts.....	151
Concluding Remarks .....	154
References.....	155
Biographical note.....	159

**LIST OF TABLES**

<b>Table 1</b>	Sequences previously used for crystallization trials .....	32
<b>Table 2</b>	DNA sequences used for crystallization trials.....	34
<b>Table 3</b>	Experimental details of the X-ray diffraction study of cisplatin-modified DNA.....	50
<b>Table 4</b>	Summary of crystallographic data.....	61
<b>Table 5</b>	Comparison of selected A-DNA and B-DNA structural parameters.....	65
<b>Table 6</b>	Selected atomic positions related by noncrystallographic symmetry.....	73
<b>Table 7</b>	Backbone-backbone packing contacts between molecules A and B.....	90
<b>Table 8</b>	Water contacts within the crystal structure of cisplatin-modified DNA.....	93
<b>Table 9</b>	Base pair parameters calculated by using the program CURVES.....	98
<b>Table 10</b>	Base step parameters calculated by using the program CURVES.....	100
<b>Table 11</b>	Pseudorotation angles, sugar puckers, and torsion angles for molecules A and B.....	108
<b>Table 12</b>	Comparison of hSRY/DNA and LEF-1/DNA NMR structures and the cisplatin/DNA crystal structure.....	152

## LIST OF FIGURES

<b>Figure 1</b>	Platinum compounds that have been tested for anticancer activity .....	21
<b>Figure 2</b>	Biological cross-links caused by <i>cis</i> -diamminedichloro-platinum(II).....	23
<b>Figure 3</b>	Structure of the dodecamer d(CGCGAATTCGCG) after pre-formed crystals were soaked with cisplatin .....	25
<b>Figure 4</b>	X-ray crystal structure of <i>cis</i> -[Pt(NH <sub>3</sub> ) <sub>2</sub> ] <sup>2+</sup> bound to d(pGpG).....	26
<b>Figure 5</b>	A representative molecular mechanics model of <i>cis</i> -[Pt(NH <sub>3</sub> ) <sub>2</sub> ] <sup>2+</sup> bound to duplex DNA .....	28
<b>Figure 6</b>	NMR model of <i>cis</i> -[Pt(NH <sub>3</sub> ) <sub>2</sub> ] <sup>2+</sup> bound to duplex DNA.....	30
<b>Figure 7</b>	HPLC purification of a platinated deoxyoligonucleotide.....	38
<b>Figure 8</b>	HPLC purification an unplatinated, complementary deoxyoligonucleotide strand .....	40
<b>Figure 9</b>	A sitting drop crystallization and conditions for cisplatin-modified DNA.....	44
<b>Figure 10</b>	Photomicrograph of a cluster of cisplatin-modified DNA crystals .....	45
<b>Figure 11</b>	Digestion analysis of the platinated oligonucleotide, d(CCTCTG*G*TCTCC) where the -G*G*- site is coordinated to platinum, from crystals of TT12d.....	46
<b>Figure 12</b>	Photomicrograph of a crystal of cisplatin-modified DNA in a glass capillary.....	48
<b>Figure 13</b>	CCD detector image collected on a frozen crystal of platinated DNA at NSLS-X8C.....	52
<b>Figure 14</b>	Fluorescence intensity scan of a crystal of platinated DNA.....	53
<b>Figure 15</b>	Patterson maps (010 projections) calculated with native data .....	55
<b>Figure 16</b>	Difference Patterson maps (010 projections) calculated with native and derivative data.....	56

<b>Figure 17</b>	Maps of molecule A, residues C19-A20-G21-A22, generated during refinement of the structure.....	59
<b>Figure 18</b>	$\sigma_a$ plot for the estimated coordinate error for the final model.....	60
<b>Figure 19</b>	DNA is composed of bases connected by a sugar phosphate backbone.....	66
<b>Figure 20</b>	The Watson-Crick base pairs of DNA.....	67
<b>Figure 21</b>	Labeling of the torsion angles and deoxyribose ring along the sugar-phosphate backbone of a segment of DNA.....	68
<b>Figure 22</b>	The structures of B-DNA and A-DNA.....	69
<b>Figure 23</b>	Space filling diagram of the structure of cisplatin-modified duplex DNA.....	71
<b>Figure 24</b>	Ball and stick models of d(CCTCTG*G*TCTCC)·d(GGAGACCAGAGG) where -G*G*- is modified by <i>cis</i> -[Pt(NH <sub>3</sub> ) <sub>2</sub> ] <sup>2+</sup> .....	74
<b>Figure 25</b>	The numbering schemes for individual bases, base pairs, and base steps are shown schematically.....	75
<b>Figure 26</b>	Rotation axis relating the two molecules in each unit cell.....	76
<b>Figure 27</b>	Rotation axis relating molecules A and B.....	77
<b>Figure 28</b>	Rotation axis relating the two molecules in each unit cell shown with neighboring molecules.....	78
<b>Figure 29</b>	Superposition of molecules A and B.....	79
<b>Figure 30</b>	Packing diagram of cisplatin-modified DNA.....	81
<b>Figure 31</b>	Packing diagrams showing the large solvent channels which run through the crystal of cisplatin-modified DNA.....	82
<b>Figure 32</b>	End-to-end packing interaction of molecule A stacking on molecule B.....	83
<b>Figure 33</b>	End-to-groove packing interaction: the end of molecule A packing into the minor groove of molecule B.....	85

<b>Figure 34</b>	End-to-groove packing interaction: the end of molecule B packing against the minor groove of molecule A.....	86
<b>Figure 35</b>	The C1-G24 base pair of molecules A and B packing against the sugar-phosphate backbone of molecules B and A, respectively.....	87
<b>Figure 36</b>	The hydrogen bonding interactions between the C1-G24 base pair of molecule A and the G6-C19 base pair of molecule B.....	88
<b>Figure 37</b>	Backbone-to-backbone packing interaction between molecule A and molecule B.....	89
<b>Figure 38</b>	Schematic diagram of the water positions in the crystal structure of cisplatin-modified DNA .....	92
<b>Figure 39</b>	Views of the B-like and A-like ends of cisplatin-modified DNA.....	95
<b>Figure 40</b>	Base pair parameters for nucleic acids.....	96
<b>Figure 41</b>	Base step parameters for nucleic acids.....	97
<b>Figure 42</b>	Graphical representations of the base pair parameters for molecules A and B.....	102
<b>Figure 43</b>	Graphical representations of the base step parameters for molecules A and B.....	103
<b>Figure 44</b>	Schematic diagrams of phosphorus atom distances in the structure of cisplatin-modified DNA .....	106
<b>Figure 45</b>	Graphs of the phosphorus atoms distances in the structure of cisplatin-modified DNA.....	110
<b>Figure 46</b>	Base stacking patterns for the different types of steps of A-DNA and B-DNA.....	113
<b>Figure 47</b>	Stacking arrangement in base step 1, C1-G24/C2-G23.....	114
<b>Figure 48</b>	Stacking arrangement in base step 2, C2-G23/U <sup>Br3</sup> -A22 .....	115
<b>Figure 49</b>	Stacking arrangement in base step 3, U <sup>Br3</sup> -A22/C4-G21 .....	116
<b>Figure 50</b>	Stacking arrangement in base step 4, C4-G21/T5-A20.....	117

<b>Figure 51</b>	Stacking arrangement in base step 5, T5-A20/G6-C19.....	118
<b>Figure 52</b>	Stacking arrangement in base step 6, G*6-C19/G*7-C18.....	119
<b>Figure 53</b>	Stacking arrangement in base step 7, G7-C18/T8-A17.....	120
<b>Figure 54</b>	Stacking arrangement in base step 8, T8-A17/C9-G16.....	121
<b>Figure 55</b>	Stacking arrangement in base step 9, C9-G16/T10-A15.....	122
<b>Figure 56</b>	Stacking arrangement in base step 10, T10-A15/C11-G14.....	123
<b>Figure 57</b>	Stacking arrangement in base step 11, C11-G14/C12-G13.....	124
<b>Figure 58</b>	Hydrogen bonding in base step 7, G7-C18/T8-A17.....	125
<b>Figure 59</b>	Helical axes calculated with the program CURVES.....	131
<b>Figure 60</b>	The -G*G*- platination site.....	132
<b>Figure 61</b>	Electron density map and stereo image of <i>cis</i> -{Pt(NH <sub>3</sub> ) <sub>2</sub> } <sup>2+</sup> bound to a d(GpG) site on duplex DNA.....	133
<b>Figure 62</b>	The platination sites of cisplatin-modified DNA from the crystal structure and the NMR solution structure.....	140
<b>Figure 63</b>	The structures of cisplatin-modified DNA determined by X-ray crystallography and by NMR.....	141
<b>Figure 64</b>	Space-filling picture of cisplatin-modified DNA, an octahedral metal complex docked in the major groove at the site of platinum binding, and a platinum-lysine complex docked in place of <i>cis</i> -{Pt(NH <sub>3</sub> ) <sub>2</sub> } <sup>2+</sup> .....	144
<b>Figure 65</b>	-TG*G*- segment from the crystal structure of cisplatin-modified DNA and model with -TG*G*- replaced by -CG*G*-, -AG*G*-, and -GG*G-.....	147
<b>Figure 66</b>	NMR solution structure of SRY bound to its DNA sequence.....	150
<b>Figure 67</b>	NMR solution structure of an interstrand cross-link of <i>cis</i> -{Pt(NH <sub>3</sub> ) <sub>2</sub> } <sup>2+</sup> on duplex DNA.....	153

**ABBREVIATIONS**

CCD	charge coupled device
DDP	diamminedichloroplatinum(II)
DNA	deoxyribonucleic acid
HMG	high mobility group
HPLC	high pressure liquid chromatography
MIR	multiple isomorphous replacement
NMR	nuclear magnetic resonance
NLS	National Synchrotron Light Source (Brookhaven)
rmsd	root-mean-square deviation
RNA	ribonucleic acid
SIR	single isomorphous replacement
SSRL	Stanford Synchrotron Radiation Laboratory

**PHYSICAL CONSTANTS**

$$1 \text{ eV} = 1.6021892 \times 10^{-19} \text{ J}$$

$$h = 6.626176 \times 10^{-34} \text{ J}\cdot\text{s}$$

$$c = 2.9979258 \times 10^8 \text{ m/s}$$

$$1 \text{ \AA} = 1 \times 10^{-10} \text{ m}$$





*To Mark*

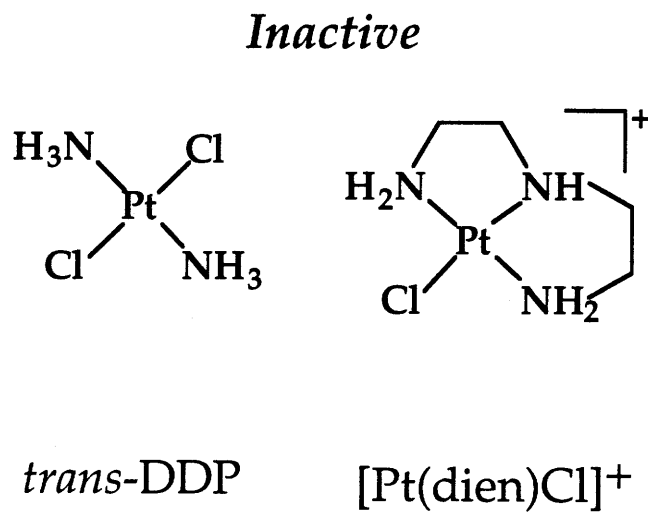
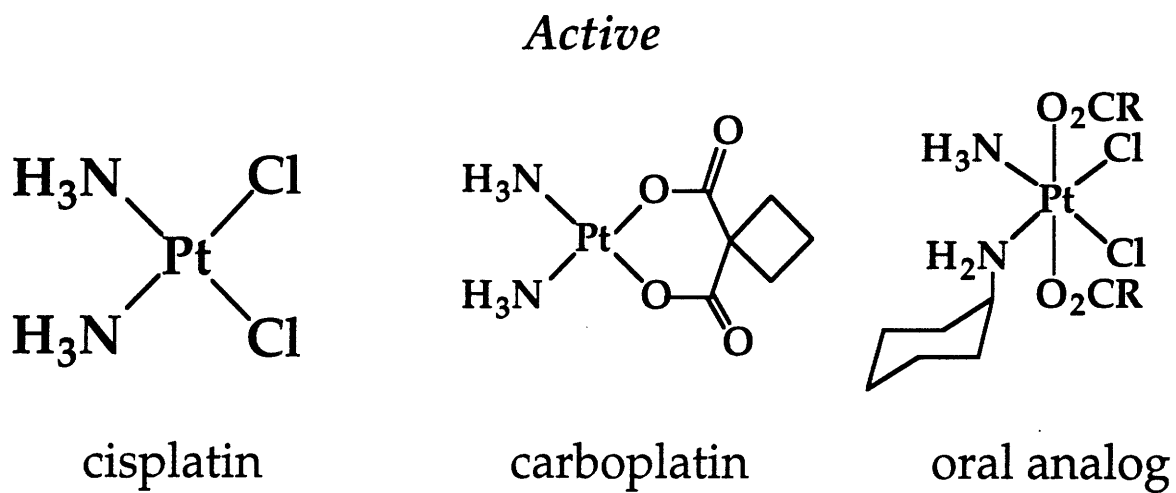


**CHAPTER 1**  
**INTRODUCTION**

Cisplatin, or *cis*-diamminedichloroplatinum(II) (*cis*-DDP), is an anticancer drug used against bladder, ovarian, head, and neck cancers, and its use in chemotherapeutic regimens has been important in achieving a cure rate of approximately 95% for testicular cancer (Comess & Lippard, 1993). Because cisplatin is effectively a cure for testicular cancer, much research has gone into understanding the molecular basis for its mechanism of anticancer activity so that drugs effective against a wider variety of tumors might be developed. Some basic information about how cisplatin works as an antitumor agent came from tests of the biological activity of other platinum compounds (Figure 1) (McA'Nulty & Lippard, 1995). The geometric isomer of cisplatin, *trans*-DDP, is not an effective antitumor agent. Also ineffective are square-planar platinum(II) complexes with only one labile ligand such as a platinum(II) diethylenetriamine complex,  $[\text{Pt}(\text{dien})\text{Cl}]^+$ . Carboplatin, an analog of cisplatin, has good activity as well as reduced toxicity and has been in clinical use since 1990. Also in clinical trials is an oral analog of cisplatin which contains an octahedral platinum(IV) atom. This compound loses two axial ligands and is reduced to a square-planar platinum(II) complex in cells. It was concluded that a platinum(II) atom with two labile *cis* ligands as well as two stable *cis* ammine moieties is necessary for the anticancer activity of platinum compounds, and that the effect of the drug is related to specific bifunctional adducts formed with biological targets *in vivo*.

Cisplatin, carboplatin, and the Pt(IV) oral analog have the ability to react with many biomolecules *in vivo* (Bruhn et al., 1990). In chemotherapy, cisplatin and carboplatin are administered intravenously and the Pt(IV) complex is administered orally. The drugs enter the bloodstream in their neutral states, and in this environment, the chloride ion concentration is about 100 mM. The neutral complexes enter cells by passive diffusion and are

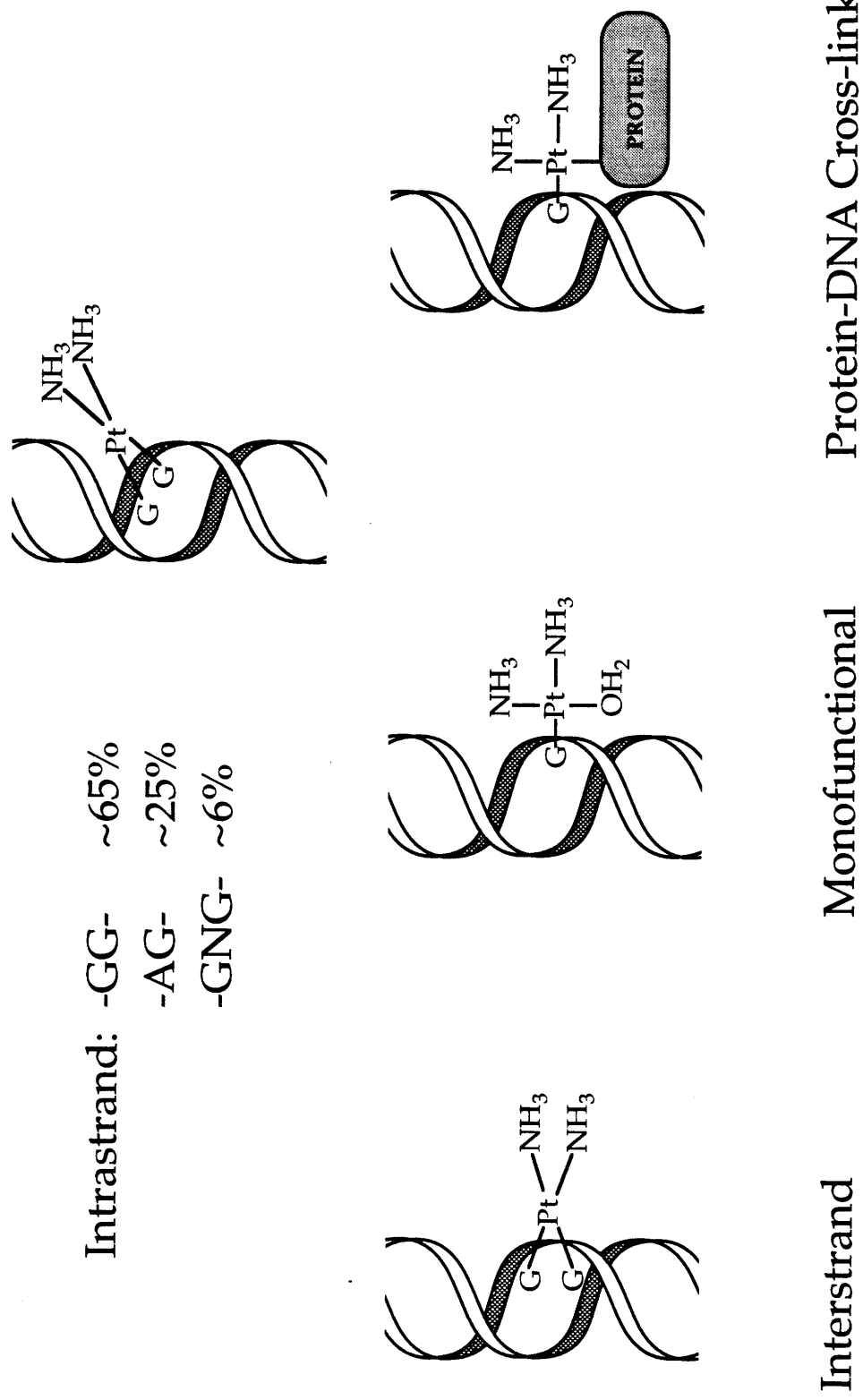
Figure 1. Platinum compounds that have been tested for anticancer activity.



immersed in a medium where the chloride ion concentration is 20 mM to 55 mM (Jennerwein & Andrews, 1995). The chloride ligands in the case of cisplatin and its oral analog and the carboxy ligands in the case of carboplatin are displaced by water and *cis*-[Pt(NH<sub>3</sub>)<sub>2</sub>(H<sub>2</sub>O)<sub>2</sub>]<sup>2+</sup> forms. This Pt(II) diaqua species has the ability to react with many biomolecules within the cell. The water ligands can readily be displaced by sulfur, nitrogen, or oxygen atoms on the side chains of peptides or proteins or by nitrogen or oxygen atoms on the nucleobases of deoxyribonucleic acid (DNA) or ribonucleic acid (RNA). Studies have shown that the most persistent adducts formed in vivo and those likely to be responsible for the antitumor activity of cisplatin are the ones in which platinum binds to the N7 atoms of the purine bases on DNA. Studies in vitro have shown that when cisplatin is allowed to react with DNA, 65% of adducts formed are intrastrand cross-links where platinum is coordinated to two adjacent guanine residues, 25% are intrastrand adducts with the platinum atom coordinated to an adjacent adenine and guanine, and the remaining 10% are other intrastrand cross-links, interstrand cross-links, monofunctional adducts, or protein-DNA cross-links (Figure 2) (Eastman, 1986; Fichtinger-Schepman et al., 1985).

Recent studies have shown that certain cellular proteins which contain a region of about 80 amino acids known as the high mobility group (HMG) domain bind to DNA modified by cisplatin (Pil & Lippard, 1992; Whitehead & Lippard, 1995). HMG proteins bind to intrastrand Pt-GpG and Pt-ApG adducts in a structure specific manner and the proteins may potentiate the antitumor activity of the drug by interfering with cellular repair processes (Huang et al., 1994). It is therefore important to understand the detailed molecular structures of cisplatin-DNA adducts and how these structures correlate with HMG protein binding.

Figure 2. Biological cross-links caused by *cis*-diamminedichloroplatinum(II).



When *cis*-[Pt(NH<sub>3</sub>)<sub>2</sub>(H<sub>2</sub>O)<sub>2</sub>]<sup>2+</sup> interacts with duplex DNA, significant disruptions in base stacking must occur in order to accommodate the square-planar coordination requirements of the platinum(II) atom. In an attempt to understand the structural perturbations caused by platinum binding to DNA, many structural studies have been undertaken (Sherman & Lippard, 1987). The first crystallographic studies were attempted by soaking cisplatin into crystals of the self-complementary B-DNA dodecamer sequence d(CGCGAATTCGCG) (Wing et al., 1984). In this work, three of the eight guanine residues, G4, G10, and G16, appeared to have affinity for cisplatin but all the platinum sites in the crystal had only partial occupancy (Figure 3). Crystal structures with three different levels of cisplatin substitution were solved, and the most occupied platinum site, near the N7 atom of residue G16, was compared. The crystals had platinum-G16(N7) bond lengths of 2.51 Å, 2.43 Å, and 2.16 Å with occupancies of 20%, 38%, and 61%, respectively. Attempts to obtain more highly substituted platinum sites resulted in degradation of the crystals. The authors reasoned, from a linear plot of bond length versus percent substitution, that the platinum-N7 bond length would be 1.8 Å at 100% occupancy. This conclusion was only for a monofunctional cisplatin-DNA adduct and yielded no information about the bifunctional adducts thought to be responsible for the antitumor activity of the drug.

The structure of the major adduct formed, *cis*-[Pt(NH<sub>3</sub>)<sub>2</sub>{d(pGpG)-N7(G<sub>1</sub>),-N7(G<sub>2</sub>)}], has been probed on short segments of single-stranded DNA by X-ray crystallography. These studies showed coordination at the N7 atoms of adjacent guanine bases causes a head-to-head orientation of the bases and a dihedral angle of about 80° between the planes of the guanine rings (Figure 4) (Admiraal et al., 1987; Sherman et al., 1985; Sherman et al., 1988). On a segment of short, single-stranded DNA, the sugar pucker of the 5' nucleotide



**Figure 3.** Structure of the dodecamer d(CGCGAATTCGCG) after preformed crystals were soaked with cisplatin.

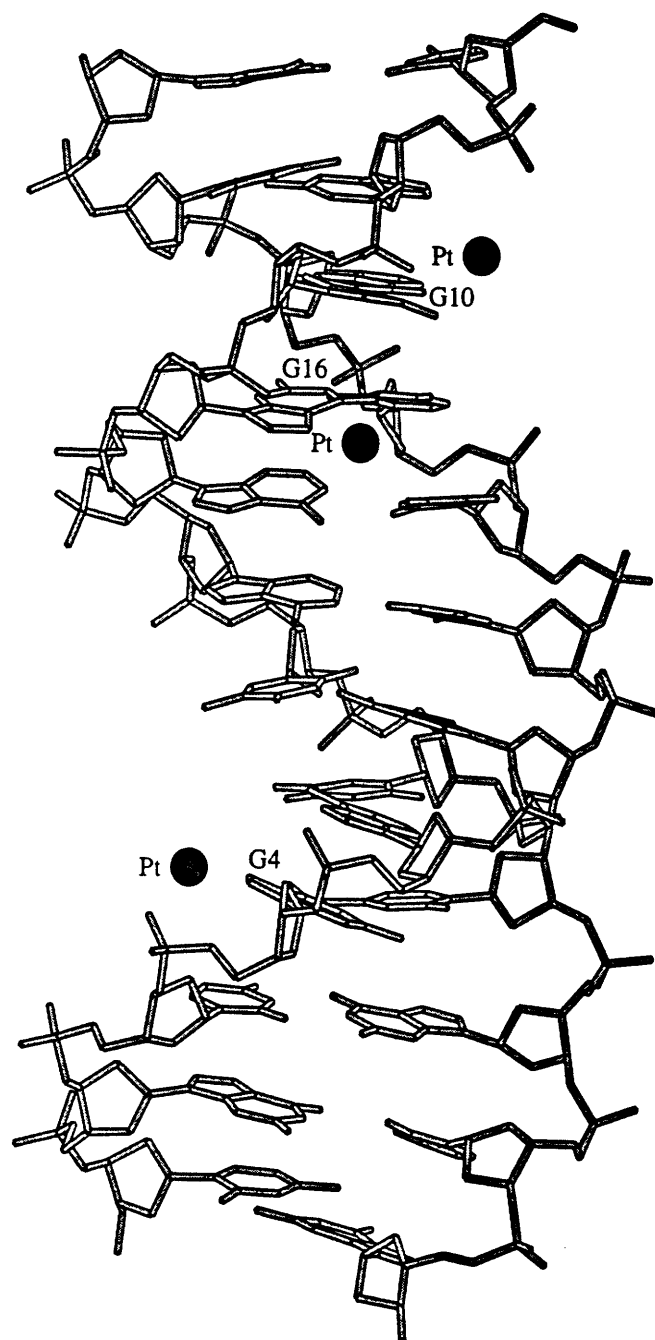
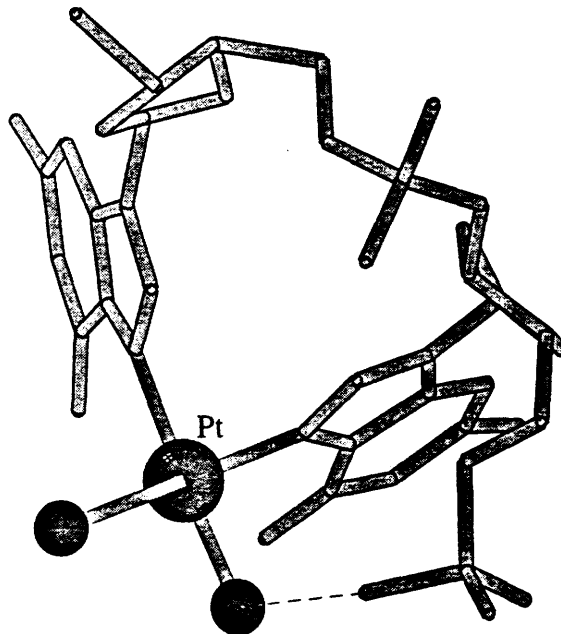


**Figure 4.** X-ray crystal structure of *cis*-[Pt(NH<sub>3</sub>)<sub>2</sub>]<sup>2+</sup> bound to d(pGpG). Cisplatin binds to the N7 atoms on each guanine base and causes a roll of ~80° between the guanine ring planes. A hydrogen bond forms between an ammine on the platinum atom and a phosphate oxygen.

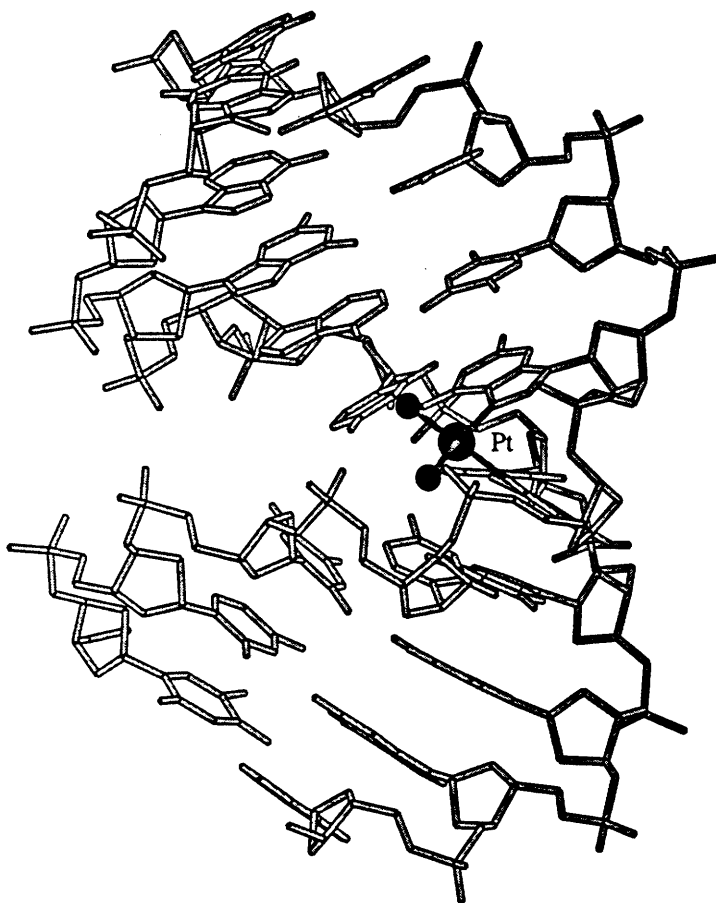


adopts a C3'-endo conformation whereas the 3' ribose ring is C2'-endo. Another interesting aspect of the structure is the hydrogen bond formed between an ammine on the platinum atom and a phosphate oxygen 5' to the platinum lesion. It was hypothesized that this hydrogen bond plays a role in stabilizing the adduct and may therefore be important for the anticancer activity of the drug. Because single-stranded DNA molecules lack the constraints of base stacking and Watson-Crick hydrogen bonding, further studies of specific platinum adducts were carried out on segments of duplex DNA.

Nuclear magnetic resonance (NMR) studies of a specific adduct of *cis*-[Pt(NH<sub>3</sub>)<sub>2</sub>]<sup>2+</sup> on duplex DNA suggested a 40-70° bend as a possible deformation of the double helix and showed a C3'-endo sugar pucker to the 5' side of the platinum lesion and a C2'-endo sugar pucker on the 3' side (den Hartog et al., 1985). Later, NMR data were combined with geometric parameters from the crystal structure of the *cis*-[Pt(NH<sub>3</sub>)<sub>2</sub>{d(pGpG)-N7(G<sub>1</sub>)-N7(G<sub>2</sub>)}] adduct and used in molecular mechanics studies (Kozelka et al., 1987; Kozelka & Chottard, 1990; Kozelka et al., 1985). These studies confirmed the head-to-head orientation of the bases, the presence of a bend, the sugar pucker alternation across the platinum lesion, and the hydrogen bond between a phosphate oxygen and an ammine on the platinum atom. Because DNA is such a large and complex molecule, it was not possible to derive a single best structure for the adduct. Instead, several models resulted from these studies, all energetically feasible and all with a bend of about 60° toward the major groove and unwound by 12-19° (Figure 5).

The bend angle of duplex DNA with an intrastrand *cis*-[Pt(NH<sub>3</sub>)<sub>2</sub>]<sup>2+</sup> cross-link seen in molecular mechanics models was much larger than the

**Figure 5.** A representative molecular mechanics model of *cis*-[Pt(NH<sub>3</sub>)<sub>2</sub>]<sup>2+</sup> bound to duplex DNA. The overall bend in the duplex was estimated to be ~60°.

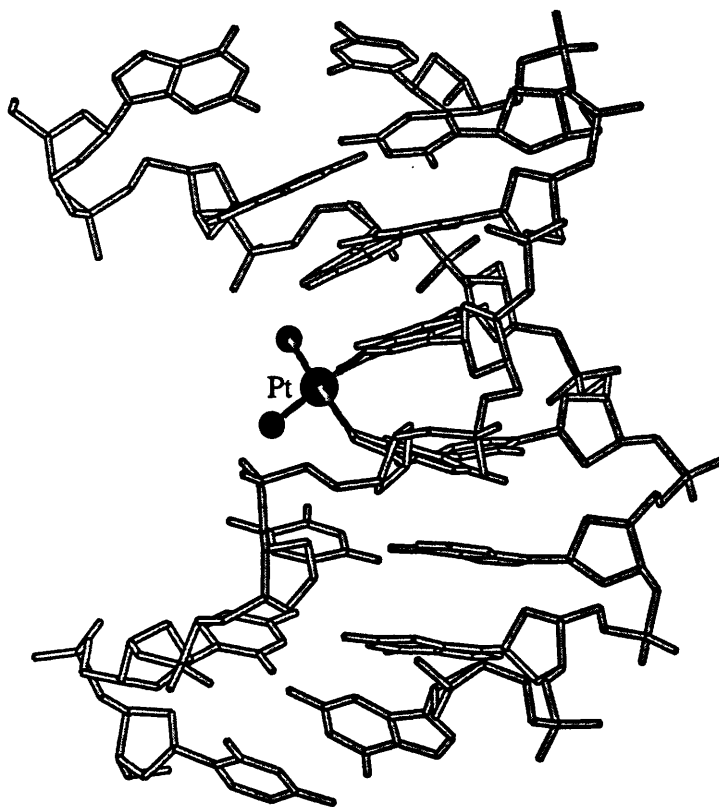


bend observed by gel electrophoresis studies on site-specifically modified platinum-DNA adducts. Multimers of a duplex containing a specific intrastrand *cis*-[Pt(NH<sub>3</sub>)<sub>2</sub>{d(GpG)-N7(G),-N7(G)}] site showed anomalous electrophoretic mobility and a bend of ~40° toward the major groove was calculated (Rice et al., 1988). Further gel electrophoresis studies on intrastrand site-specific cisplatin/DNA adducts showed that the major intrastrand cross-links *cis*-[Pt(NH<sub>3</sub>)<sub>2</sub>{d(GpG)-N7(G),-N7(G)}] and *cis*-[Pt(NH<sub>3</sub>)<sub>2</sub>{d(ApG)-N7(A),-N7(G)}] bend the double helix by ~35° and unwind it by ~13° (Bellon et al., 1991; Bellon & Lippard, 1990).

Recently, an NMR structure of a double-stranded DNA octamer, d(CCTG\*G\*TCC)·d(GGACCAGG) with an intrastrand *cis*-[Pt(NH<sub>3</sub>)<sub>2</sub>{d(GpG)-N7(G<sub>4</sub>),-N7(G<sub>5</sub>)}] cross-link at the -G\*G\*- site was reported (Yang et al., 1995). The duplex exhibits a bend of ~58°, an unwinding angle of ~-21°, a C3'-endo sugar pucker on the 5' side of the platinum lesion, and a C2'-endo sugar conformation on the 3' side of the platinum cross-link (Figure 6). This study afforded a significantly more detailed description of the cisplatin adduct than previous NMR studies. In particular, it showed that the minor groove of the octamer opposite the platinum binding site had widened to about 8 Å, as compared to the width of 5.7 Å for canonical B-DNA. The platinated octamer used in the NMR analysis was metastable, however. The intrastrand cross-link rearranged to an interstrand cross-link under the experimental conditions employed, but the significance of such a rearrangement is not yet clear.

Although the experimental NMR and gel electrophoresis studies provided important information about the distortions caused by cisplatin-DNA cross-links, structural details of bifunctional platinum adducts were limited to short single-stranded DNA oligonucleotides. The one

**Figure 6.** NMR model of *cis*-[Pt(NH<sub>3</sub>)<sub>2</sub>]<sup>2+</sup> bound to duplex DNA. The overall bend in the structure was reported to be 58°.



crystallographic attempt to study duplex DNA crystals soaked with cisplatin did not result in cisplatin-DNA cross-links and provided no structural information about biologically relevant adducts. It was therefore an extremely important objective to obtain the X-ray crystal structure of a specific and biologically relevant intrastrand cisplatin cross-link on duplex DNA.

Crystallographic studies of such a site, a specific cisplatin cross-link on duplex DNA were first undertaken in the laboratory of Stephen J. Lippard by Steven F. Bellon (Bellon, 1992). His work involved the self-complementary dodecamer DNA oligonucleotide d(GCTG\*G\*TTAACCA) with an intrastrand *cis*-{Pt(NH<sub>3</sub>)<sub>2</sub>}<sup>2+</sup> cross-link at the -G\*G\*- site. The platinated dodecamer was synthesized, purified, and annealed to afford a duplex with two cisplatin cross-links per double helical turn. The cisplatin adducts were strategically placed such that the bends in each helical turn would be 180° apart. The annealed duplex DNA also had a 5' -GC- overhang on each end for base pairing with the 5' ends of neighboring helices. The bend placements and the overhangs on the ends of the helices were designed to create a structure which was effectively a long, continuous, albeit curved helix that might pack well in crystals. Crystals with a flat plate-like morphology were obtained but diffracted poorly. An analogous sequence, d(ATTG\*G\*TTAACCA), was also synthesized, purified, annealed, and crystallized. Again, the crystals diffracted poorly and were not suitable for study by X-ray crystallography. The unit cell dimensions and space groups for the crystals of the sequences described above are listed in Table 1.

Further attempts at obtaining diffraction quality crystals of an intrastrand cisplatin cross-link on duplex DNA involved a more conventional approach. Oligonucleotides with a single -GG- site for platination were synthesized and, in order to increase the yield of purified

**Table 1.** Platinated deoxyoligonucleotides duplexes crystallized by Steven F. Bellon (Bellon, 1992). The -GG- sites were coordinated to *cis*-{Pt(NH<sub>3</sub>)<sub>2</sub>}<sup>2+</sup>.

Sequence	Unit cell parameters
GCT <b>GG</b> TTAACCA ACCAATT <b>GG</b> TTCG	Trigonal: a = 30 Å      a = 90° b = 30 Å      b = 90° c = 83 Å      g = 120°
ATT <b>GG</b> TTAACCA ACCAATT <b>GG</b> TTA	P2 <sub>1</sub> : a = 27 Å      a = 90° b = 87 Å      b = 111° c = 36 Å      g = 90°

platinated product, the oligonucleotide contained no purines other than the -GG- platination site. The pure platinated oligonucleotide was then annealed to its purified, complementary strand to form duplex DNA with an intrastrand cisplatin cross-link. Many cisplatin-modified DNA duplexes were synthesized and all were screened for crystallization (Table 2), but only one sequence yielded diffraction quality crystals. Crystals of the sequence d(CCTCTG\*G\*TCTCC)·d(GGAGACCAGAGG) were obtained and the X-ray crystal structure was solved by multiple isomorphous replacement. One of the brominated derivatives diffracted to 2.6 Å and data from this crystal were used to obtain the structure described in this thesis.

The structure of the platinated duplex dodecamer, d(CCU<sup>Br</sup>CTG\*G\*TCTCC)·d(GGAGACCAGAGG) where the -G\*G\*- site was modified with a cisplatin intrastrand cross-link, was solved by conventional



multiple isomorphous replacement (MIR) methods with brominated derivatives. The numbering scheme for the oligonucleotide is as follows:

**5' -C1 -C2 -U\*3-C4 -T5 -G\*6-G\*7-T8 -C9 -T10-C11-C12-3'**  
**3' -G24-G23-A22-G21-A20-C19-C18-A17-G16-A15-G14-G13-5'**

where U\*3 is 5-bromouridine and platinum binds to the N7 atoms of G\*6 and G\*7. In this thesis, the ends of the double helix will be referred to as the "3' end" and "5' end" with respect to the platinated deoxyoligonucleotide. Crystals of this cisplatin-modified duplex diffracted to 2.6 Å and these data provide the basis for the structure discussed. A preliminary report of this crystal structure has been published (Takahara et al., 1995). The structure shows how a segment of platinated DNA flexes to accommodate a platinum lesion and packing interactions in the crystal illustrate how a cisplatin-modified duplex might come in close contact with other biomolecules.

**Table 2.** Deoxyoligonucleotides used for crystallization trials.

Name	Sequence
TT8d	5' -CTCGGTTC-3' 3' -GAGCCAAG-5'
TT6d	5' -CCGGTC-3' 3' -GGCCAG-5'
TT12d	5' -CCTCTGGTCTCC-3' 3' -GGAGACCAGAGG-5'
TT12-3d	5' -CCCCTGGTTTCC-3' 3' -GGGGACCAAAGG-5'
TT12-4d	5' -CTCTTGGCCTAC-3' 3' -GAGAACCGGATG-5'
TT12-5d	5' -CCCCCGGTCCCC-3' 3' -GGGGGCCAGGGG-5'
TT12-2A	5' -CTGGC-3'
TT12-2B	5' -CGGCCAG-3'
TT32A	5' -CCTCTCTGGTCTTC-3'
TT32B	5' -CGGAAGAACCAGAGAGG-3'
TT12Br-a	5' -CCU <sup>Br</sup> CTGGTCTCC-3'
TT12Br-b	5' -CC <sup>Br</sup> TCTGGTCTCC-3'
TT12Br-c	5' -CCTCTGGT <sup>Br</sup> TCC-3'
TT12Br-d	5' -CCTCTGGU <sup>Br</sup> CTCC-3'
TT12Br-e	5' -CCTCU <sup>Br</sup> GGTCTCC-3'
TT12Br-f	5' -CCTCTGGTCU <sup>Br</sup> CC-3'
CD13-1d	5' -CTCTTGTGTCTC-3' 3' -GAGAACACAGGAG-5'
CD13-2d	5' -CTCCTGTGTCTC-3' 3' -GAGGACACAAGAG-5'
CD13-3d	5' -CCCTTGTGTCCCC-3' 3' -GGGAACACAGGGG-5'
CD12d	5' -CCTCTGTGTCTC-3' 3' -GGAGACACAGAG-5'
CD20	5' -TCTCCTTCTGGTCTCTTCTC-3' 3' -AGAGGAAGACCAGAGAAGAG-5'

---

\*Strands with GG sites or GTG sites for platination were reacted with cisplatin. Top and bottom strands of TT6, TT8, TT12, TT12-3, CD13-1, CD13-2, CD13-3, and CD12 were annealed to form duplexes. TT12Br-a, TT12Br-b, TT12Br-c, TT12Br-d, TT12Br-e, and TT12Br-f were mixed in a 1:1 molar ratio with TT12b. TT12A and TT12B were mixed in a 1:1 molar ratio and annealed to form a 12-mer. TT32A and TT32B were mixed in a 1:1 molar ratio and annealed to form a 32-mer. TT12A/B and TT32A/B were designed with the help of Professor Carl Pabo.

**CHAPTER 2**  
**MATERIALS AND METHODS**

*Materials.* Phosphoramidites and DNA synthesis reagents were purchased from Cruachem and Glen Research. Crystallization reagents were obtained from Fluka or Aldrich. *cis*-Diamminedichloroplatinum(II) was a gift from the Engelhard Corporation. DNase 1 and alkaline phosphatase were obtained from Boehringer Mannheim and P1 Nuclease was purchased from Gibco BRL. Reverse phase C4 and C18 high pressure liquid chromatography (HPLC) columns were purchased from Vydac, and ion exchange HPLC columns were purchased from Dionex.

Large scale HPLC was performed on a Waters 600E pumping system with either a Waters 486 or Waters 484 ultraviolet detector set at 260 nm. Analytical HPLC was done by using a Perkin-Elmer Series 4 Liquid Chromatograph with an LC-95 UV/vis detector set at 260 nm. Atomic absorption was done by using a Varian AA1475 instrument. X-ray diffraction data were collected on a Marresearch imaging plate system equipped with a Rigaku Cu K $\alpha$  rotating anode radiation source.

#### *Deoxyoligonucleotide Synthesis and Purification.*

Deoxyoligonucleotides were prepared on a Cruachem synthesizer by using standard solid phase phosphoramidite methods. Deoxyoligonucleotides were deprotected by using concentrated NH<sub>4</sub>OH at 55 °C for 12 hours. Protecting groups and excess trityl groups were removed by G25 Sephadex size exclusion chromatography, and the deoxyoligonucleotides were then lyophilized to dryness. Deoxyoligonucleotides were then converted to their sodium salts by using a Dowex cation exchange column and quantitated by optical spectroscopy with calculated extinction coefficients (A<sub>260</sub>) (Borer, 1975).

The diaqua complex of cisplatin was prepared by allowing 1.97 equivalents of AgNO<sub>3</sub> to react with *cis*-[Pt(NH<sub>3</sub>)<sub>2</sub>Cl<sub>2</sub>] in water at room

temperature in the dark. AgCl, a white precipitate, formed after about 30 min. After 12 h, the reaction mixture was centrifuged at 13000 rpm for ten min. The aqueous layer was drawn away from the AgCl pellet by using a pipet and centrifuged for another ten min. This process was repeated twice, and the final platinum solution was allowed to react with deoxyoligonucleotides with a -GpG- site for platination at 37 °C in the dark for 6-8 h.

Platinated deoxyoligonucleotides and their complementary strands were initially purified by an NaCl gradient on an ion exchange HPLC column. HPLC buffer A was composed of 25 mM NH<sub>4</sub>OAc, 10% CH<sub>3</sub>CN, and distilled, deionized H<sub>2</sub>O (ddH<sub>2</sub>O). Buffer B was composed of 25 mM NH<sub>4</sub>OAc, 10% CH<sub>3</sub>CN, 1 M NaCl, and ddH<sub>2</sub>O. Oligonucleotides were eluted from the column by using a gradient of 90% A and 10% B to 50% A and 50% B over 30 min. Oligonucleotide fractions were collected and desalted by dialysis against a solution of 0.1 M NH<sub>4</sub>OAc in ddH<sub>2</sub>O. Oligonucleotides rich in adenine or guanine residues were sometimes difficult to purify because they tended to aggregate on the ion exchange columns. In these cases, 50% formamide was used as a denaturing agent in the ion exchange HPLC solutions.

The DNA strands were then purified by an acetonitrile gradient on a C4 or C18 reverse phase HPLC column. Reverse phase HPLC buffer A was composed of 0.1 M NH<sub>4</sub>OAc in ddH<sub>2</sub>O and buffer B was 50% buffer A and 50% HPLC grade CH<sub>3</sub>CN. The typical gradient used was 95% A and 5% B to 60% A and 40% B over 30 minutes. DNA sequences used in this study are listed in Table 2 and example purification schemes are shown in Figures 7 and 8.

*Crystallization.* Purified complementary strands of each deoxyoligonucleotide were mixed in a 1:1 molar ratio and diluted to a

**Figure 7.** HPLC purification of a platinated deoxyoligonucleotide. (a) Dodecamer oligonucleotide after reaction with cisplatin. Ion exchange gradient B: 10-40% over 30 min. (b) Platinated oligonucleotide after ion exchange purification. Reverse phase gradient B: 5-40% over 30 min. (c) Platinated oligonucleotide after ion exchange and reverse phase purification. Reverse phase B: 5-40% over 30 min.

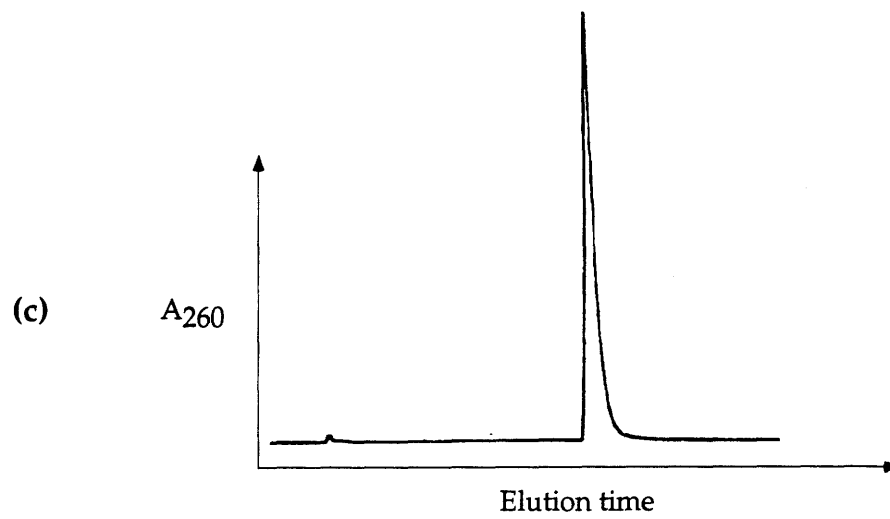
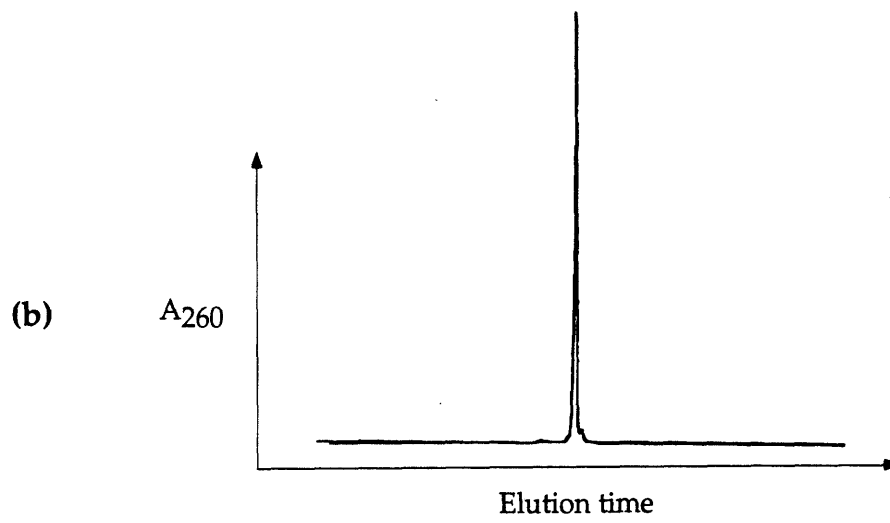
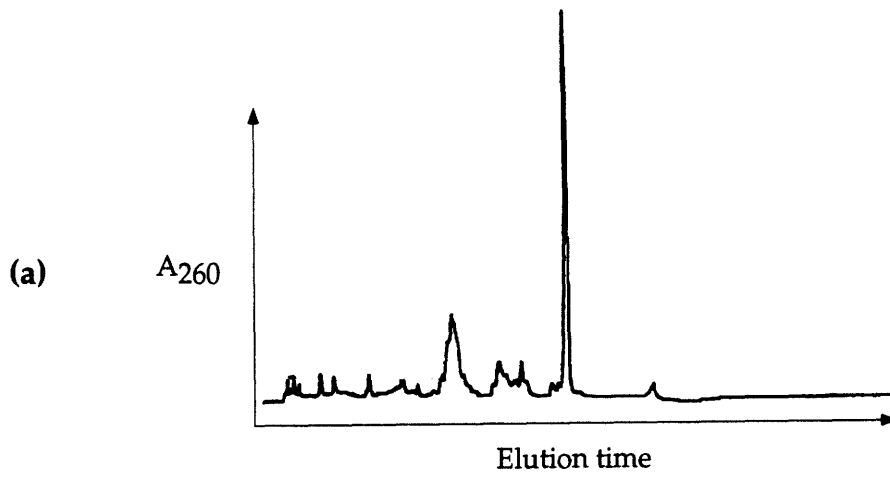
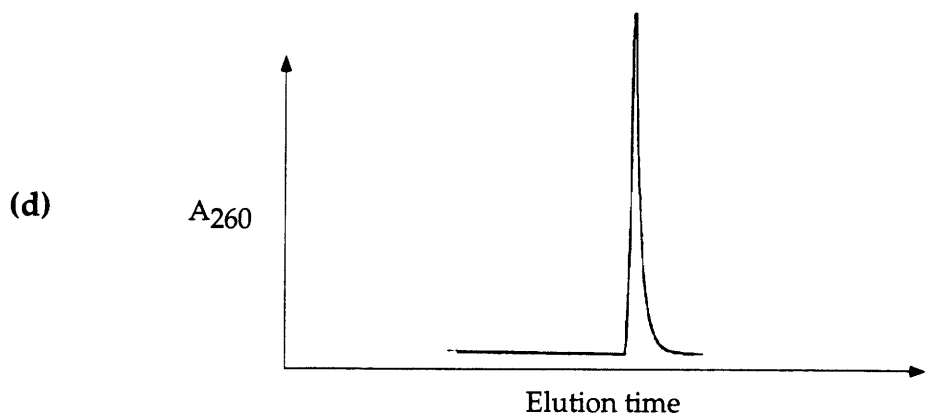
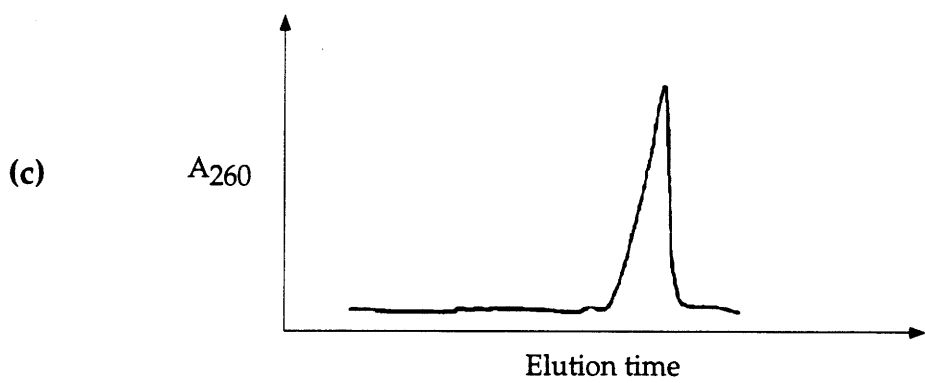
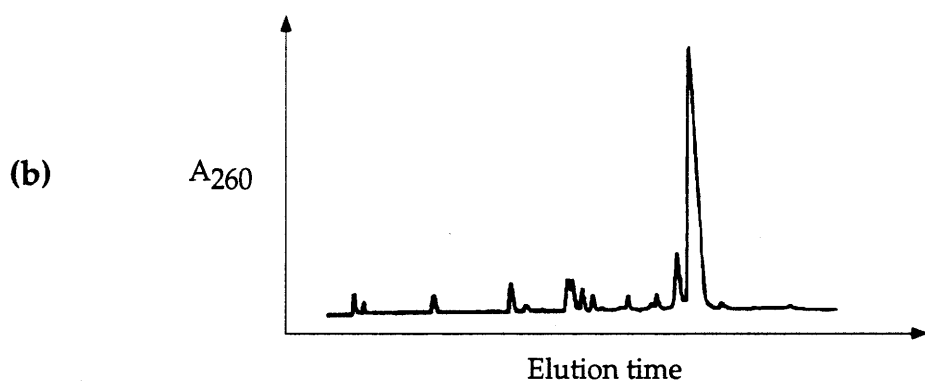
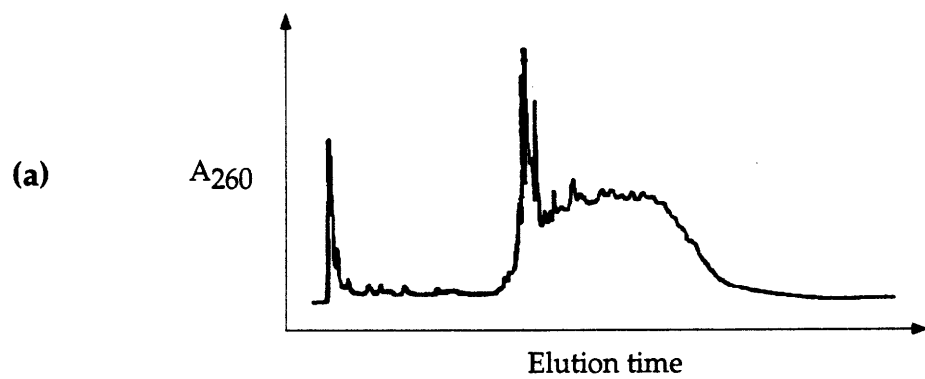


**Figure 8.** HPLC purification an unplatinated, complementary deoxyoligonucleotide strand. (a) Crude oligonucleotide after deprotection. Ion exchange B: 20-80% over 30 min. (b) Crude oligonucleotide after deprotection. Ion exchange B with 50% formamide: 10-50% over 30 min. (c) Oligonucleotide after ion exchange purification. Reverse phase B: 5-40% over 30 min. (d) Oligonucleotide after ion exchange and reverse phase purification. Ion exchange B with 50% formamide: 10-50% over 30 min.





concentration of 2.5 mM. Crystals were grown by using sitting drops (Figure 9) (Drenth, 1994). Each crystallization trial drop contained deoxyoligonucleotide, sodium cacodylate, magnesium chloride, and 2-methyl-2,4-pentanediol (MPD). Drops also contained a polyamine; spermine hydrochloride or  $[\text{Co}(\text{NH}_3)_6]\text{Cl}_3$  were most often used. Crystallization drops were mixed at room temperature and equilibrated against a 5% MPD reservoir at 4 °C. In successful trials, clusters of crystals appeared after 3-30 days and were allowed to grow for 9-12 months.

Successful crystallizations of TT12d and its derivatives resulted in clusters of thin rods. The small dimensions of the rods are usually 0.01 - 0.07 mm x 0.01 - 0.10 mm, too thin to be studied by X-ray diffraction. In order to get crystals with dimensions of about 0.05 x 0.10 x 1.0 mm<sup>3</sup>, a slow cooling technique was employed. Crystallization drops were constructed as described in the previous section, the crystallization boxes were sealed, and the boxes were then covered with three layers of bubble wrap. Wrapped boxes were then packed into a styrofoam box at room temperature. The styrofoam box was sealed and placed in the cold room and allowed to equilibrate to 4 °C. After 9-12 months, the drops produced diffraction quality crystals.

Clusters of TT12d and its brominated derivatives TT12-Br1, TT12-Br2, and TT12-Br3 (Table 3) were grown in drops containing 0.2 mM duplex DNA (TT12), 52 mM cacodylic acid (sodium salt, pH 6.0), 15 mM magnesium chloride, 6 mM  $[\text{Co}(\text{NH}_3)_6]\text{Cl}_3$  and 3% 2-methyl-2,4-pentanediol (MPD) (Figure 10). Diffraction quality crystals of the other sequences listed in Table 2 were not obtained.

*Analysis of Platinum/DNA Ratios in the Crystals.* Ten TT12d crystals were removed from crystallization drops, washed three times with 20% MPD,

and dissolved in water. The platinated oligonucleotide was separated from its complementary strand by reverse phase HPLC. The *cis*-[Pt(NH<sub>3</sub>)<sub>2</sub>{d(GpG)-N7(G<sub>6</sub>),-N7(G<sub>7</sub>)}] adduct was confirmed by enzymatic digestion analysis of the platinated oligonucleotide. 1 nmol of single-stranded platinated oligonucleotide from TT12d crystals was dissolved in 50 mM NaOAc and 10 mM MgCl<sub>2</sub> at pH 5.6 and digested with DNase I (40 units) and P1 Nuclease (2 units) at 37 °C for 24 h. An aliquot of this digestion solution was diluted ten-fold and digested further with alkaline phosphatase (5 units) in a 100 mM EDTA and 50 mM Tris-HCl buffer at 37 °C for 24 h. The final digestion solution was then analyzed by reverse phase HPLC. The presence of cytosine and thymine were confirmed by comparison with standards purchased from Aldrich, and the ratio of 6 cytosine residues to 4 thymine residues was confirmed by peak integration. The cisplatin intrastrand cross-link was confirmed by coinjection with authentic *cis*-[Pt(NH<sub>3</sub>)<sub>2</sub>{d(GpG)-N7(G<sub>1</sub>),-N7(G<sub>2</sub>)}] and unplatinated d(GpG). The digestion analysis of the platinated oligonucleotide isolated from TT12d crystals is shown in Figure 11.

The platinated oligonucleotide isolated from TT12d crystals by using HPLC was also analyzed twice by using flameless atomic absorption spectroscopy and yielded platinum per single-stranded oligonucleotide ratios of 0.98 and 0.96.

*X-ray Data Collection.* Crystals cut from clusters were mounted in sealed glass capillaries containing a drop of mother liquor (Figure 12) and sealed with melted wax. The capillaries were attached to pre-cooled brass pins and secured with epoxy resin. The brass pins were then attached to pre-cooled goniometer heads and stored in a styrofoam box packed with ice.

**Figure 9.** A sitting drop crystallization and conditions for cisplatin-modified DNA.

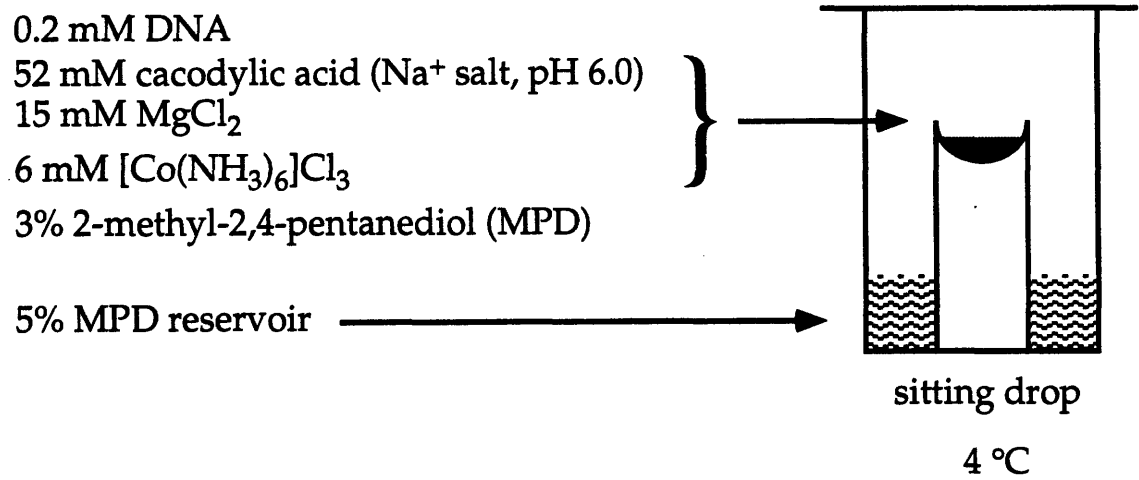


**Figure 10.** Photomicrograph of a cluster of cisplatin-modified DNA crystals. The picture was taken under polarized light and the crystals are actually colorless.

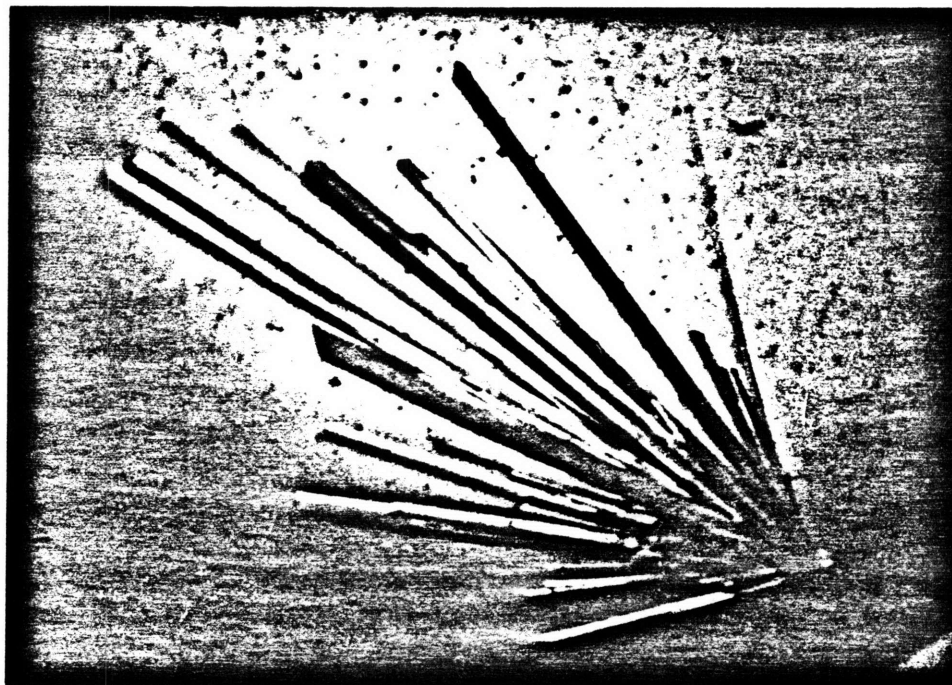


**Figure 11.** Digestion analysis of the platinated oligonucleotide, d(CCTCTG\*G\*TCTCC) where the -G\*G\* site is coordinated to *cis*-[Pt(NH<sub>3</sub>)<sub>2</sub>]<sup>2+</sup>, from crystals of TT12d. (a) Digestion products from the platinated oligonucleotide. (b) Coinjection of d(GpG) and *cis*-[Pt(NH<sub>3</sub>)<sub>2</sub>{d(GpG)}]<sup>+</sup> with the digestion products. (c) d(GpG) and *cis*-[Pt(NH<sub>3</sub>)<sub>2</sub>{d(GpG)}]<sup>+</sup> standards. Peaks are as follows: (1) digestion buffer, (2) dC, (3) dT, (4) *cis*-[Pt(NH<sub>3</sub>)<sub>2</sub>{d(GpG)}]<sup>+</sup>, (5) undigested platinated oligonucleotide, (6) d(GpG), (7) solvents from a previous purification of *cis*-[Pt(NH<sub>3</sub>)<sub>2</sub>{d(GpG)}]<sup>+</sup>.

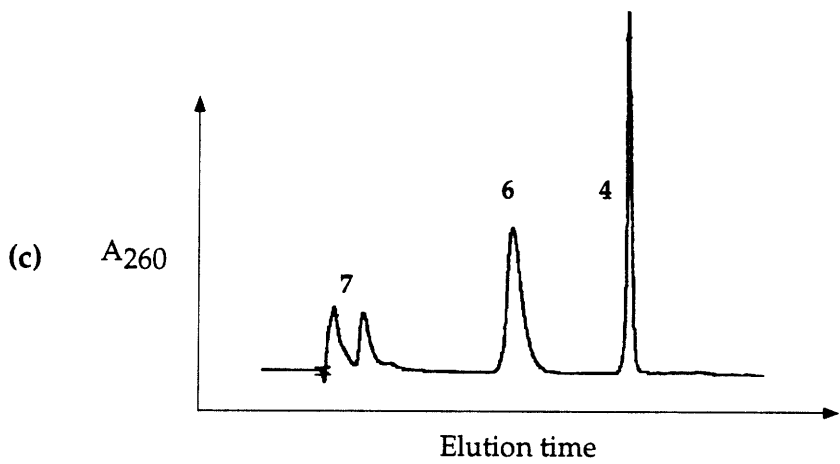
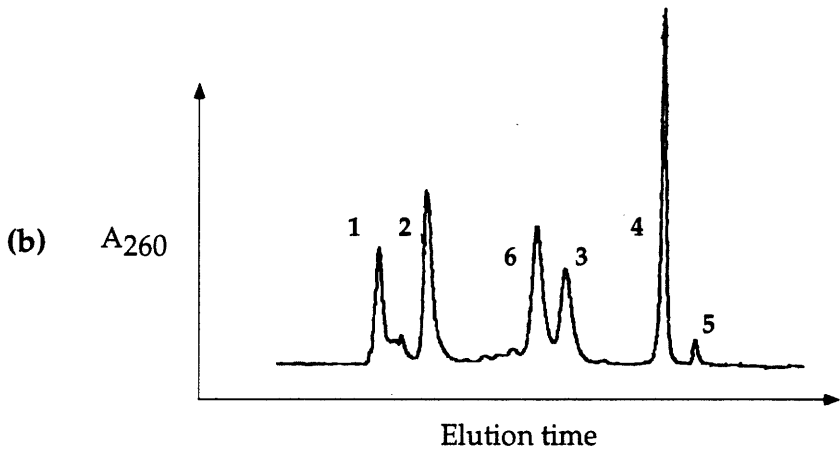
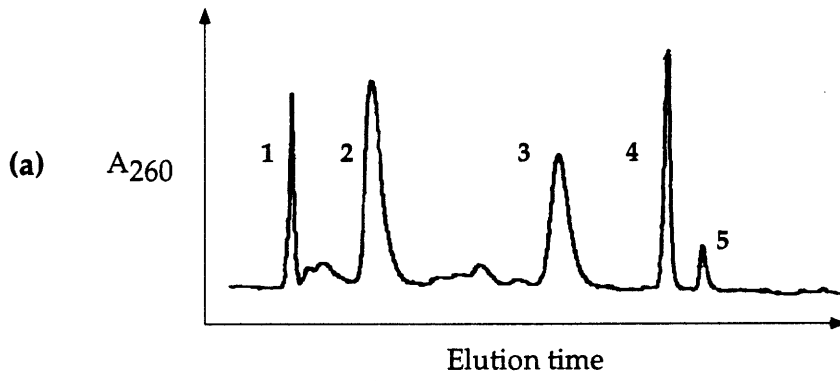
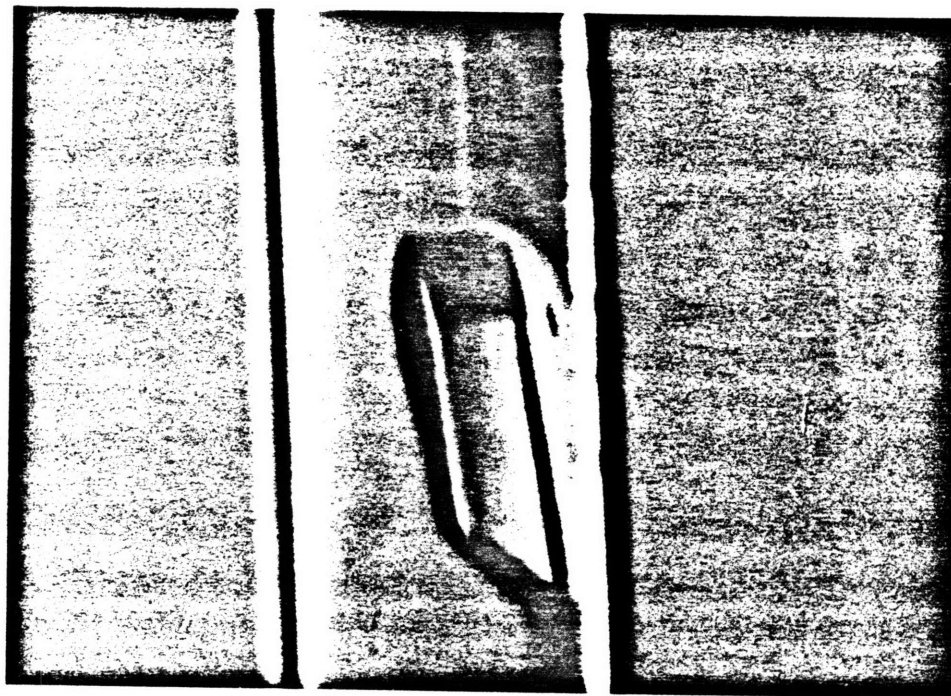


**Figure 12.** Photomicrograph of a crystal of cisplatin-modified DNA in a glass capillary. The capillary contains the crystal and a plug of mother liquor and is sealed on both ends by wax.





The cold stream on the X-ray instrument to be used was adjusted to 4 °C and allowed to equilibrate for 30-60 min. The temperature was monitored with a thermocouple. After the cold stream was stabilized at 4 °C, the styrofoam box containing the goniometer head was removed from the cold room, transported to the machine and mounted as quickly as possible. Crystals were optically centered by using a videomicroscope.

Data sets for TT12d and its derivatives were collected on a Marresearch image plate with  $\text{CuK}\alpha$  ( $\lambda = 1.5418 \text{ \AA}$ ) radiation. Unit cell parameters were determined by autoindexing several images in each data set separately with the program DENZO (Z. Otwinowski, University of Texas, Southwestern Medical Center). The unit cell volume was determined to be  $50,770 \text{ \AA}^3$  and indicated the presence of two DNA duplexes in each asymmetric unit. For each data set, rotation images were collected in  $3^\circ$  increments with a total rotation of  $360^\circ$  about phi. Unit cell parameters, sequences used, and additional X-ray information are summarized in Table 3.

Crystals of TT12d, TT12Br2, and TT12Br3, in the original drops from which they were grown, were packed in a styrofoam box fitted with several cold packs and foam and were transported to the Stanford Synchrotron Radiation Laboratory (SSRL). At SSRL, the crystallization plates were immediately transferred to a cold room (4 °C) and removed from the styrofoam box. The crystals were visually inspected by using a microscope, and no damage was seen. Several crystals of TT12d, TT12Br2, and TT12Br3 were mounted in a loops made from strands of dental floss and fastened to the end of brass pins with epoxy. Crystals mounted in loops were flash frozen in a nitrogen cold stream (-170 °C). No diffraction was seen for the frozen crystals. The remaining crystals were mounted in sealed capillaries and tested

**Table 3.** Experimental details of the X-ray diffraction study of cisplatin-modified DNA.

Unit cell parameters:      $a = 31.3 \text{ \AA}$       $\alpha = 79.8^\circ$   
                                    $b = 35.5 \text{ \AA}$       $\beta = 84.8^\circ$   
                                    $c = 47.0 \text{ \AA}$       $\gamma = 82.8^\circ$

Unit cell volume:  $50,770 \text{ \AA}^3$   
 Space group: P1  
 Molecules per asymmetric unit: 2  
 Instrument: Mar Research Imaging Plate  
 Radiation: Cu  $K_\alpha$   
 Diffraction limit:  $2.6 \text{ \AA}$  for Br1  
 Structure solution method: multiple isomorphous replacement (MIR)

Sequences used for MIR:

Native	d(CCTCTG*G*TCTCC)·d(GGAGACCAGAGG)
Br1	d(CCUBrCTG*G*TCTCC)·d(GGAGACCAGAGG)
Br2	d(CCTCTG*G*UBrCTCC)·d(GGAGACCAGAGG)
Br3	d(CCTCTG*G*TCBrTCC)·d(GGAGACCAGAGG)

for diffraction. Many of the crystals failed to diffract at all, and the ones that did diffract had split spots throughout the diffraction pattern indicating that the crystal had cracked during the trip or during mounting. The best crystals, TT12d, were split badly but diffracted to about 2.8 Å.

Crystals were packed and transported to the Brookhaven National Synchrotron Light Source Beamline X-8C in the manner described for the Stanford experiments. The crystals were inspected under a microscope after they had been transferred to the cold room. Several were cracked and a few had disintegrated, but there were also many crystals which showed no visible signs of damage. Two TT12d crystals were mounted in loops and frozen by immersion in liquid propane. The frozen crystals were then transferred into a nitrogen cold stream set at -165 °C. The first frozen crystal diffracted to about 2.7 angstroms but had many split spots indicating that the crystals were damaged either by the transportation or freezing procedure (Figure 13). No data were collected on the first crystal but it was used to tune the wavelength of the radiation to the platinum edge. The edge was found by monitoring fluorescence while stepping the energy of the X-ray beam. The maximum fluorescence for platinum foil was found to be 11550 eV. The maximum fluorescence for a TT12d crystal was found to be 11574 eV and corresponded to a wavelength of 1.072 Å (Figure 14). This experiment provided further confirmation that crystals contained platinum.

A partial data set was collected on a second crystal that had been frozen in liquid propane. The data were collected on a charge coupled device (CCD) imaging plate with rotation increments of 0.2°. 492 pictures corresponding to a total rotation of 98.4° were collected. The data could not be indexed.

**Figure 13.** CCD detector image collected on a frozen crystal of platinated DNA at NSLS-X8C. The outer spots on the image correspond to 2.7 Å diffraction. Many spots are split and indicate crystal damage.

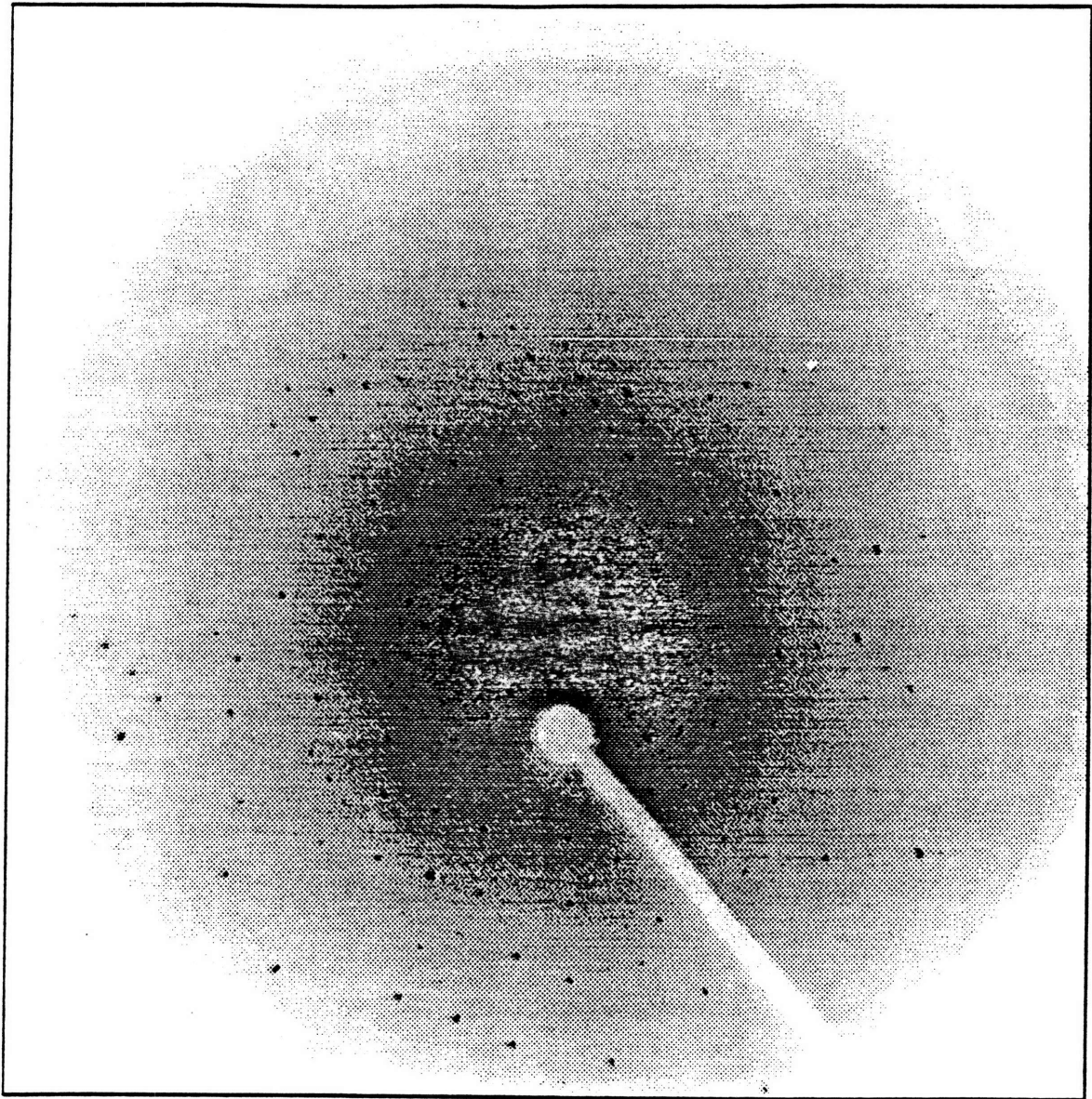
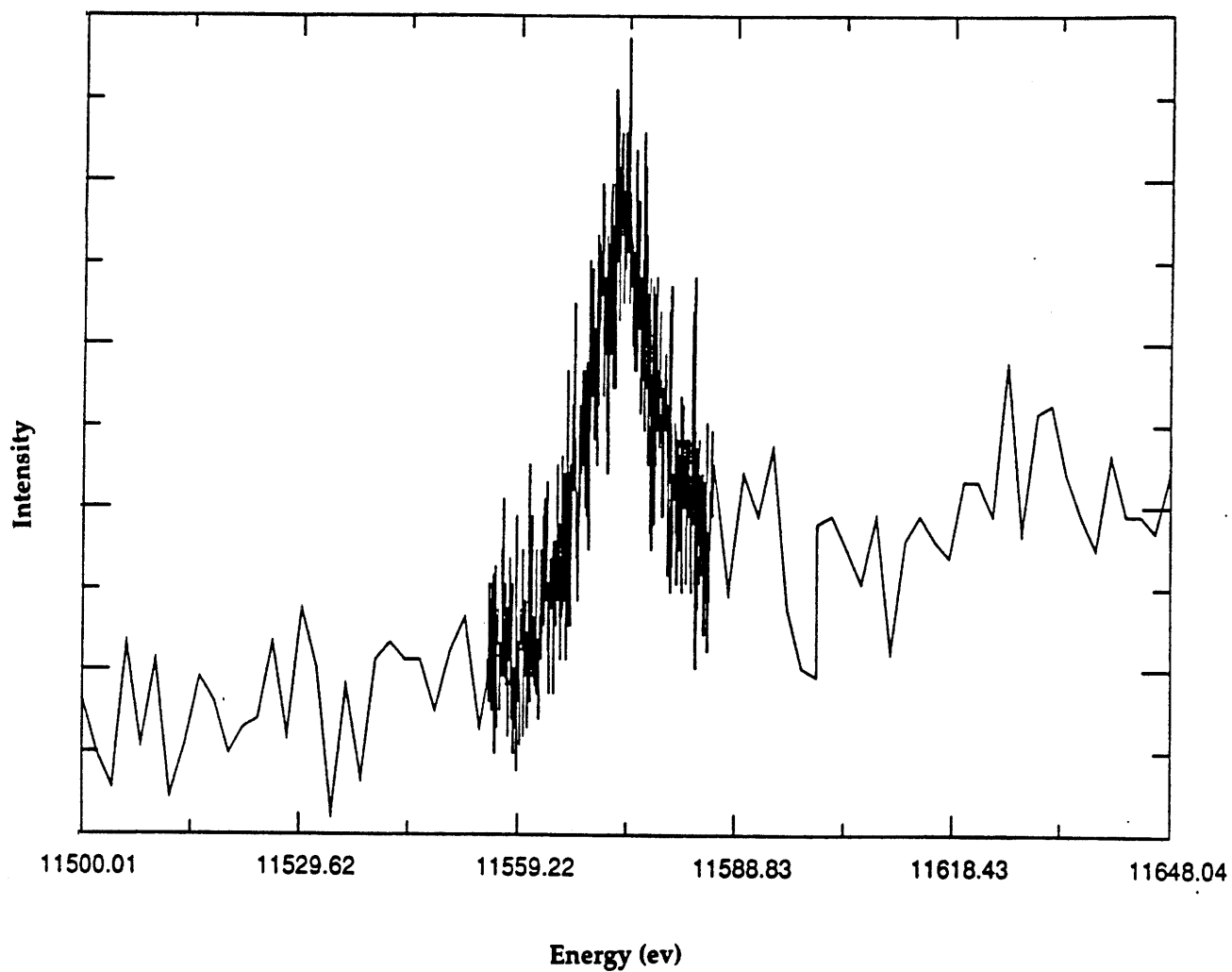


**Figure 14.** Fluorescence intensity scan of a crystal of platinated DNA. The maximum energy corresponds to an energy of 11574 eV and a wavelength of 1.072 Å.

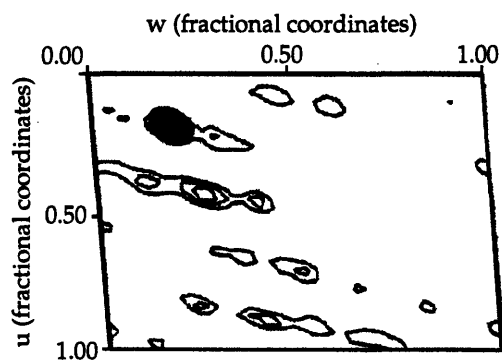


*Data Reduction and Structure Determination.* Data sets collected on a Marresearch imaging plate were used to solve the structure of the cisplatin-modified dodecamer, d(CCTCTG\*G\*TCTCC)·d(GGAGACCAGAGG), where the -G\*G\*- site has been modified with *cis*-[Pt(NH<sub>3</sub>)<sub>2</sub>]<sup>2+</sup>. Data were processed and merged by using DENZO and SCALEPACK (Z. Otwinowski) and further processed by using the CCP4 program suite (CCP4, 1994). An anomalous difference Patterson map was calculated from the native data and used to determine the relative positions of the platinum atoms and this map confirmed the presence of two platinated duplexes in each unit cell with the platinum atoms 15.1 Å apart (Figure 15 a). A conventional Patterson map was calculated by using the data from 3.2 Å to 3.5 Å and showed a slight bend in the stacking pattern of the bases (Figure 15 b).

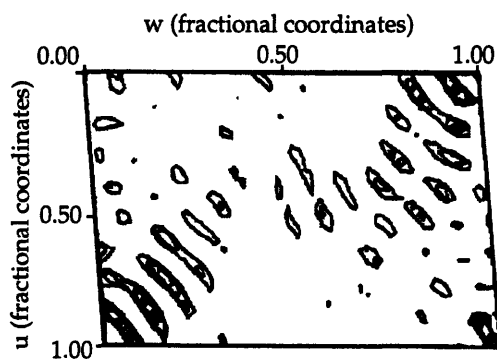
Difference Patterson maps between the native and derivative data were calculated for each brominated duplex for which data were collected. Each derivative DNA duplex was synthesized with one bromine placed specifically in the sequence (Table 3). Difference Patterson maps clearly showed one peak corresponding to a bromine-bromine vector, in accord with the presence of two DNA duplexes in the asymmetric unit (Figures 16 a-c).

The bromine positions were used to calculate single isomorphous replacement (SIR) phases for each heavy atom derivative. Fourier maps were then calculated by using the SIR phases and the native structure factor amplitudes. Since Patterson maps are centrosymmetric, the Fourier map derived was superimposed on its inverse. From each map, two pairs of possible platinum atoms positions were obtained. Shifting one platinum atom to the origin of the unit cell with concomitant shifting of the bromine atoms afforded two possible pairs of bromine positions for each derivative.

**Figure 15.** (a) Anomalous difference Patterson map (010 projection) calculated with native data from 12.0 to 3.0 Å. The peak is at fractional coordinates (0.18, 0.24, 0.19) and corresponds to a platinum-platinum vector of 15.1 Å. (b) Patterson map (010 projection) calculated with native data from 3.2 to 3.5 Å.

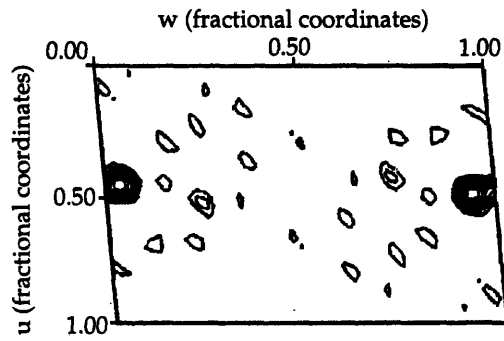


(a)

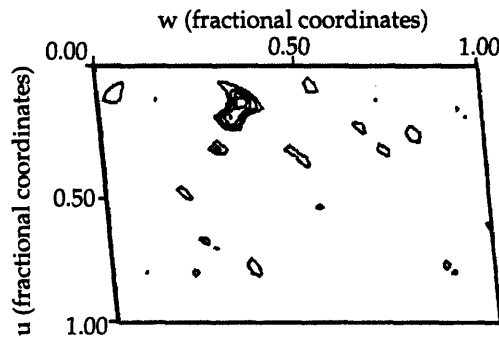


(b)

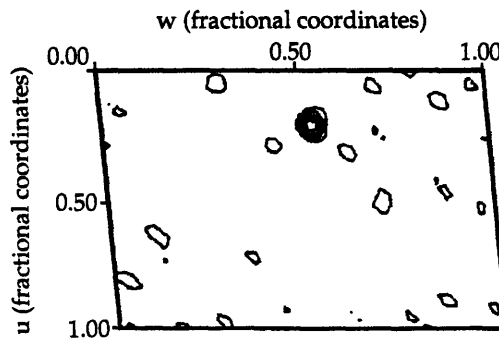
**Figure 16.** Difference Patterson maps (010 projections) calculated with native and derivative data from crystals of (a) Br1, (b) Br2, and (c) Br3. The fractional coordinates for the main peaks are (a) (0.48, 0.50, 0.06), (b) (0.16, 0.19, 0.35), and (c) (0.20, 0.20, 0.53).



(a)



(b)



(c)



The possible pairs of heavy atom positions afforded eight possible combinations of heavy atom positions, each of which was used to calculate trial phases. The correct bromine coordinates for each derivative were found by choosing the best multiple isomorphous replacement (MIR) electron density map. Bromine positions were confirmed by calculating electron density maps with MIR phases and  $|F_{\text{nat}} - F_{\text{der}}|$  structure factor amplitudes. The platinum atom positions were confirmed by calculating maps with MIR phases and the anomalous differences in the native data as the structure factor amplitudes.

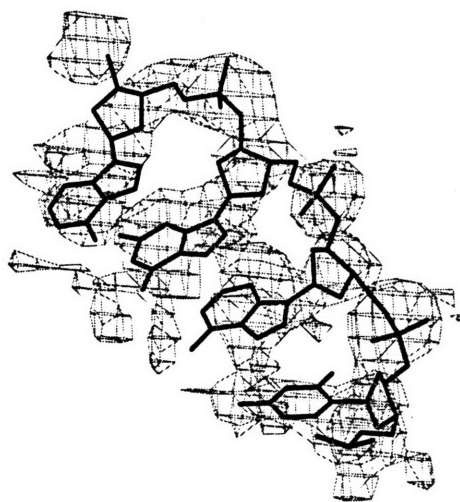
The MIR maps calculated at this stage of the refinement clearly showed the platinum atoms, spherical electron density for the phosphate groups, and elongated electron density for a few of the bases. An initial model of B-DNA modified with *cis*- $\{\text{Pt}(\text{NH}_3)_2\}^{2+}$  was built with the program INSIGHT II (Biosym). Model manipulation was done by using the program O (Jones et al., 1989). No symmetry restraints between the two molecules in the unit cell were used during refinement. The initial model was fit to the MIR maps calculated with native structure factor amplitudes to 3.0 Å. After positional refinement in X-PLOR (Brünger, 1992b; Brünger et al., 1987), the phases obtained were applied to Br1 derivative data with  $|F_{\text{obs}}|$  to 2.6 Å. 10% of the reflections were set aside for the free-*R* factor calculation prior to model building and refinement (Brünger, 1992a; Brünger, 1993). Seventeen cycles of model building, positional refinement, and phase combination, yielded a model for which  $R = \Sigma(|F_{\text{obs}}| - |F_{\text{calc}}|) / \Sigma |F_{\text{obs}}| = 0.25$ . Another round of positional refinement in which all restraints on the platinum geometry were removed, followed by temperature factor (B) refinement resulted in  $R = 0.225$ . Finally, 31 water molecules were added to the model and gave a final structure with a free-*R* = 0.249 and  $R = 0.203$ . The final structure was checked

by using a series of simulated annealing omit maps in which one base step at a time was left out of the calculation. Refinement statistics are given in Table 4 and examples of maps obtained and models built during the refinement are shown in Figure 17. The overall estimated coordinate error for this structure is 0.46 Å and was determined by using a plot of  $\ln(\sigma_A)$  vs. resolution (Figure 18) (Drenth, 1994; Read, 1986) which is based on equation (1):

$$\ln \sigma_A = 1/2 [\ln(\Sigma_P/\Sigma_N)] - \pi^3(|\Delta r|)^2(\sin\theta/\lambda)^2 \quad (1)$$

where  $\sigma_A$  is  $D(\Sigma_P/\Sigma_N)^{1/2}$ ,  $\Sigma_P$  and  $\Sigma_N$  are the summations of the squares of atomic structure factors for all atoms in the full and partial structures, respectively,  $|\Delta r|$  is the average coordinate error for the model, and  $D$  is the Fourier transform of the probability distribution of  $|\Delta r|$ .

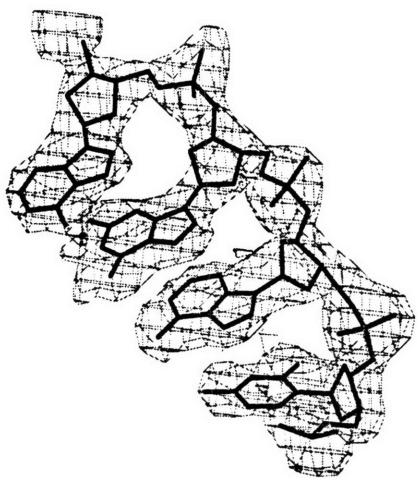
**Figure 17.** Maps of molecule A, residues C19-A20-G21-A22, generated during refinement of the structure. (a) is the MIR map, (b) is a 2Fo-Fc map calculated from a partial structure after five rounds of model building, (c) is a 2Fo-Fc map calculated after ten rounds of model building, and (d) is the final 2Fo-Fc map with the final model superimposed.



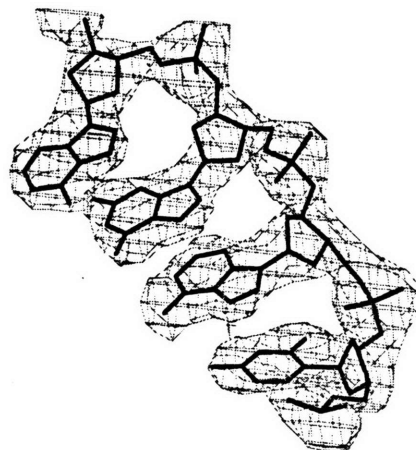
(a)



(b)



(c)



(d)

Figure 18.  $\sigma_a$  plot for the estimated coordinate error for the final model.

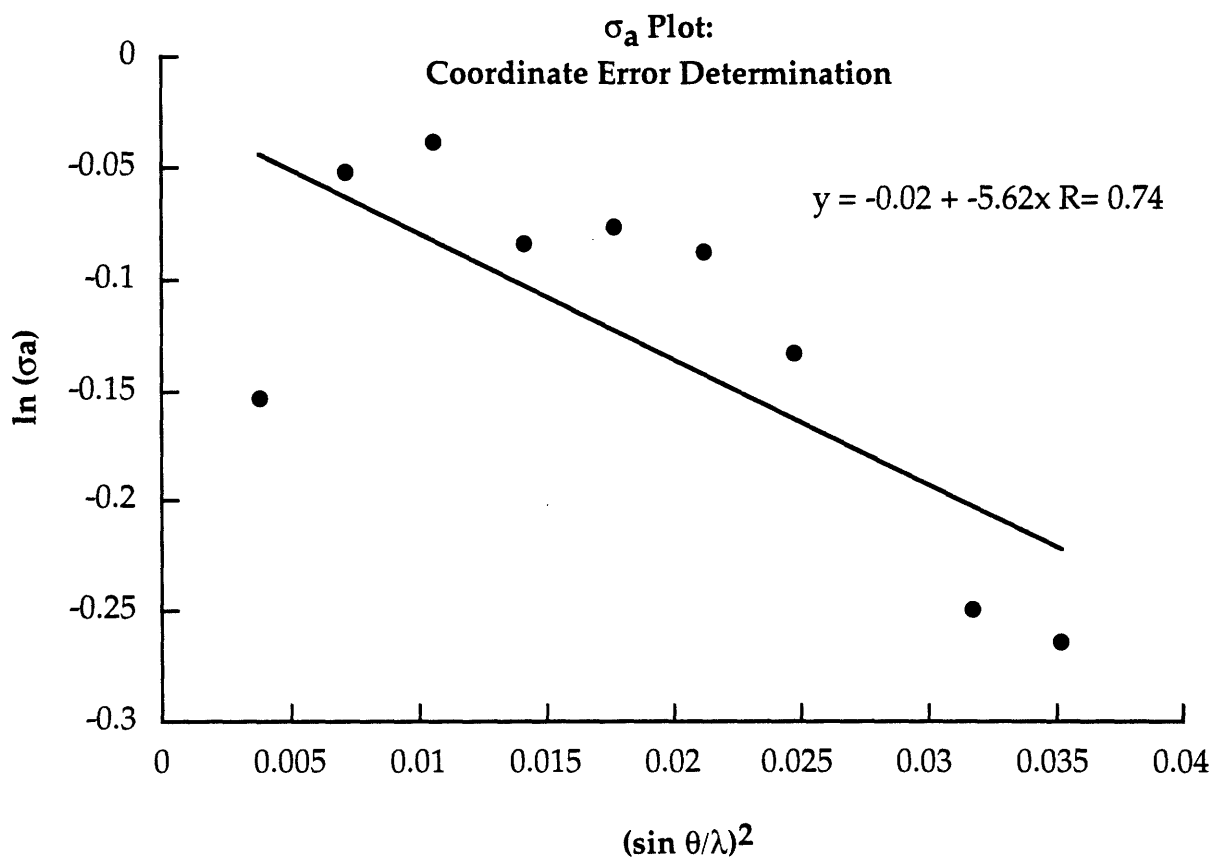


**Table 4.** Summary of crystallographic data.

Crystal	Resolution (Å)	Unique reflections	Completeness (%)	R <sub>sym</sub> (%)	Isomorphous difference (%)	Phasing power
Native	3.0	3793	97.7	6.2		
Br1	2.6	5797	97.0	6.2	13.4	1.4
Br2	3.0	3380	86.8	8.7	16.1	0.9
Br3	3.0	3488	89.9	7.5	17.1	0.9

R-factor = 0.203

R-free = 0.245

rmsd:

distances = 0.015 Å

angles = 3.1°

temperature factors = 1.9 Å<sup>2</sup>

$$R\text{-factor} = [\sum(hkl) | |F_{obs} | - k |F_{calc} | | ] / \sum(hkl) | F_{obs} |$$

$$R\text{-free} = [\sum(hkl) | |F_{obs} | - k |F_{calc} | | ] / \sum(hkl) | F_{obs} | \text{ for reflections set aside before refinement}$$

$$R_{sym} = [\sum(hkl)\Sigma(i) | I(hkl) - I(\overline{hkl}) | ] / \sum(hkl)\Sigma(i) I(hkl)$$

$$\text{Isomorphous difference} = R_{iso} = [\sum(hkl) | |F_{nat} | | - |F_{nat} | | ] / \sum(hkl) | F_{nat} |$$

$$\text{Phasing power} = [\sum |F_H |^2 / \sum |E|^2] \text{ with } \Sigma |E|^2 = \Sigma [ |F_{PH} |_{obs} - |F_{PH} |_{calc} ]$$



**CHAPTER 3**

**RESULTS**

*Canonical DNA Structures*

DNA is a biopolymer composed of four bases, adenine, thymine, guanine, and cytosine, arranged in various sequences and connected by a deoxyribose-phosphate backbone (Figure 19) (Sriram & Wang, 1996). DNA exists mainly in the form of a double helix with antiparallel strands and specific nucleotide base pairs. Adenine forms two hydrogen bonds with thymine and guanine forms three hydrogen bonds with cytosine to form these base pairs through what has been termed Watson-Crick hydrogen bonding (Saenger, 1984). The base pairs, their numbering schemes, and the labels used to describe the DNA sugar phosphate backbone are shown in Figures 20 and 21, respectively. The hydrophobic surfaces of the base pairs of DNA stack on top of one another and are connected in a helical arrangement by negatively charged sugar-phosphate backbones which run antiparallel to one another.

DNA predominantly exists in two right handed helical forms, B-DNA and A-DNA. Both B-DNA and A-DNA have been extensively characterized by X-ray diffraction techniques (Kennard & Hunter, 1989; Kennard & Salisbury, 1993). The structures of B-DNA and A-DNA are shown in Figure 22 and selected metrical parameters are summarized in Table 5. B- and A-DNA differ in the conformations of their sugar rings, groove widths, positions of their helical axes, and overall helix shapes. The differences in their structures arise from variations in hydration conditions and the composition of the environment in which the molecule is being studied (Saenger, 1984).



**Table 5.** Comparison of selected A-DNA and B-DNA structural parameters.

Helix type	A-DNA	B-DNA
Rise per base pair	2.3 Å	3.4 Å
Base pairs per turn of helix	11	10.4
Pitch per turn of helix	25.3 Å	35.4 Å
Propeller twist	11.44°	-1.29°
Roll	10.78°	-2.80°
Slide	-2.08 Å	-0.62 Å
Twist	31°	36°
Major groove	11.7 Å	2.8 Å
Minor groove	5.7 Å	11.0 Å
Sugar pucker	C3'-endo	C2'-endo

**Figure 19.** DNA is composed of bases connected by a sugar phosphate backbone. The four bases contained in normal DNA sequences are adenine, guanine, cytosine, and thymine.

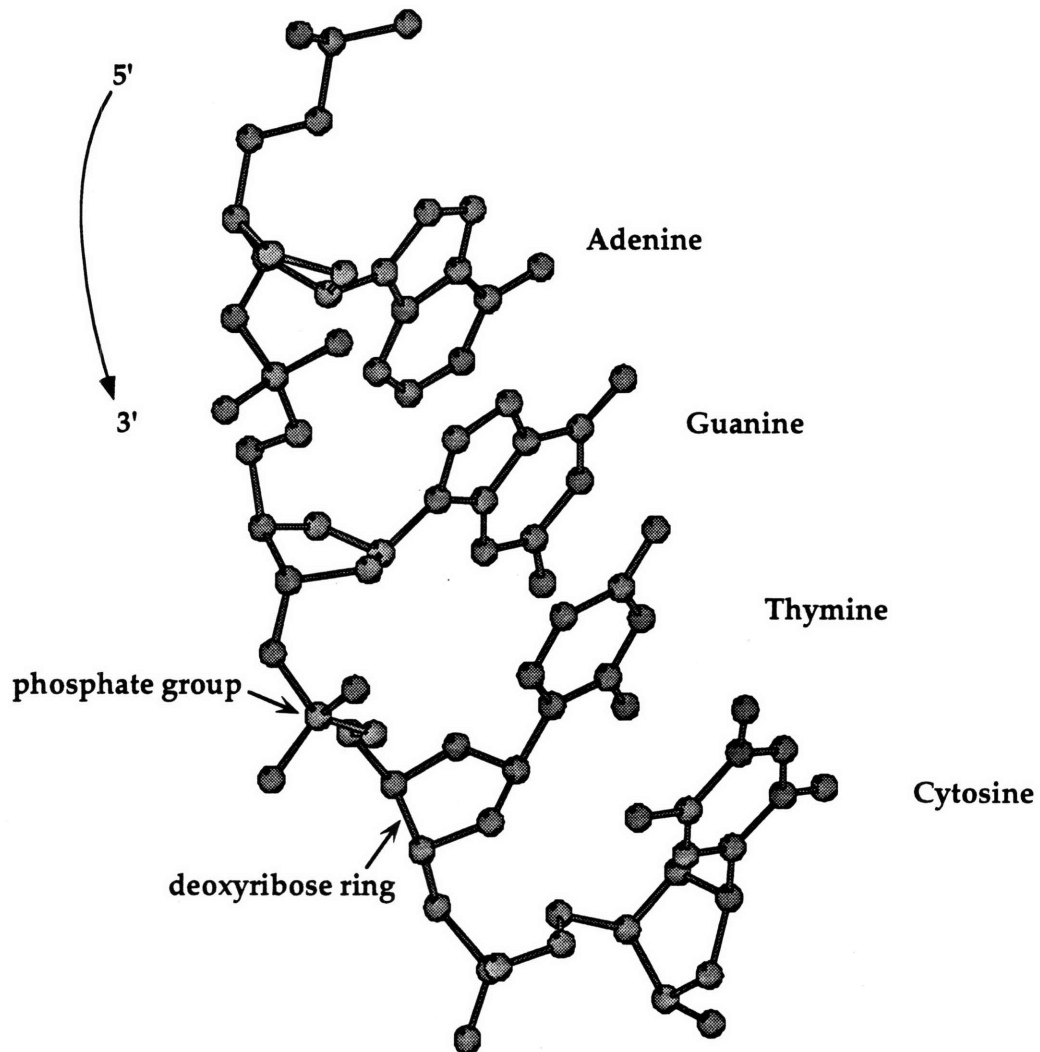


**Figure 20.** The Watson-Crick base pairs of DNA. Adenine pairs with thymine and guanine with cytosine through the hydrogen bonds shown. Also shown are the numbering schemes normally used for the base atoms and the atoms in the major groove and minor groove when the base pairs are incorporated into double helical DNA.

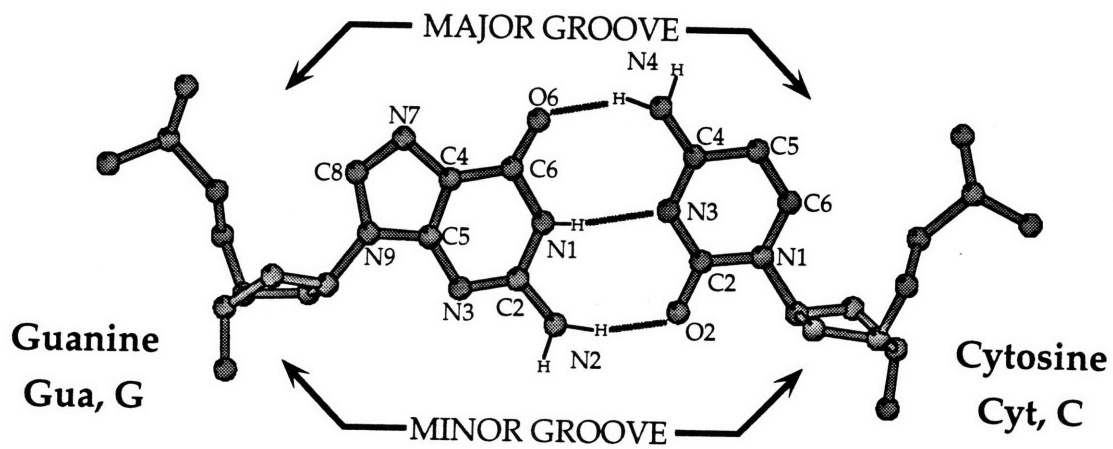
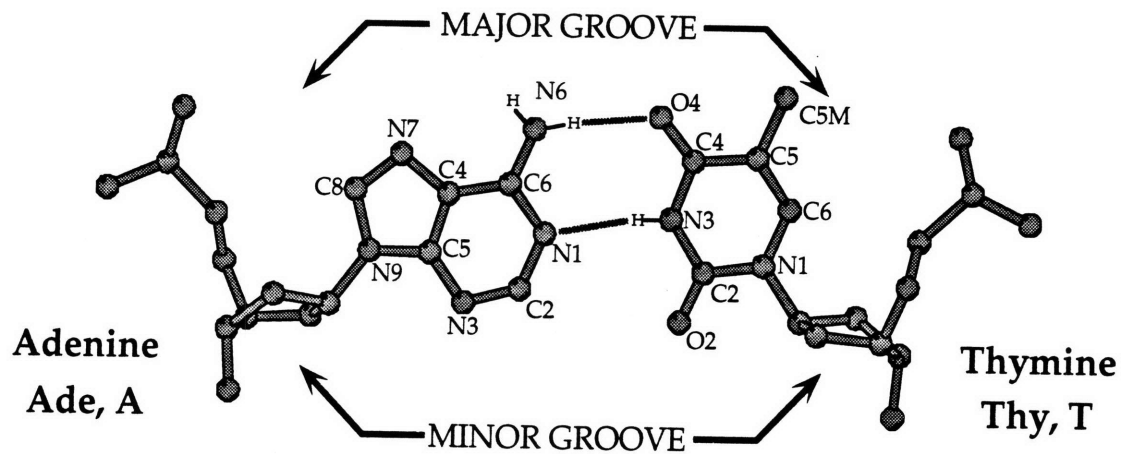


**Figure 21.** Labeling of the torsion angles and deoxyribose ring along the sugar-phosphate backbone of a segment of DNA.

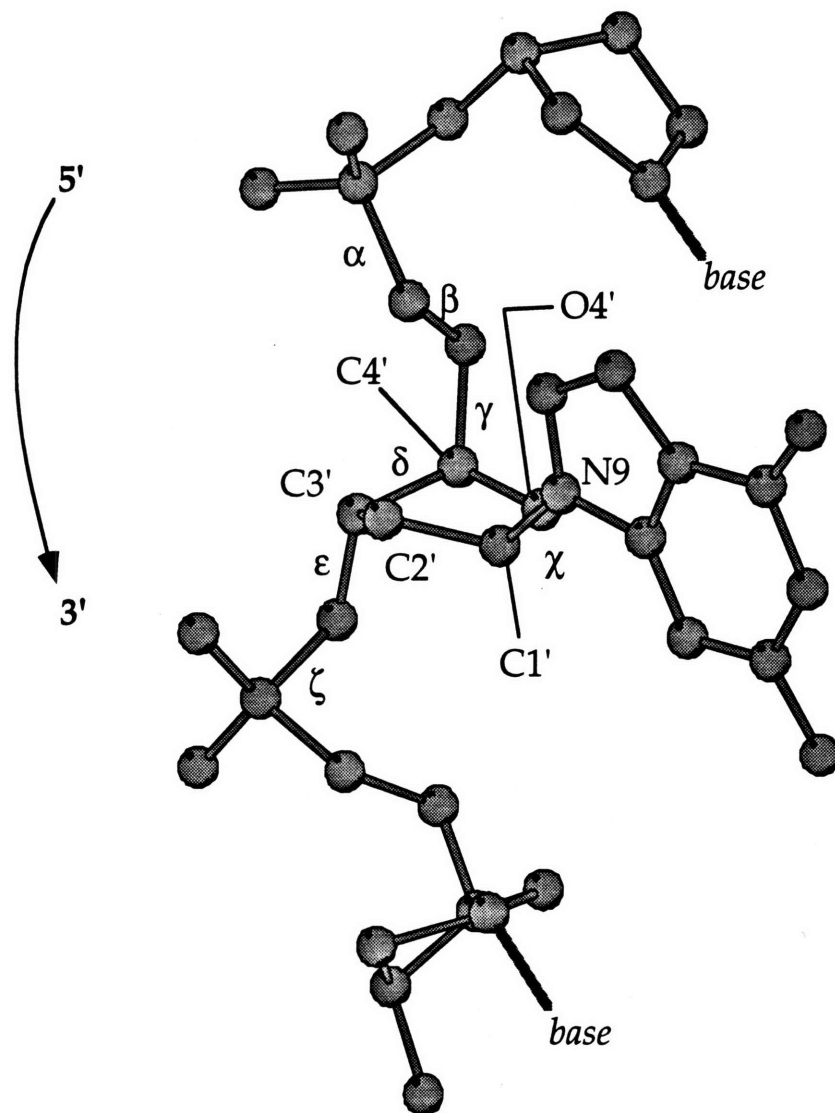
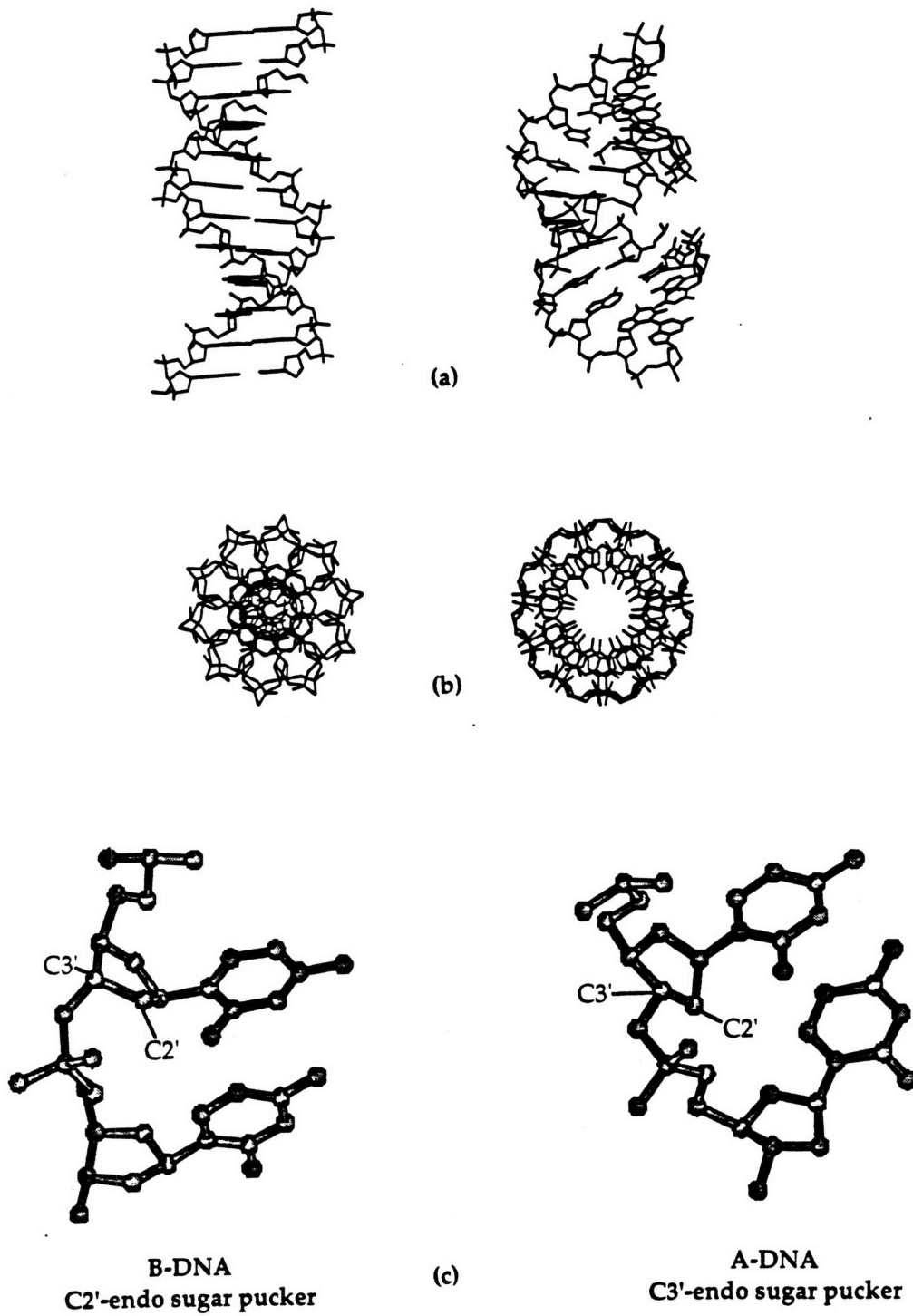


**Figure 22.** (a) The structures of B-DNA and A-DNA. (b) B-DNA and A-DNA viewed down their helical axes. (c) The structure of the deoxyribose rings in B-DNA (C2'-endo) and A-DNA (C3'-endo).

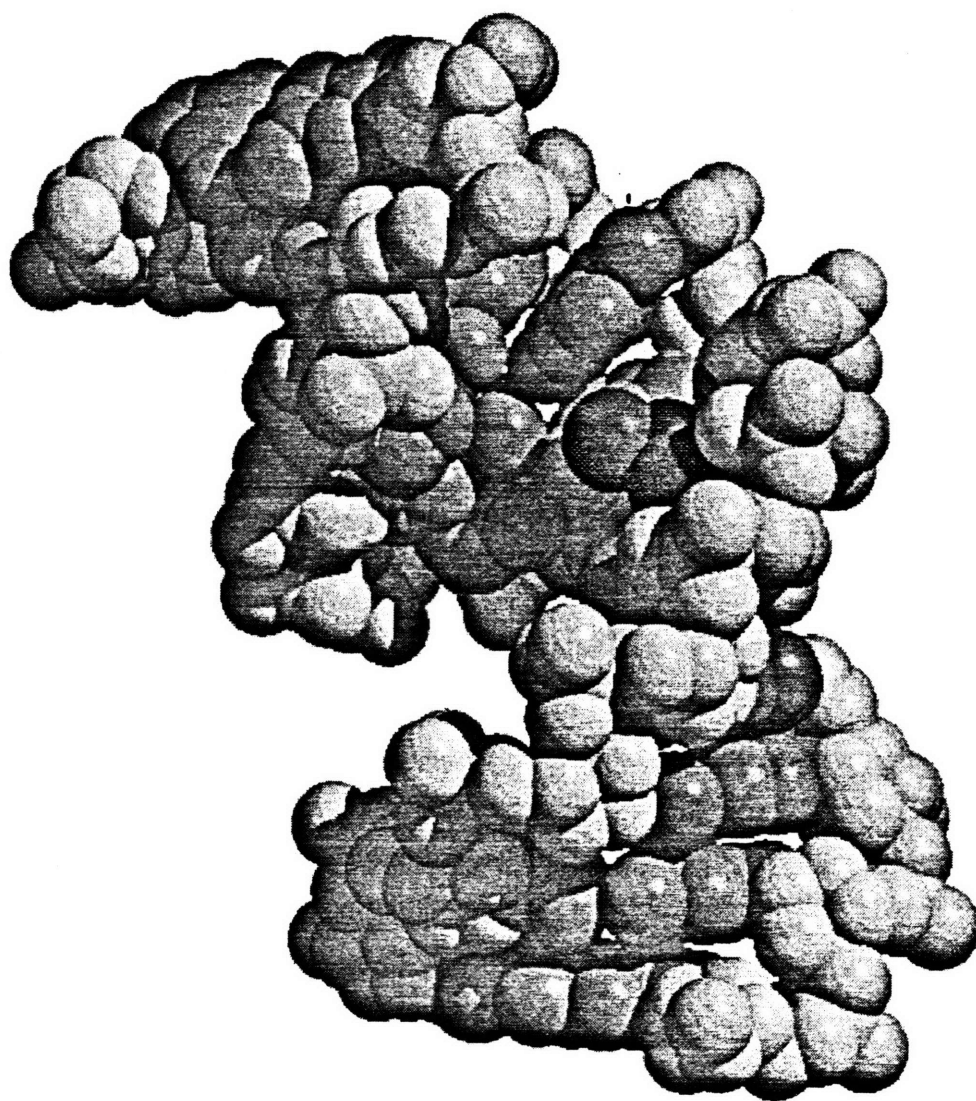


This thesis focuses on how DNA structure is affected by cisplatin binding to a specific site on the double helix. It is important to understand the detailed structural perturbations caused by platinum adducts on DNA because cisplatin/DNA cross-links are generally accepted to be responsible for the antitumor activity of the drug.

### *The Unit Cell*

The DNA duplex, d(CCTCTG\*G\*TCTCC)-d(GGAGACCAGAGG), where the N7 atoms of G6 and G7 are coordinated to the *cis*-{Pt(NH<sub>3</sub>)<sub>2</sub>}<sup>2+</sup> moiety was crystallized and the X-ray structure was solved to a resolution of 2.6 Å. The platinated duplex crystallizes in the triclinic spacegroup P1 with the cell constants listed in Table 3. From the volume of the unit cell and the approximate volume of a B-DNA base pair, 1700 Å<sup>3</sup>, we estimated that there would be two duplexes per unit cell (Kennard & Hunter, 1989). This estimate was confirmed by the presence of one large peak in the anomalous difference Patterson map corresponding to a vector between two crystallographically independent platinum atoms in the unit cell. The Patterson map calculated by using native data from 3.2 Å to 3.5 Å showed a stacking pattern of base pairs with a significant bend from linearity, a feature that was subsequently confirmed with the complete crystal structure (Figure 23).

**Figure 23.** Space filling diagram of the structure of cisplatin-modified duplex DNA. The platinum atom and the ammine ligands are dark gray.



Since there are two molecules in the asymmetric unit, and because molecular averaging was not used during the refinement, two independent determinations of the structure were obtained. We hereafter refer to these as molecule A and molecule B, the nucleotide numbering scheme for which are designated in Figures 24 and 25. A and B are related by the following normalized operator:

$$\begin{array}{ccc} -0.275 & -0.961 & -0.012 \\ -0.961 & 0.275 & -0.016 \\ 0.019 & 0.007 & -0.999 \\ 44.904 & 37.586 & 45.968 \end{array}$$

The rotation axis and relationship of the molecules in the unit cell are shown in Figures 26 and 27. The relationship between the coordinates for selected atoms in molecule A and molecule B are listed in Table 6. The rotation axis shown is a local symmetry element. It does not run along any of the crystallographic axes and is not indicative of higher crystal symmetry. This conclusion is supported by a more extended view of the crystal lattice (Figure 28) in which the local two-fold is seen not to extend to the neighboring unit cells.

Molecules A and B have very similar structures even though they are not related by crystallographic symmetry. The root-mean-square deviation (rmsd) between all atoms is 0.38 Å and an overlay of the two structures is given in Figure 29.



**Table 6.** Selected atomic positions related by the noncrystallographic symmetry operator given in the text. The rotation and translation were applied to the coordinates of an atom in molecule A to afford the calculated coordinates. The actual coordinates of the symmetry-related atom from molecule B are listed for comparison. Units are in Å.

<b>Atom</b>	<b>Molecule A</b>	<b>Calculated</b>	<b>Molecule B</b>
Pt	x = 16.243 y = 17.019 z = 18.691	x = 23.858 y = 26.956 z = 27.723	x = 23.832 y = 26.809 z = 27.606
N7 (G6)	x = 16.313 y = 16.504 z = 20.539	x = 24.310 y = 26.776 z = 25.875	x = 24.315 y = 26.648 z = 25.641
N7 (G7)	x = 16.156 y = 15.209 z = 17.844	x = 25.630 y = 26.528 z = 28.555	x = 25.490 y = 26.345 z = 28.455
Br (UBr <sub>3</sub> )	x = 4.758 y = 21.898 z = 21.882	x = 22.289 y = 39.386 z = 24.352	x = 21.917 y = 39.014 z = 24.348

**Figure 24.** Ball and stick models of the duplex DNA, d(CCTCTG\*G\*TCTCC).d(GGAGACCAGAGG), where -G\*G\*- is modified by cis-[Pt(NH<sub>3</sub>)<sub>2</sub>]<sup>2+</sup>. There are two molecules in each unit cell, (a) molecule A and (b) molecule B.

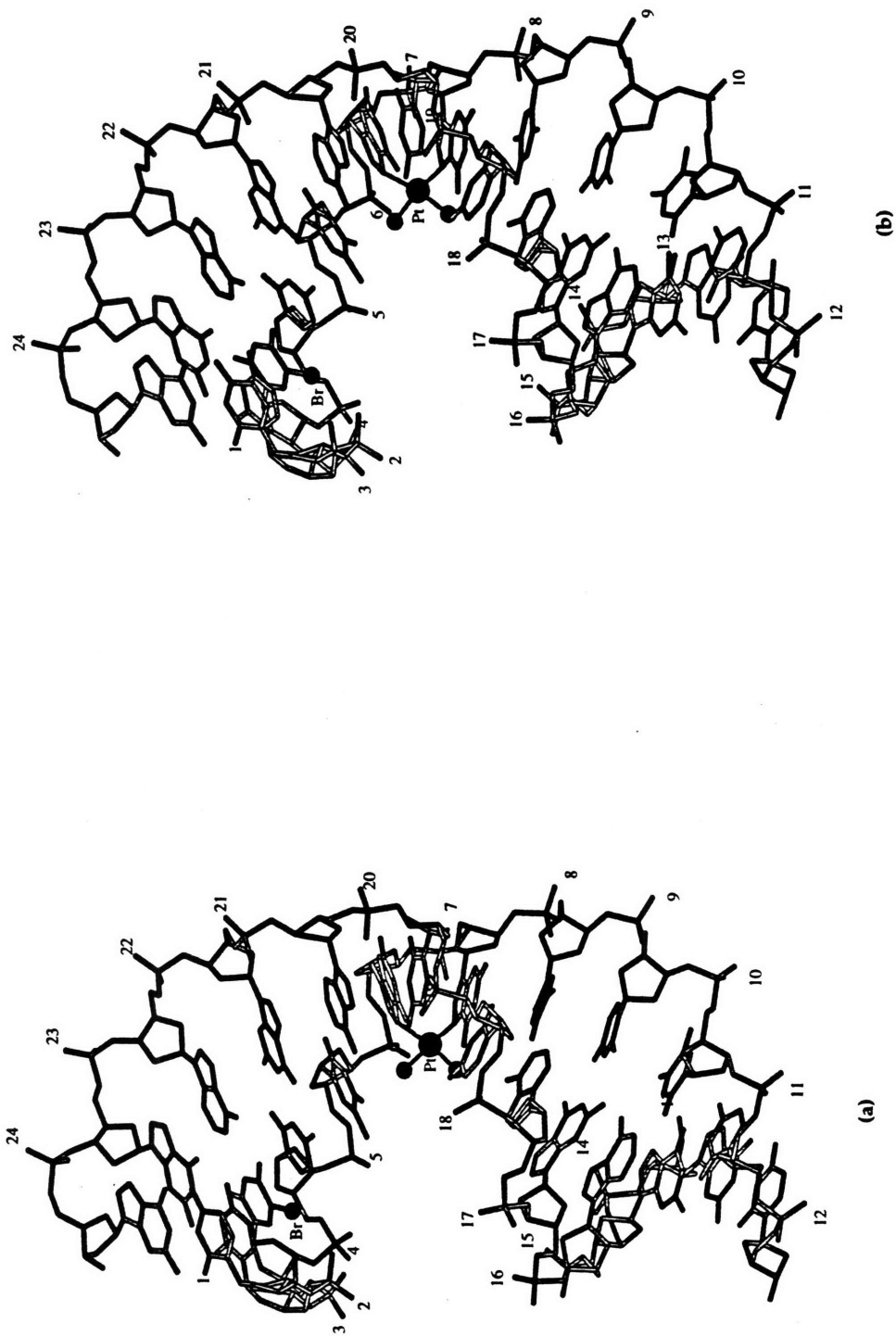


**Figure 25.** The numbering schemes for individual bases, base pairs, and base steps used in this paper are shown.

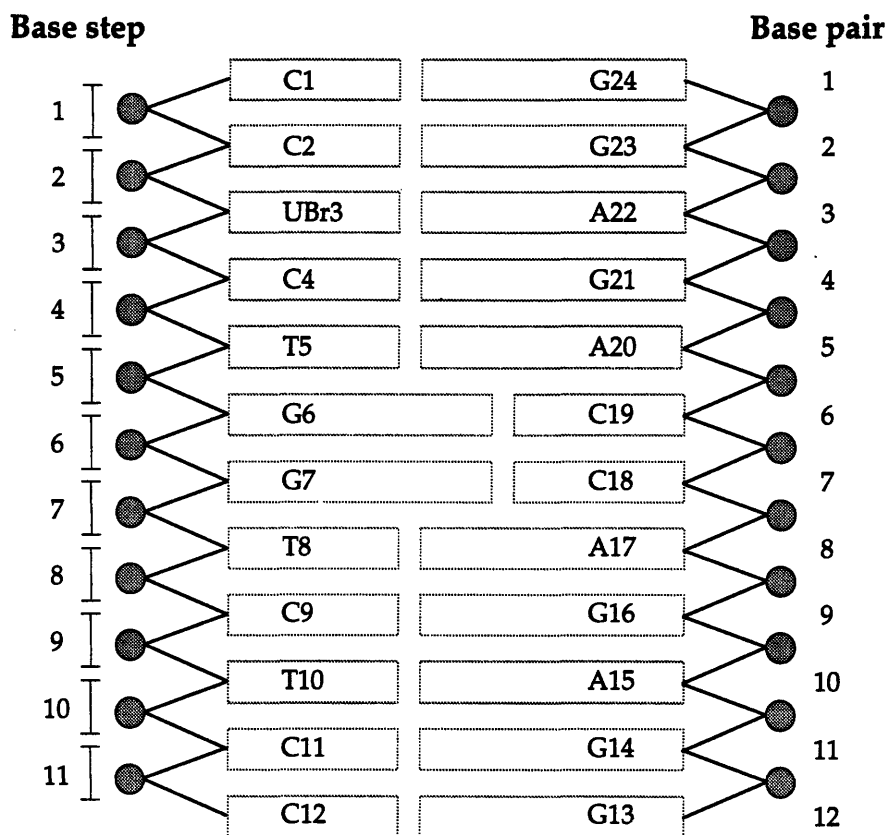


**Figure 26.** (a) Rotation axis (black line) relating the two molecules in each unit cell. The outline of the unit cell is shown in dark gray. (b) View down the rotation axis.

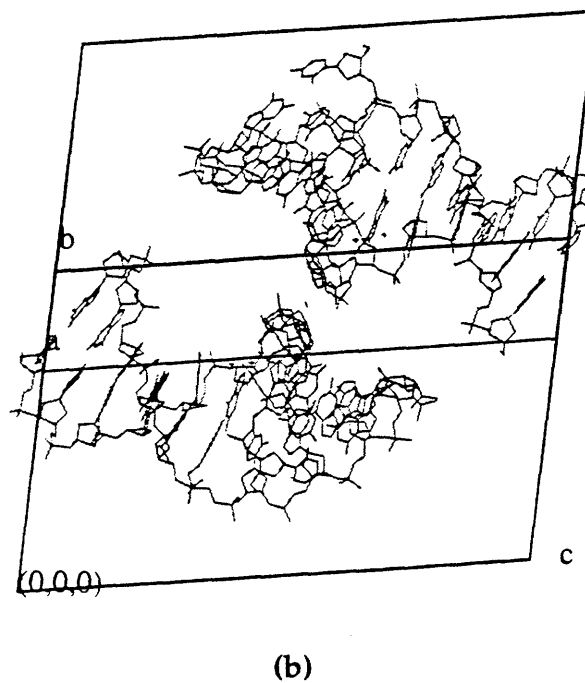
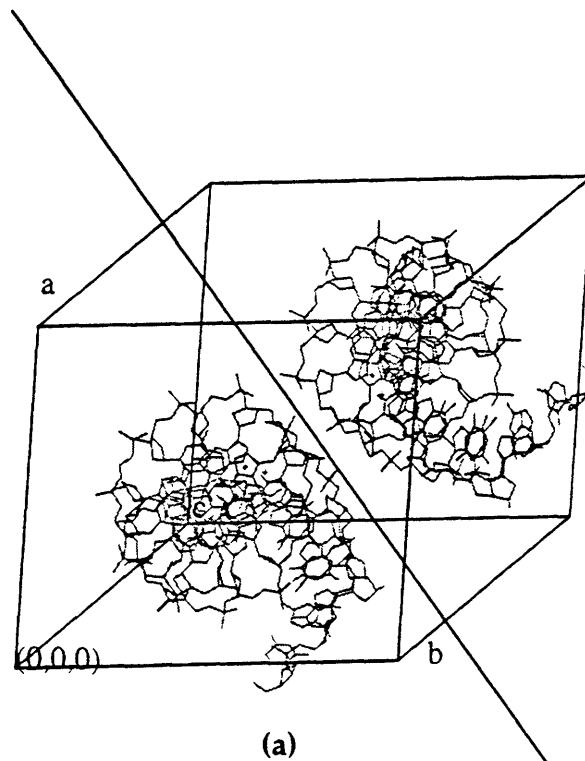


**Figure 27.** Rotation axis (black line) relating molecules A and B. View down (a) the crystallographic a-axis, (b) the b-axis, and (c) the c-axis.

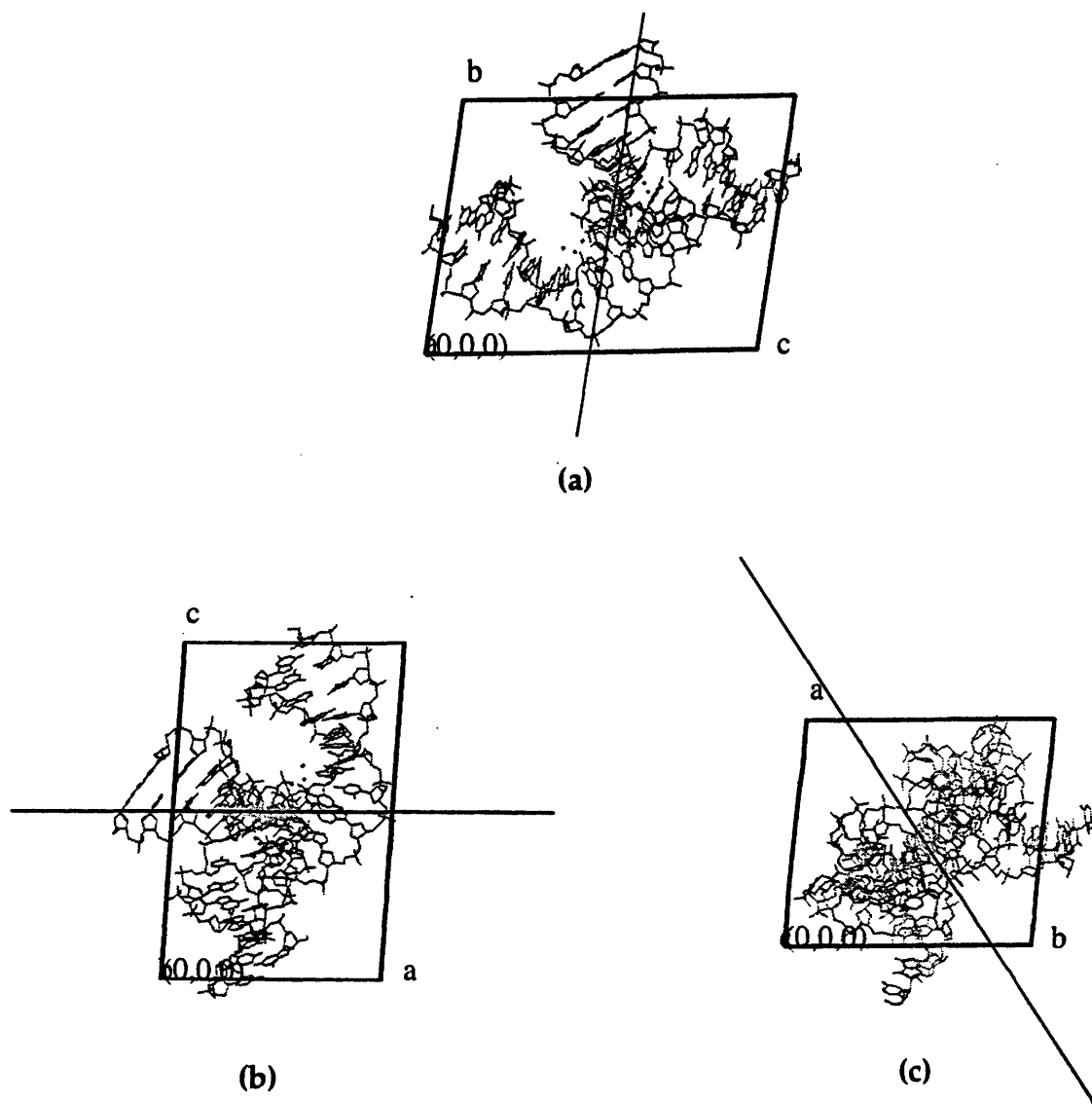


**Figure 28.** Rotation axis (black line piercing the unit cell) relating the two molecules in each unit cell shown with neighboring molecules. The rotation axis is non-crystallographic.

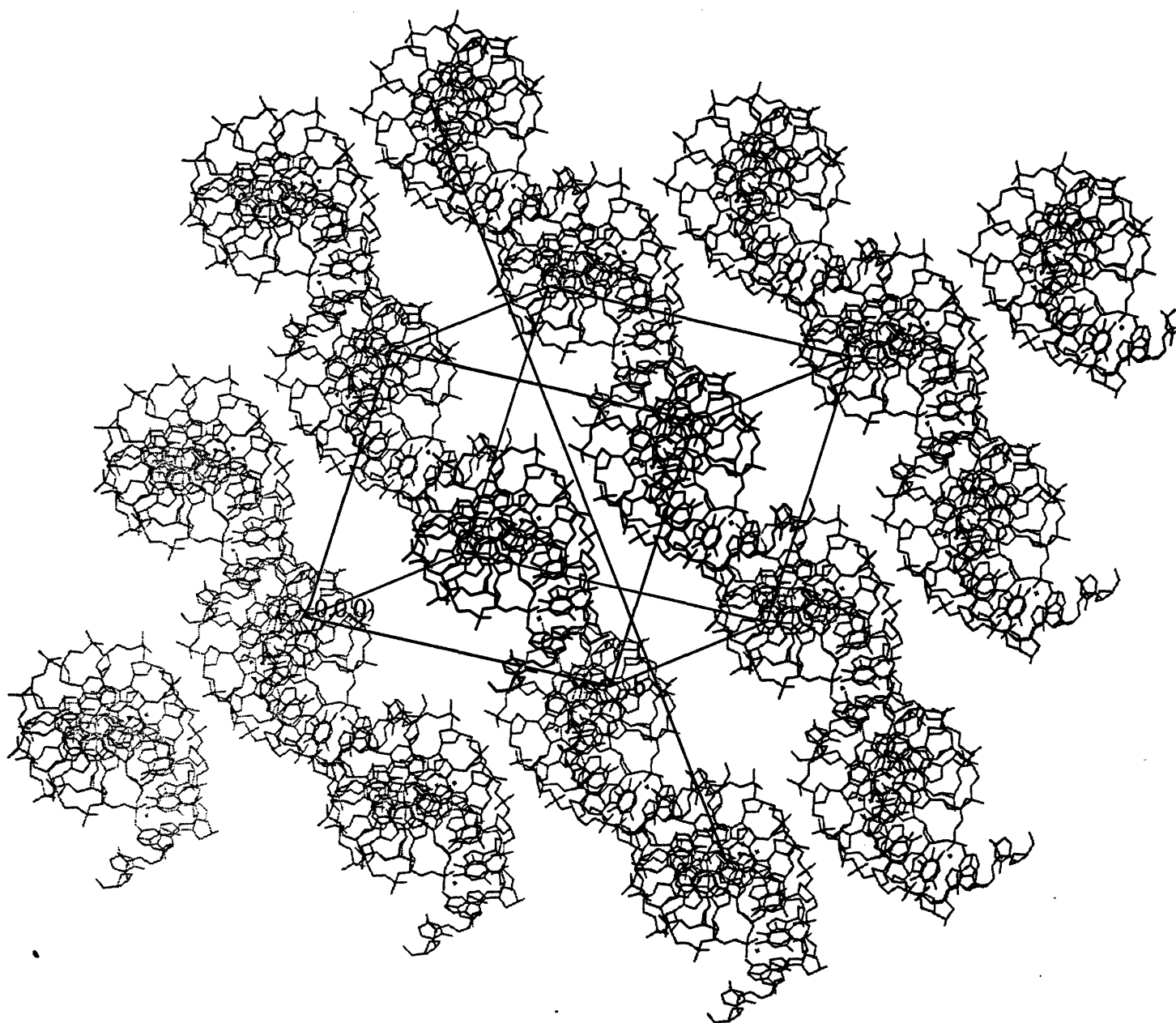
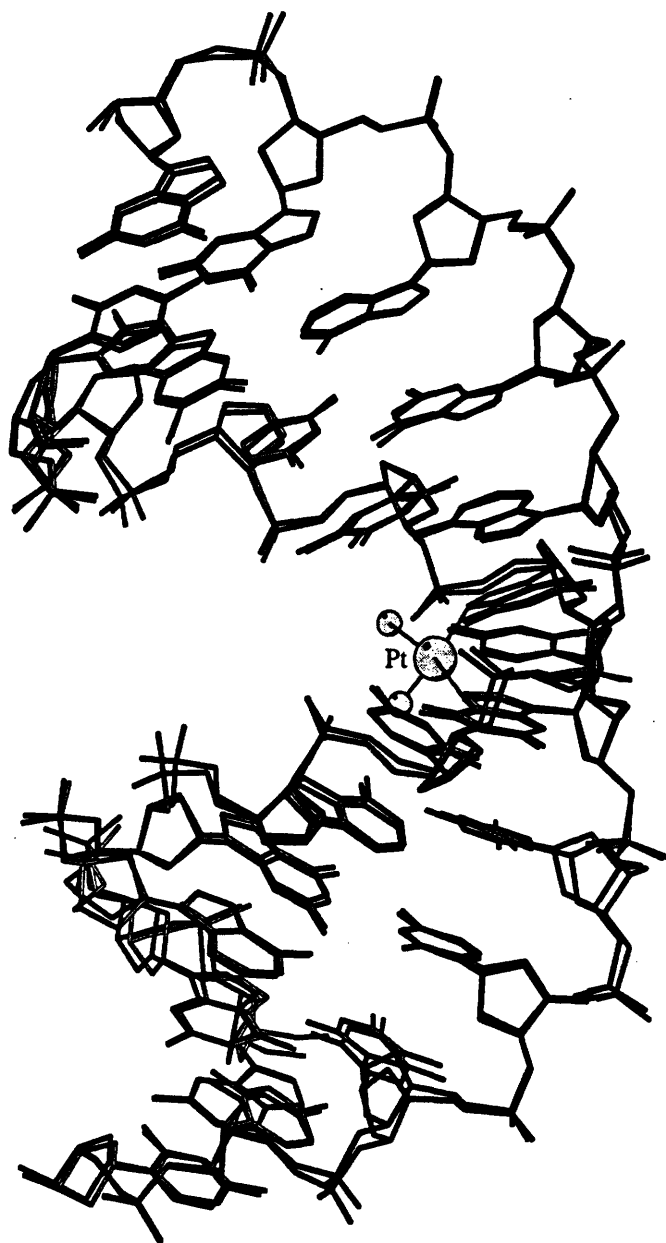


**Figure 29.** Superposition of molecules A and B. The rmsd is 0.38 Å for all atoms and 0.10 Å for the atoms in the base pairs at the site of platinum coordination.



## *Packing*

The two duplexes in the asymmetric unit pack in a novel manner. There are three types of contacts: end-to-end, end-to-groove, and backbone-to-backbone (Figure 30). These packing interactions combine to form an intricate network of DNA molecules containing large solvent channels (Figure 31). Large channels running through the crystal are 10 Å to 30 Å in diameter and reflect the high solvent content of the crystal. The crystals used in this study have a solvent content of ~60%, which was calculated by computing the volume of the DNA from a mask generated in the program O and then assuming that the rest of the unit cell was filled with solvent.

The platinated DNA duplexes in the crystal structure interact with each other through two types of hydrophobic packing contacts. In one such interaction, the 3' end of a duplex, comprising base pair C12-G13, stacks against the 3' end of another duplex such that a pseudo-continuous helix forms (Figure 32). This type of packing is often observed in crystals of B-DNA (Wang & Teng, 1987). The ends are held together by the hydrophobic stacking interaction of the terminal base pairs on each duplex, with 3' C12 base of one dodecamer stacking on the 5' G13 of another. Along with directly stacking on the C12-G13 base pair of an adjacent duplex, the terminal base pair is also positioned in space directly above the C11-G14 base pair of the next helix. This interaction can be seen when the stacking is viewed down the helix axis (Figure 30). If the two stacked helices are considered to be a pseudo-continuous segment of B-DNA, then at the base step contact between the C12-G13 terminal base pairs of adjacent helices, the DNA has a twist of  $-35^\circ$  and unwinds a full step before resuming normal helical twisting at the next base step. This unwinding is possible because the interaction between the



**Figure 30.** Packing diagram of cisplatin-modified DNA. There are two molecules in each unit cell. One is shown in dark gray and one in light gray.

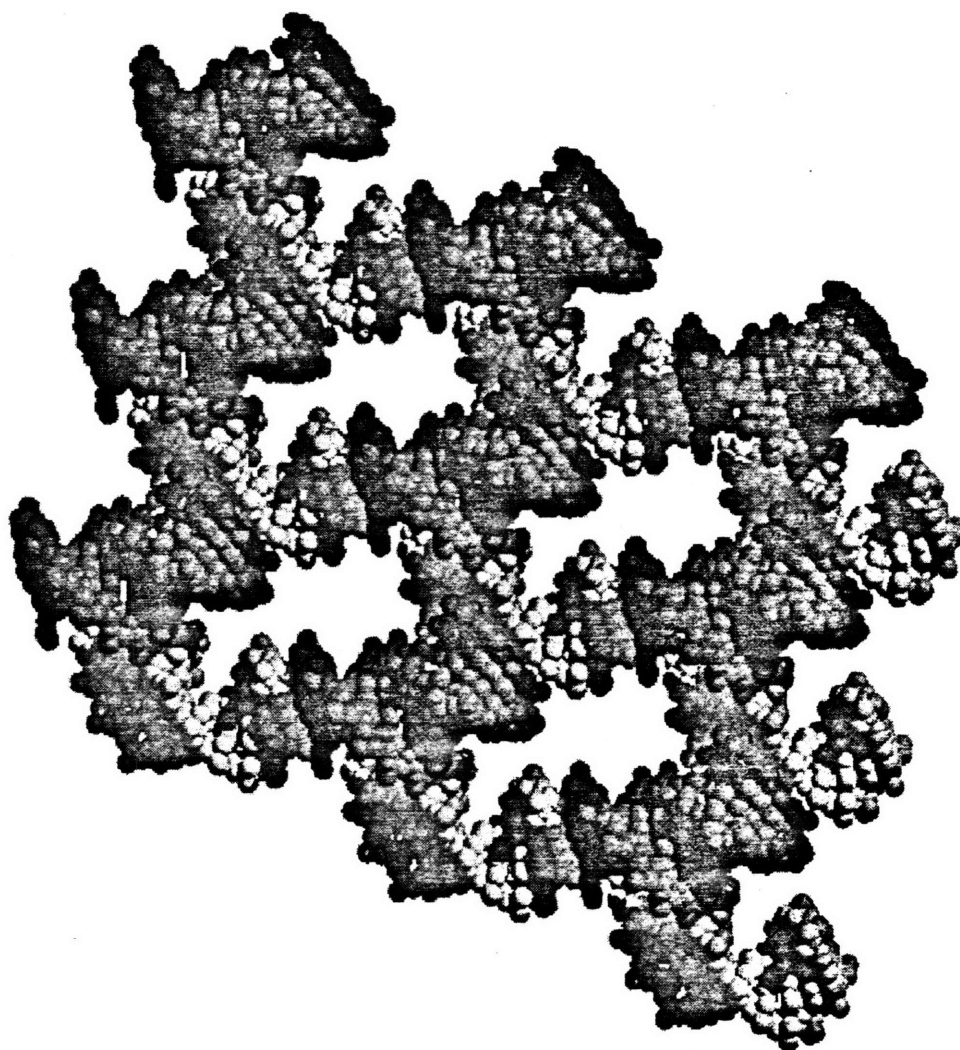


**Figure 31.** Packing diagrams showing the large solvent channels which run through the crystal of cisplatin-modified DNA.

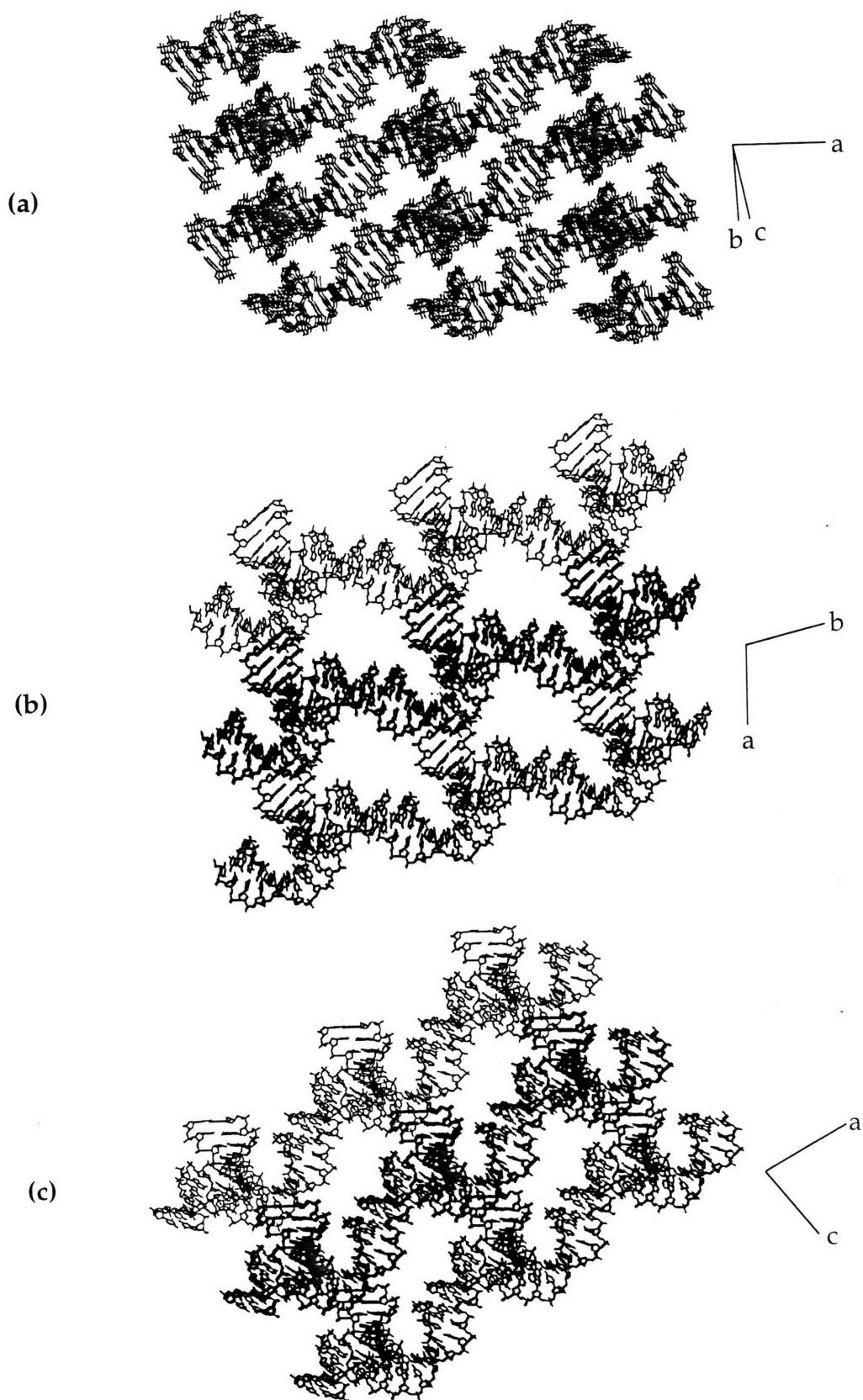
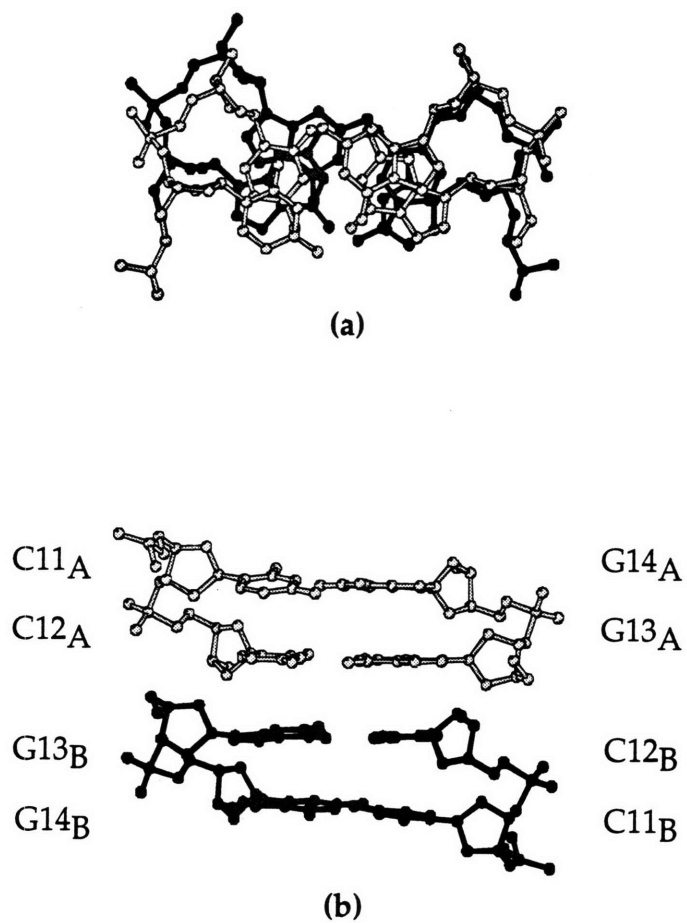


**Figure 32.** End-to-end packing interaction of molecule A (light) stacking on molecule B (dark). The interaction is depicted viewing down the helix axis (a) and perpendicular to the helix axis (b).



terminal C12-G13 base pairs of adjacent helices lacks the constraints of the sugar phosphate linkage that would be present in a segment of continuous DNA.

In the second type of hydrophobic packing interaction, the 5' terminal base pair, C1-G24, of each duplex abuts the minor groove of a neighboring helix (Figures 33 and 34), as often seen in crystals of A-DNA (Frederick et al., 1989; Wang et al., 1982). The end base pair of helix A packs against the hydrophobic surface of the sugar phosphate backbone on helix B (Figure 35 a,b). The C1 base of helix A stacks over the deoxyribose C3' atom of residue G7 on helix B, and G24 of helix A packs closely against the C1' region of the deoxyribose ring of T8 on helix B. This interaction is hydrophobic in nature although the overlap between the base and the ribose ring is less pronounced than the C1-G7 ribose interaction. A slightly different interaction takes place between the C1-G24 of helix B when it packs against the deoxyribose rings of G7 and T8 on helix A (Figure 35 c,d). In this case, the purine ring of helix B G24 packs directly against the sugar of T8 on helix A. As in the case of helix A packing against the minor groove of helix B, C1 of helix B packs against the deoxyribose ring of G7, but to a lesser extent. The end-groove interactions are also stabilized by hydrogen bonds between the terminal C1-G24 base pair and the G6-C19 base pair of the helix which accommodates its neighbor by opening and flattening its minor groove. The hydrogen bonding interactions are between the N2 of G24 and the O2 of C19 and the O2 of C1 and the N2 of G6 and their distances are (Figure 36).

The two duplexes in each unit cell also have very close contacts between their backbones (Figure 37 and Table 7). We ascribe this packing to C-H...O hydrogen bonding (Derewenda et al., 1995; Desiraju, 1991). Such hydrogen bonds have been postulated to play an important role in the

**Figure 33.** End-to-groove packing interaction: the end of molecule A (light) packing into the minor groove of molecule B (dark).

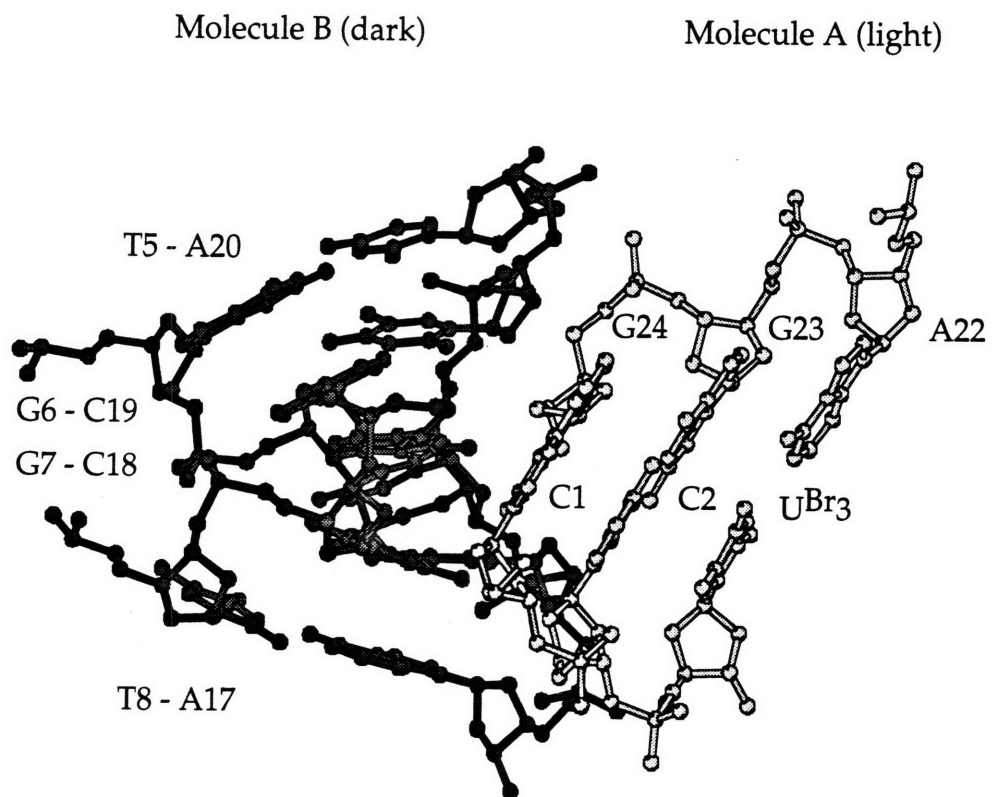


**Figure 34.** End-to-groove packing interaction: the end of molecule B (dark) packing into the minor groove of molecule A (light).

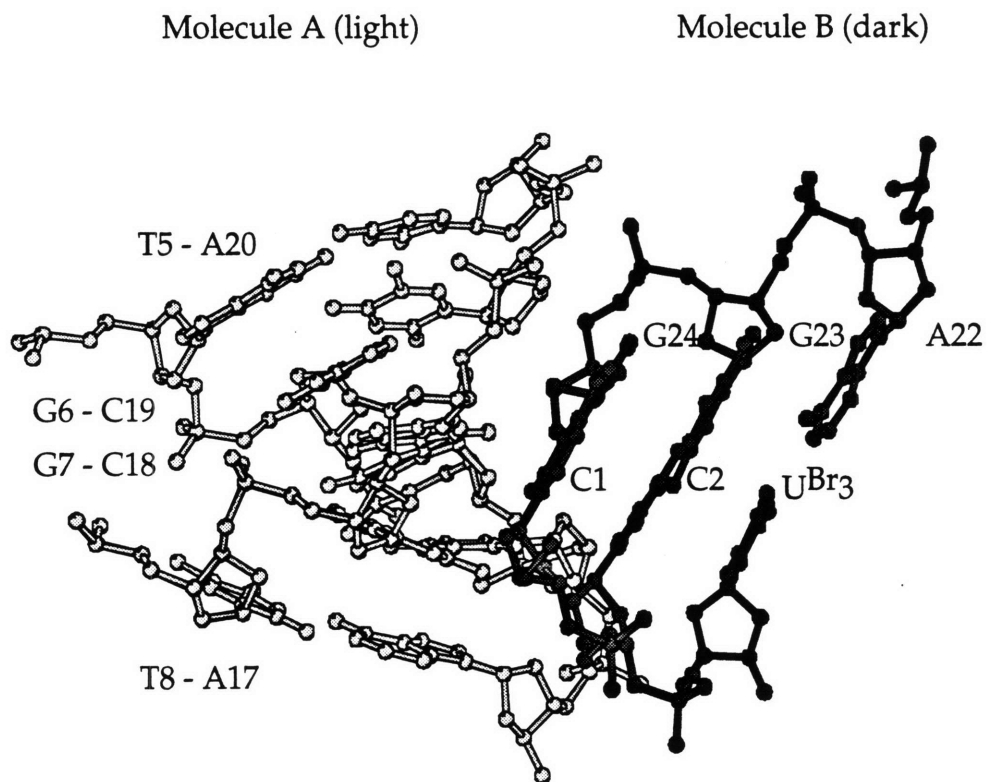


**Figure 35.** (a) The C1-G24 base pair of molecule A packing against the sugar-phosphate backbone of molecule B, and (b) a side view of the packing interaction. (c) The C1-G24 base pair of molecule B packing against the sugar phosphate backbone of molecule A, and (d) a side view of the interaction.

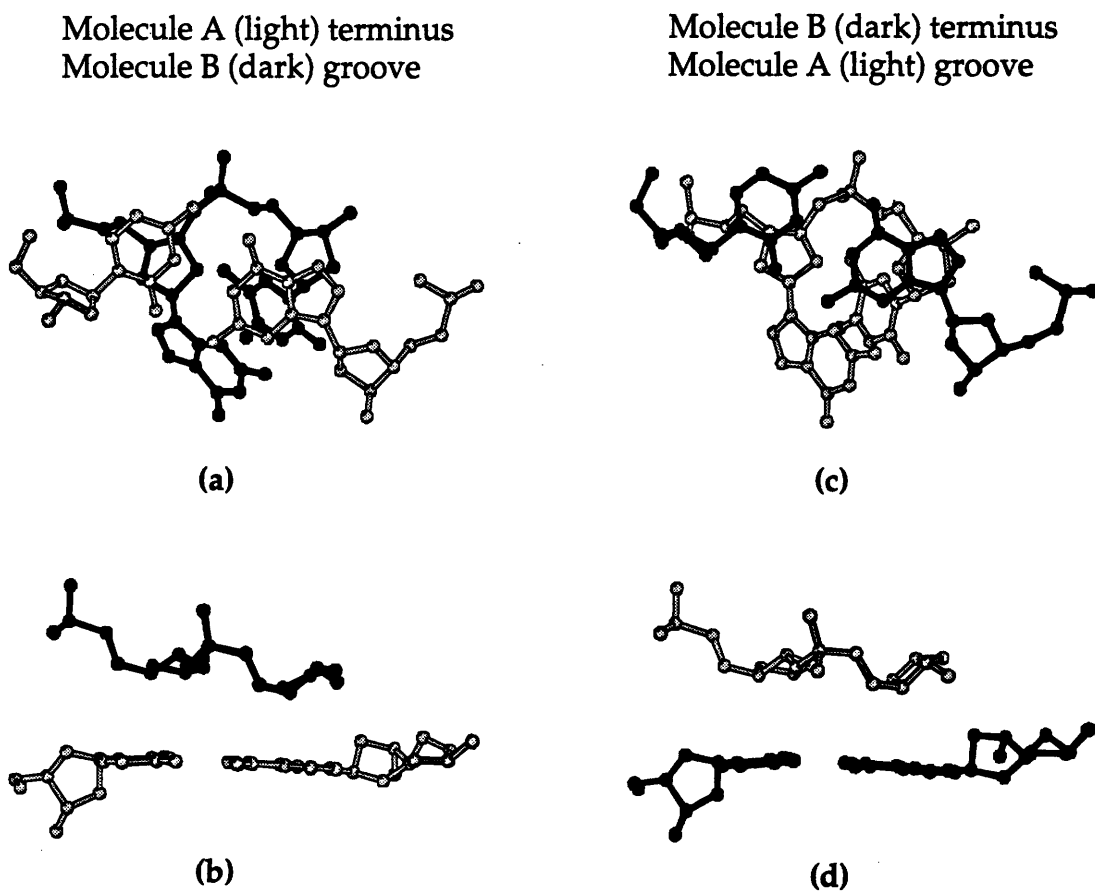
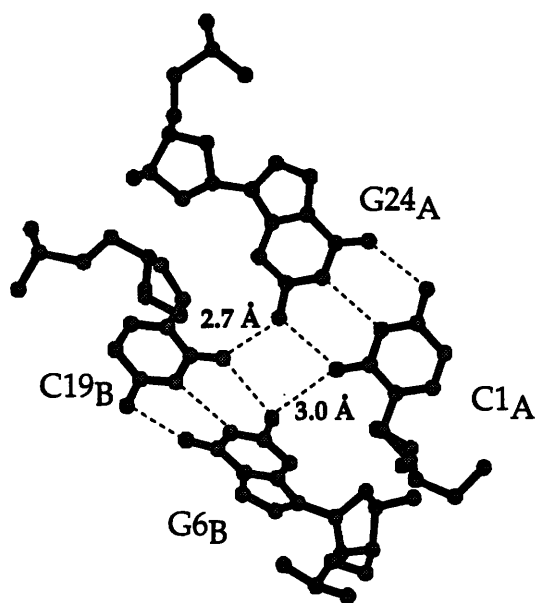
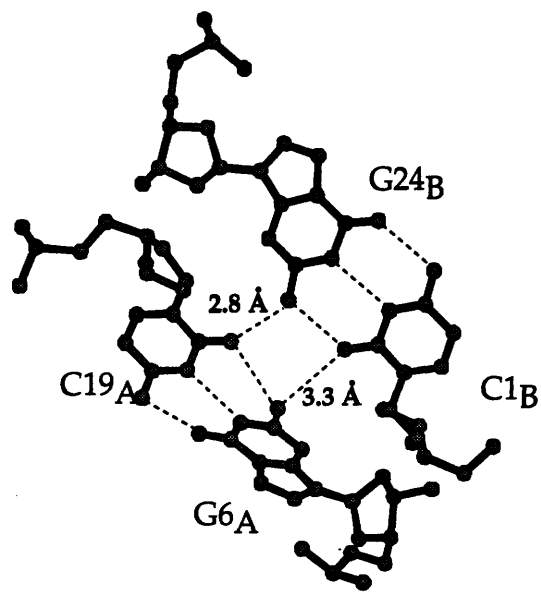


**Figure 36.** (a) The hydrogen bonding interactions between the C1-G24 base pair of molecule A and the G6-C19 base pair of molecule B. (b) The hydrogen bonding interactions between the C1-G24 base pair of molecule B and the G6-C19 base pair of molecule A.



(a)



(b)



**Figure 37.** Backbone-to-backbone packing interaction between molecule A and molecule B. The interactions are listed in Table 7 and show that molecules A and B are in slightly different packing environments and are crystallographically independent.

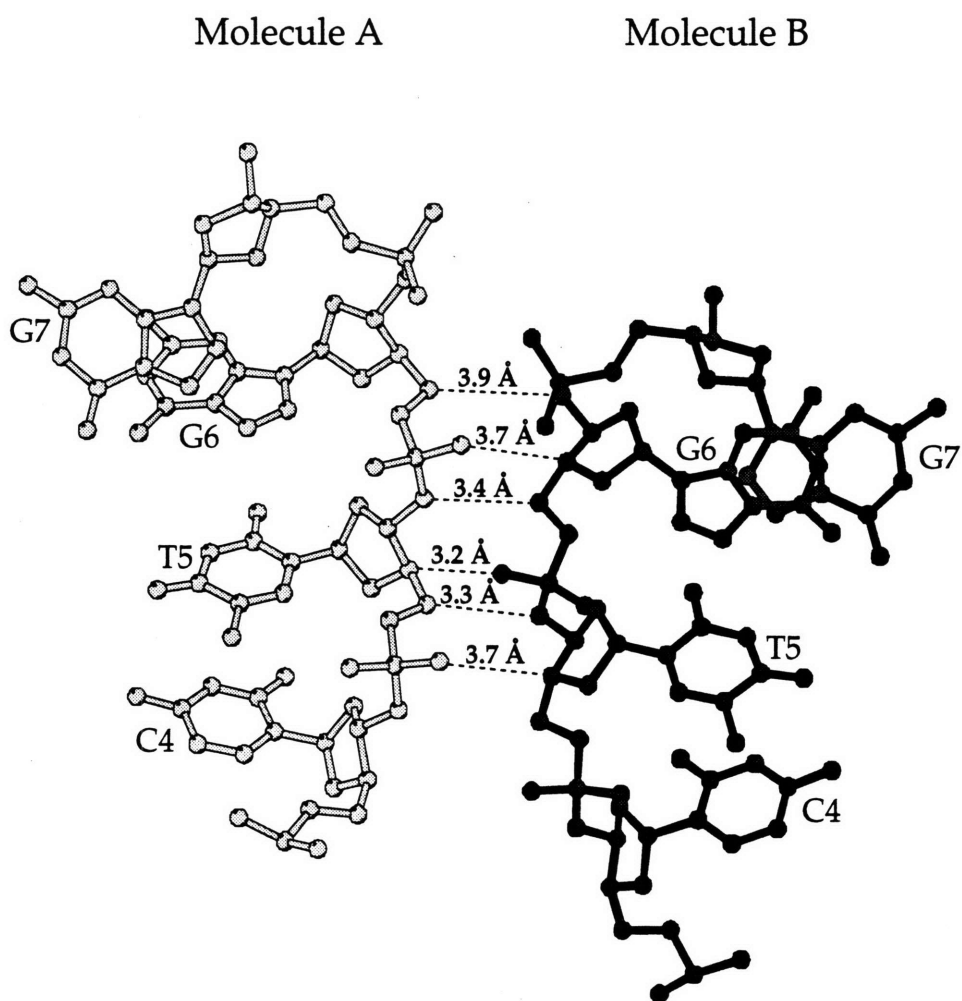


**Table 7.** Backbone-backbone packing contacts between molecules A and B.

<b>Donor</b>		<b>Acceptor</b>		<b>Distance (Å)</b>
T5 <sub>B</sub>	C4'	T5 <sub>A</sub>	O1P	3.7
T5 <sub>A</sub>	C5'	T5 <sub>B</sub>	O3'	3.3
T5 <sub>A</sub>	C4'	G6 <sub>B</sub>	O1P	3.4
G6 <sub>B</sub>	C5'	T5 <sub>A</sub>	O3'	3.2
G6 <sub>B</sub>	C4'	G6 <sub>A</sub>	O1P	3.7
G6 <sub>A</sub>	C5'	G6 <sub>B</sub>	O3'	3.9

stabilization of unusual DNA strand interactions such as A-T base pairs involving O2 of thymine and the C2-H of adenine (Leonard et al., 1995). In the present structure, a phosphate oxygen atom and C4'-H and O3' with C5'-H appear to stabilize the contacts between platinated DNA molecules. A search of the Nucleic Acid Database (H. Berman, personal communication) revealed that such contacts have been observed in other DNA structures, but they are isolated and not an extended series such as that found here.

The backbone contacts between helices A and B are listed in Table 7 and are not related by symmetry. For example the T5 C4'-H atom of molecule A forms a C-H...O hydrogen bond with a G6 OP of molecule B whereas the T5 C4'-H atom of molecule B interacts with the T5 OP atom of molecule A. Although the stacking of the 3' ends of neighboring helices appears to be identical for helices A and B, the backbones and end-groove packing clearly reveal that the contacts between the two molecules are not the same. This result further underscores that the two duplexes in each unit cell have slightly different packing environments and are crystallographically independent.

The solvent content of DNA crystals is generally very high, but most of the solvent is disordered and limits the resolution of the data (Drenth, 1994). Some ordered solvent molecules can be seen with diffraction to 2.6 Å resolution and 31 water molecules were found in this structure. The central four base pairs at the platination site of both molecules contained a high proportion of the ordered water molecules. Ten out of 18 waters associated with molecule A and 7 out of 13 waters associated with molecule B contact base pairs T5-A20 through T8-A17. The water molecules that were located are listed in Table 8 and their positions are shown schematically in Figure 38.

**Figure 38.** Schematic diagram of the water positions for (a) molecule A and (b) molecule B. The water molecules in the major groove are darkly shaded and the water molecules along the backbone or in the minor groove are lightly shaded. The atom contacts and distances are listed in Table 8.

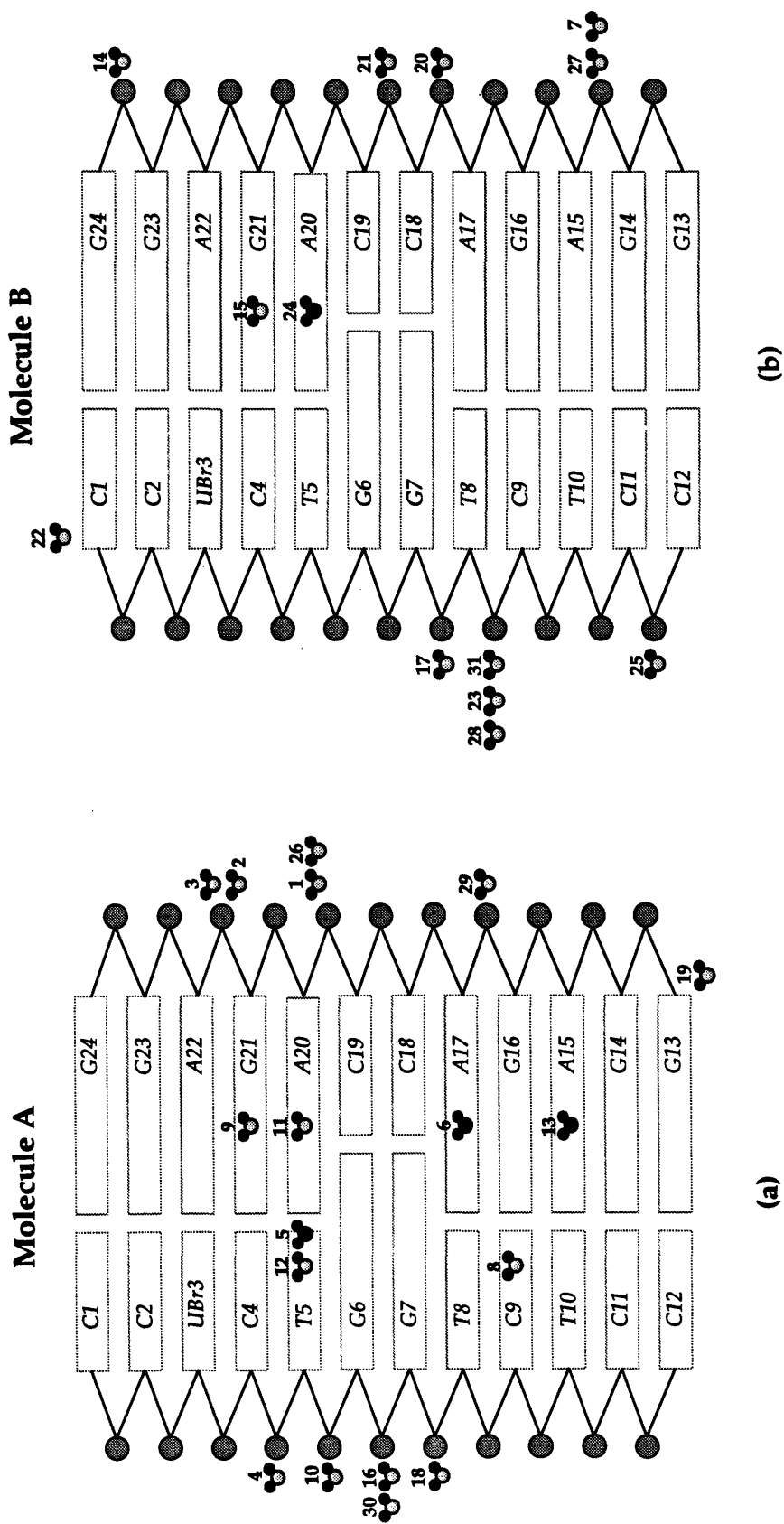


**Table 8.** Water contacts within the crystal structure of cisplatin-modified DNA. Water positions are shown schematically in Figure 37. The "residue number" for each water molecule corresponds to the numbering in the coordinate file deposited with the Protein Data Bank.

Water	Molecule	Residue	Atom	Distance (Å)
1	A	C19	O2P	2.6
	water	29	OH2	2.8
2	A	G21	O2P	3.2
3	A	G21	O1P	2.8
4	A	C4	O2P	2.6
5	A	T5	O4	2.9
6	A	A17	N7	2.7
7	water	27	OH2	3.1
8	A	C9	O2	2.8
9	A	G21	N2	3.0
10	A	T5	O2P	3.0
11	A	A20	N3	2.9
12	A	T5	O2	2.8
13	A	A15	N7	2.8
14	B	G23	O1P	2.7
15	B	G21	N2	3.1
16	A	G6	O2P	3.1
	water	30	OH2	2.6
17	B	G7	O1P	2.9
18	A	G7	O2P	3.2
	A	G6	O1P	2.7
19	A	G13	O5'	3.0
20	B	A17	O1P	2.6
21	B	C18	O2P	2.8
22	B	C1	O5'	2.9
23	water	31	OH2	2.9
24	B	A20	N7	2.7
25	B	C11	O2P	2.7
26	A	G16	O1P	3.0
27	B	G14	O1P	2.9
	water	7	OH2	2.7
28	B	T8	O2P	2.9
29	water	51	OH2	2.8
30	water	16	OH2	3.0
31	B	T8	O1P	3.1
	water	23	OH2	2.7

*The Platinated DNA Duplex*

The structures of the two crystallographically independent DNA duplexes modified by cisplatin are shown in Figure 24. The two molecules have the same general features. The 5' end of each helix is A-like and the 3' end is B-like, judging by nearest-neighbor phosphate-phosphate contacts, backbone torsion angles, and base step stacking patterns. This heterogeneity is especially clear when the helix is viewed down either end and compared to similar views of A-DNA and B-DNA (Figure 39). The entire minor groove of each duplex, however, is quite wide and bears a general resemblance to A-DNA (Figure 22). We ascribe these features to distortion of the double helix at the site of platinum coordination. Small but significant differences between the two crystallographically independent molecules are revealed by evaluation of detailed structural parameters.

Helical base-base and base-step parameters are used to describe the details of nucleic acid structures and are defined according to the EMBO Workshop on DNA Curvature and Bending (Dickerson, 1989). Base pair parameters (Figure 40) from the program CURVES (Lavery & Sklenar, 1988; Lavery & Sklenar, 1989) are calculated with respect to a global helix axis and reveal how individual base pairs shear, open, stretch, stagger, propeller twist, and buckle in order to maximize stacking interactions and Watson-Crick base pairing. The global helix axis used by CURVES is bent and is the best long-range axis for the DNA duplex under investigation. Base step parameters (Figure 41) from the program CURVES (Lavery & Sklenar, 1988; Lavery & Sklenar, 1989) are calculated for each base pair step with respect to a local helix axis and illustrate how the bases move with respect to one another

**Figure 39.** Views of the (a) B-like and (b) A-like ends of cisplatin-modified DNA. Similar views of canonical (c) B- and (d) A-DNA are included for comparison.

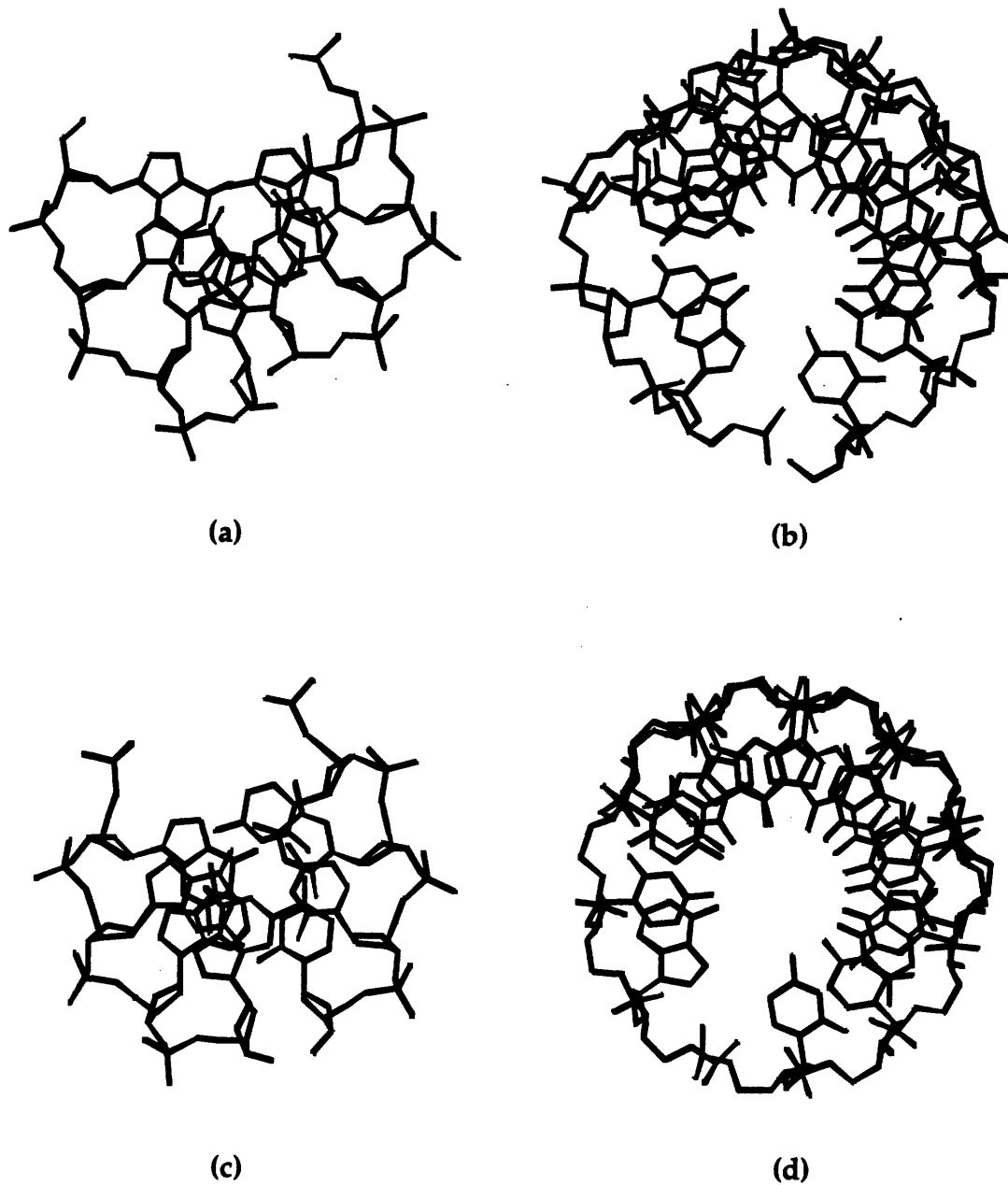


**Figure 40.** Base pair parameters for nucleic acids. The coordinate frame is shown at the top of the figure.

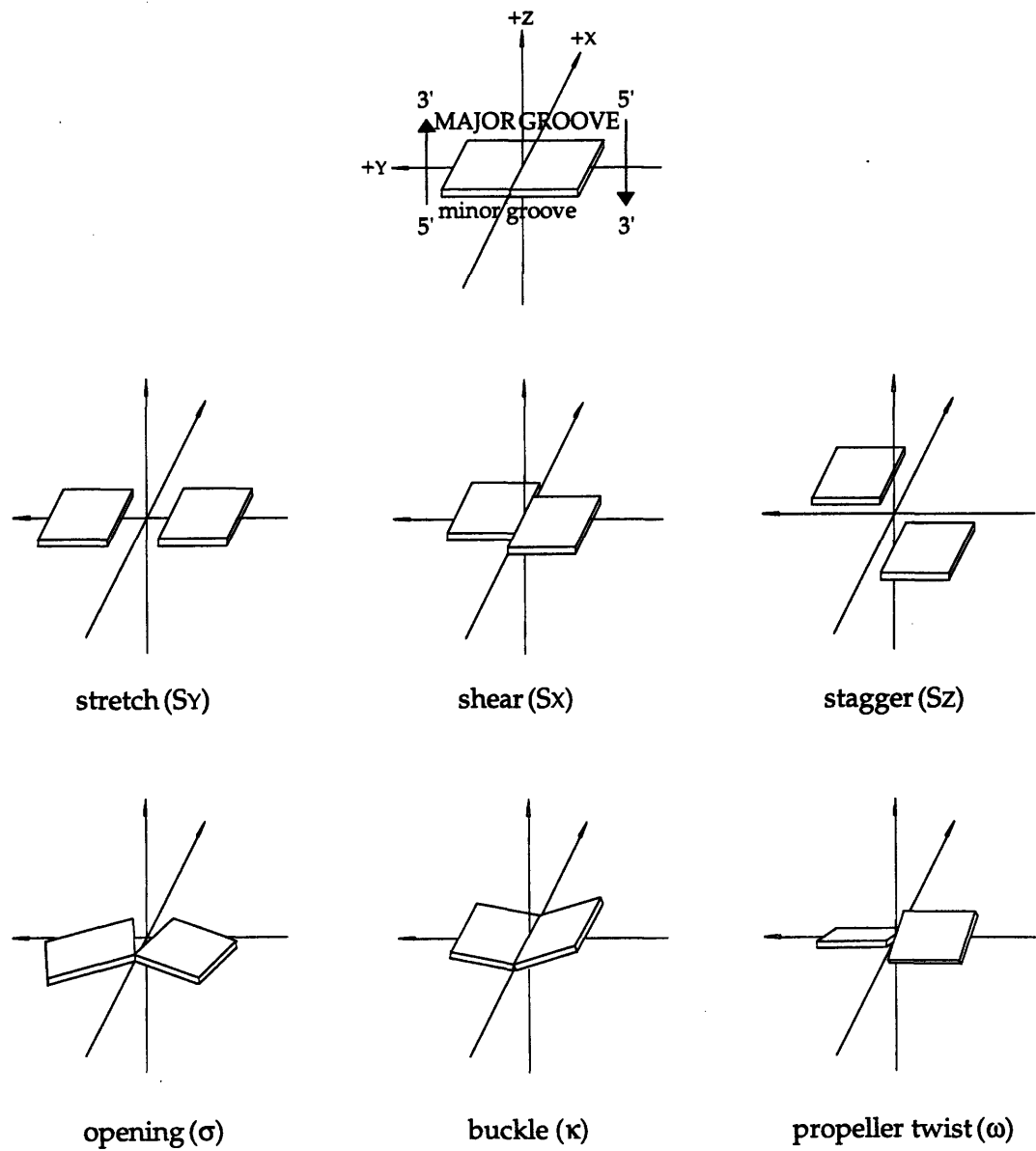




**Figure 41.** Base step parameters for nucleic acids. The coordinate frame is shown at the top of the figure.

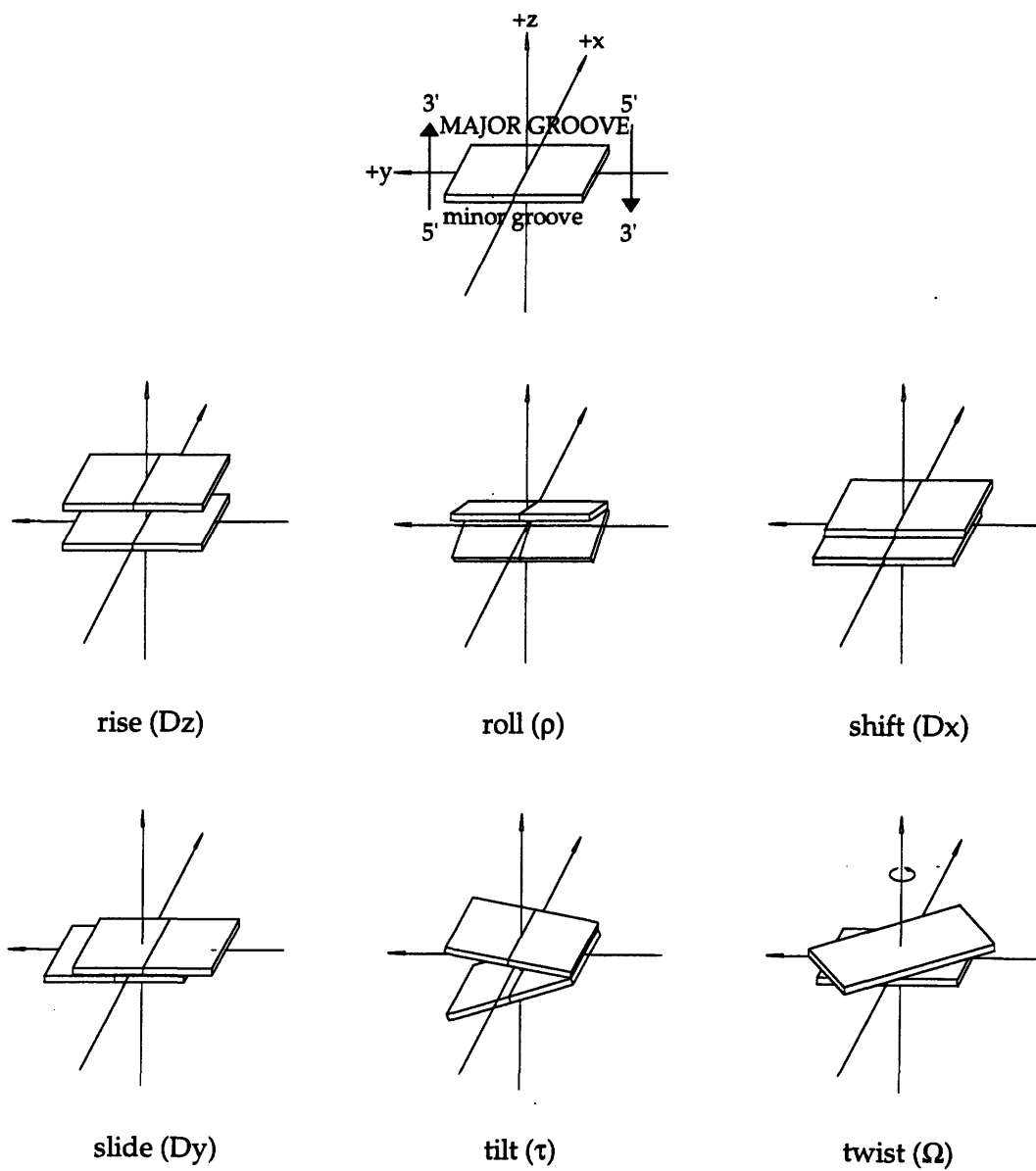


**Table 9.** Base pair parameters calculated by using the program CURVES and are defined according to the Cambridge convention (Dickerson, 1989). Signs agree with the coordinate system used in Figures 40 and 41.

Buckle ( $\kappa$ )				
Base pair	Molecule A	Molecule B	A-form DNA	B-form DNA
C1-G24	5.98	8.61	0.00	0.00
C2-G23	3.86	-2.48	0.00	0.00
U(Br)3-A22	4.56	4.32	0.00	0.00
C4-G21	-1.42	-1.76	0.00	0.00
T5-A20	4.66	6.01	0.00	0.00
G6-C19	13.07	12.96	0.00	0.00
G7-C18	0.52	-1.46	0.00	0.00
T8-A17	9.92	-5.00	0.00	0.00
C9-G16	-15.54	-14.16	0.00	0.00
T10-A15	0.01	5.87	0.00	0.00
C11-G14	4.78	2.77	0.00	0.00
C12-G13	-0.53	-2.39	0.00	0.00
Opening ( $\sigma$ )				
Base pair	Molecule A	Molecule B	A-form DNA	B-form DNA
C1-G24	-3.76	-1.01	-0.85	-0.38
C2-G23	-1.31	0.59	-0.85	-0.38
U(Br)3-A22	-1.65	1.48	-0.85	-0.38
C4-G21	6.24	5.73	-0.85	-0.38
T5-A20	8.60	2.65	-0.85	-0.38
G6-C19	-2.57	-1.49	-0.85	-0.38
G7-C18	2.00	4.74	-0.85	-0.38
T8-A17	27.71	7.82	-0.85	-0.38
C9-G16	10.21	3.48	-0.85	-0.38
T10-A15	10.13	8.59	-0.85	-0.38
C11-G14	-3.95	-0.52	-0.85	-0.38
C12-G13	-1.69	1.49	-0.85	-0.38
Propeller ( $\omega$ )				
Base pair	Molecule A	Molecule B	A-form DNA	B-form DNA
C1-G24	-5.96	-2.83	11.44	-1.29
C2-G23	-5.40	-8.15	11.44	-1.29
U(Br)3-A22	-8.78	-9.94	11.44	-1.29
C4-G21	-11.22	-10.02	11.44	-1.29
T5-A20	-7.29	-8.90	11.44	-1.29
G6-C19	-22.41	-15.66	11.44	-1.29
G7-C18	-13.52	-18.67	11.44	-1.29
T8-A17	-40.49	-33.27	11.44	-1.29
C9-G16	-14.70	-12.31	11.44	-1.29
T10-A15	-8.34	-15.90	11.44	-1.29
C11-G14	-13.48	-8.13	11.44	-1.29
C12-G13	1.31	-3.97	11.44	-1.29

**Table 9.** (continued)

<b>Shear (Sx)</b>				
Base pair	Molecule A	Molecule B	A-form DNA	B-form DNA
C1-G24	0.43	0.51	0.00	0.00
C2-G23	0.00	0.24	0.00	0.00
U(Br)3-A22	-0.53	-0.48	0.00	0.00
C4-G21	0.42	-0.10	0.00	0.00
T5-A20	0.91	0.42	0.00	0.00
G6-C19	0.47	-0.11	0.00	0.00
G7-C18	-0.61	-0.29	0.00	0.00
T8-A17	2.39	0.49	0.00	0.00
C9-G16	-0.92	-0.09	0.00	0.00
T10-A15	-0.36	0.39	0.00	0.00
C11-G14	0.39	0.51	0.00	0.00
C12-G13	0.40	0.37	0.00	0.00
<b>Stagger (Sz)</b>				
Base pair	Molecule A	Molecule B	A-form DNA	B-form DNA
C1-G24	-0.25	-0.51	0.15	-0.02
C2-G23	-0.12	-0.04	0.15	-0.02
U(Br)3-A22	-0.12	-0.31	0.15	-0.02
C4-G21	0.04	-0.05	0.15	-0.02
T5-A20	-0.05	0.01	0.15	-0.02
G6-C19	0.07	0.16	0.15	-0.02
G7-C18	0.26	0.15	0.15	-0.02
T8-A17	-0.51	0.20	0.15	-0.02
C9-G16	0.44	0.14	0.15	-0.02
T10-A15	0.03	-0.50	0.15	-0.02
C11-G14	-0.54	-0.12	0.15	-0.02
C12-G13	-0.31	-0.53	0.15	-0.02
<b>Stretch (Sy)</b>				
Base pair	Molecule A	Molecule B	A-form DNA	B-form DNA
C1-G24	-0.47	-0.30	-0.11	0.01
C2-G23	-0.33	-0.16	-0.11	0.01
U(Br)3-A22	-0.44	-0.16	-0.11	0.01
C4-G21	0.09	0.27	-0.11	0.01
T5-A20	0.11	-0.05	-0.11	0.01
G6-C19	-0.23	-0.40	-0.11	0.01
G7-C18	-0.20	-0.01	-0.11	0.01
T8-A17	0.80	0.69	-0.11	0.01
C9-G16	0.20	-0.07	-0.11	0.01
T10-A15	0.17	0.76	-0.11	0.01
C11-G14	-0.33	-0.14	-0.11	0.01
C12-G13	-0.22	-0.01	-0.11	0.01

**Table 10.** Base step parameters calculated by using the program CURVES and are defined according to the Cambridge convention (Dickerson, 1989). Signs agree with the coordinate system used in Figures 40 and 41.

Rise (Dz)				
Base pair step	Molecule A	Molecule B	A-form DNA	B-form DNA
C1-G24/C2-G23	3.58	3.75	3.18	3.34
C2-G23/U(Br)3-A22	3.38	3.22	3.18	3.34
U(Br)3-A22/C4-G21	3.63	3.58	3.18	3.34
C4-G21/T5-A20	3.26	3.25	3.18	3.34
T5-A20/G6-C19	3.26	3.40	3.18	3.34
G6-C19/G7-C18	3.69	3.63	3.18	3.34
G7-C18/T8-A17	3.45	3.43	3.18	3.34
T8-A17/C9-G16	3.76	3.53	3.18	3.34
C9-G16/T10-A15	3.02	2.97	3.18	3.34
T10-A15/C11-G14	3.16	3.46	3.18	3.34
C11-G14/C12-G13	3.57	3.38	3.18	3.34
Roll ( $\rho$ )				
Base pair step	Molecule A	Molecule B	A-form DNA	B-form DNA
C1-G24/C2-G23	-0.62	2.57	10.78	-2.80
C2-G23/U(Br)3-A22	6.08	6.80	10.78	-2.80
U(Br)3-A22/C4-G21	6.14	7.14	10.78	-2.80
C4-G21/T5-A20	2.08	3.60	10.78	-2.80
T5-A20/G6-C19	12.21	5.63	10.78	-2.80
G6-C19/G7-C18	25.17	26.94	10.78	-2.80
G7-C18/T8-A17	0.66	4.06	10.78	-2.80
T8-A17/C9-G16	3.08	-0.66	10.78	-2.80
C9-G16/T10-A15	8.33	11.66	10.78	-2.80
T10-A15/C11-G14	7.44	4.81	10.78	-2.80
C11-G14/C12-G13	4.08	5.28	10.78	-2.80
Shift (Dx)				
Base pair step	Molecule A	Molecule B	A-form DNA	B-form DNA
C1-G24/C2-G23	-0.54	-0.65	0.00	0.00
C2-G23/U(Br)3-A22	-0.47	-0.45	0.00	0.00
U(Br)3-A22/C4-G21	0.75	0.63	0.00	0.00
C4-G21/T5-A20	0.18	-0.02	0.00	0.00
T5-A20/G6-C19	-1.67	-1.08	0.00	0.00
G6-C19/G7-C18	1.37	1.66	0.00	0.00
G7-C18/T8-A17	0.61	-0.41	0.00	0.00
T8-A17/C9-G16	-0.86	0.49	0.00	0.00
C9-G16/T10-A15	-0.01	-0.10	0.00	0.00
T10-A15/C11-G14	-0.26	-0.27	0.00	0.00
C11-G14/C12-G13	0.26	0.44	0.00	0.00

**Table 10.** (continued)

## Slide (Dy)

Base pair step	Molecule A	Molecule B	A-form DNA	B-form DNA
C1-G24/C2-G23	-2.42	-2.37	-2.08	-0.62
C2-G23/U(Br)3-A22	-2.44	-2.34	-2.08	-0.62
U(Br)3-A22/C4-G21	-1.97	-1.97	-2.08	-0.62
C4-G21/T5-A20	-1.81	-1.79	-2.08	-0.62
T5-A20/G6-C19	-1.56	-1.81	-2.08	-0.62
G6-C19/G7-C18	-2.35	-2.34	-2.08	-0.62
G7-C18/T8-A17	-0.24	-1.45	-2.08	-0.62
T8-A17/C9-G16	-0.85	-0.94	-2.08	-0.62
C9-G16/T10-A15	-0.33	-0.13	-2.08	-0.62
T10-A15/C11-G14	-0.51	-0.50	-2.08	-0.62
C11-G14/C12-G13	-0.67	-0.55	-2.08	-0.62

Tilt ( $\tau$ )

Base pair step	Molecule A	Molecule B	A-form DNA	B-form DNA
C1-G24/C2-G23	-4.69	-4.38	0.00	0.00
C2-G23/U(Br)3-A22	-0.60	1.38	0.00	0.00
U(Br)3-A22/C4-G21	-0.26	-0.87	0.00	0.00
C4-G21/T5-A20	1.78	-0.20	0.00	0.00
T5-A20/G6-C19	-2.45	-3.00	0.00	0.00
G6-C19/G7-C18	1.30	3.69	0.00	0.00
G7-C18/T8-A17	9.33	2.89	0.00	0.00
T8-A17/C9-G16	-1.41	4.57	0.00	0.00
C9-G16/T10-A15	3.76	9.18	0.00	0.00
T10-A15/C11-G14	3.45	-3.88	0.00	0.00
C11-G14/C12-G13	1.63	6.05	0.00	0.00

Twist ( $\Omega$ )

Base pair step	Molecule A	Molecule B	A-form DNA	B-form DNA
C1-G24/C2-G23	25.80	26.13	30.95	35.88
C2-G23/U(Br)3-A22	29.55	29.22	30.95	35.88
U(Br)3-A22/C4-G21	36.14	29.80	30.95	35.88
C4-G21/T5-A20	30.89	34.51	30.95	35.88
T5-A20/G6-C19	27.57	24.62	30.95	35.88
G6-C19/G7-C18	24.22	29.98	30.95	35.88
G7-C18/T8-A17	51.29	39.10	30.95	35.88
T8-A17/C9-G16	23.45	34.69	30.95	35.88
C9-G16/T10-A15	29.93	30.96	30.95	35.88
T10-A15/C11-G14	39.54	35.40	30.95	35.88
C11-G14/C12-G13	34.71	36.73	30.95	35.88

**Figure 42.** Graphical representations of the base pair parameters (Table 9) for molecules A and B. Data for canonical A- and B-DNA are included for comparison.

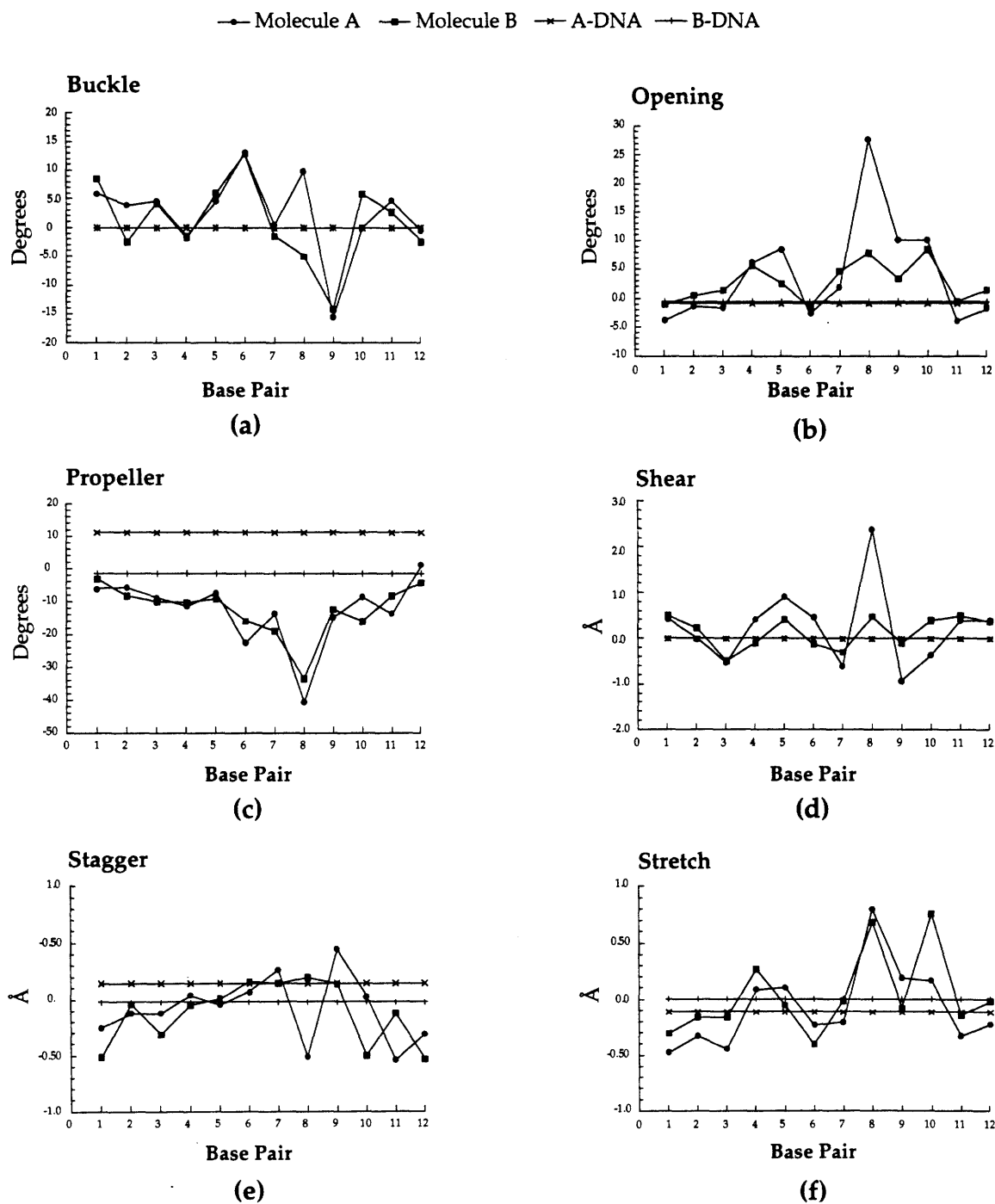
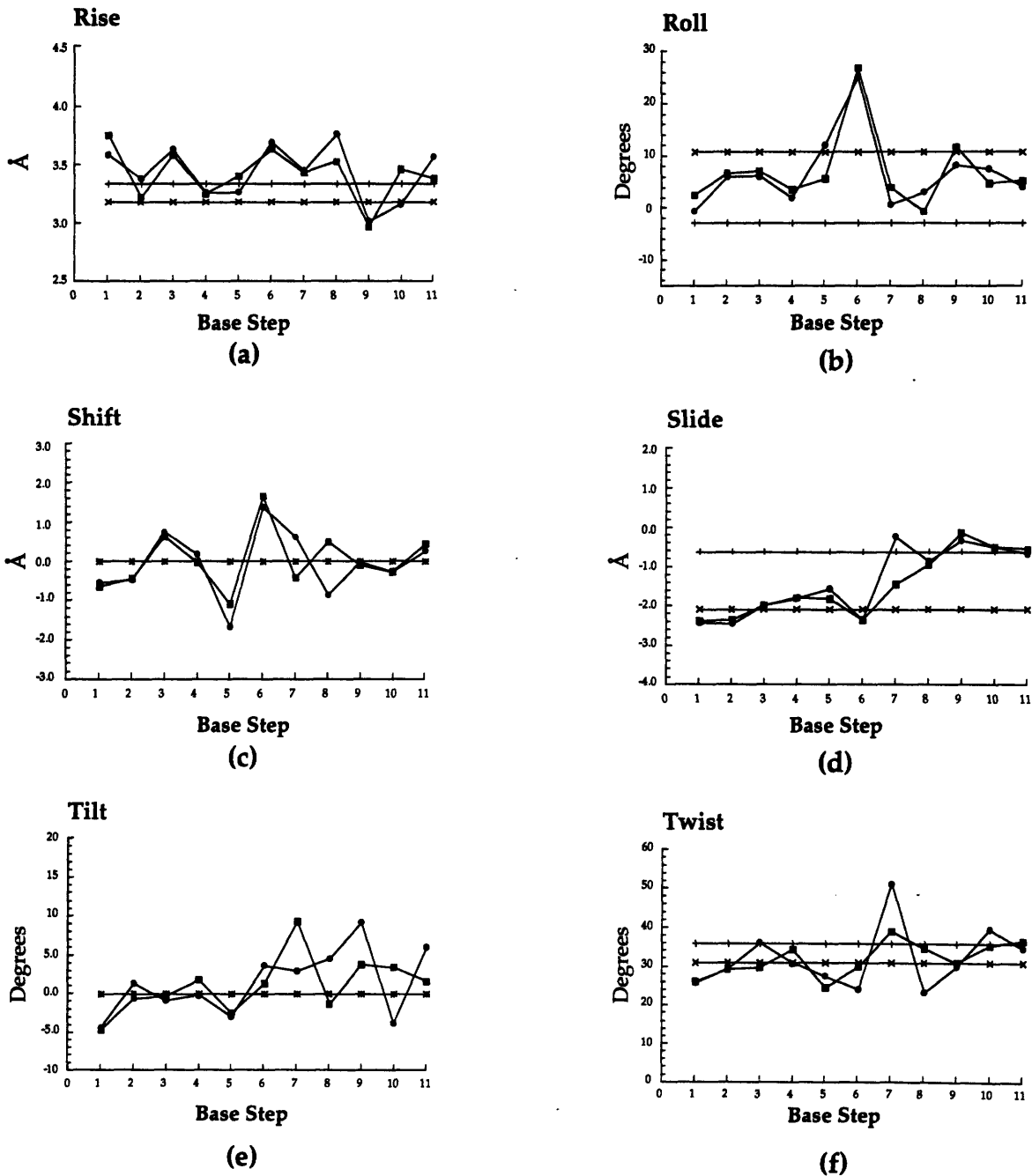


**Figure 43.** Graphical representations of the base step parameters (Table 10) for molecules A and B. Data for canonical A- and B-DNA are included for comparison.

—●— Molecule A    —■— Molecule B    —×— A-DNA    —+— B-DNA



in order to facilitate stacking interactions. These parameters reveal how a segment of DNA flexes to maintain optimal stacking for the double helix and are termed shift, slide, rise, tilt, roll, and twist. Parameters for the cisplatin-modified duplex are given and are compared to those of canonical A- and B-DNA in Tables 9 and 10 and Figures 42 and 43.

The sugar-phosphate backbone structure of a DNA oligonucleotide is described by a series of torsion angles (Figure 21). In electron density maps of a crystal structure at 2.6 Å resolution, individual atoms in the backbone cannot be resolved and many aspects of the structure must be inferred from distances between phosphate groups. The distances between phosphorus atoms along the backbone and across the grooves are known quite precisely for the two independent molecules in the present structure. These values are the same within experimental error and are shown schematically in Figure 44. Groove widths and backbone distances are shown graphically in Figure 45. The major groove is less well determined because there are few distances with which to characterize it, however.

#### *Structure of Molecule A*

The first four base steps of helix A comprise base pairs C1-G24 through T5-A18 (Figure 24). This segment of the helix has an overall resemblance canonical A-DNA. The A-like classification of this section of the helix is based on deoxyribose ring conformations and the twists of the base steps. All sugar puckers are C3'-endo or C4'-exo, a conformation very close to that of A-DNA. At 2.6 Å resolution, the conformation of the sugar rings cannot be seen in electron density maps but must be inferred from the distances between adjacent phosphate groups. The phosphate-phosphate distance is about 5.6 Å

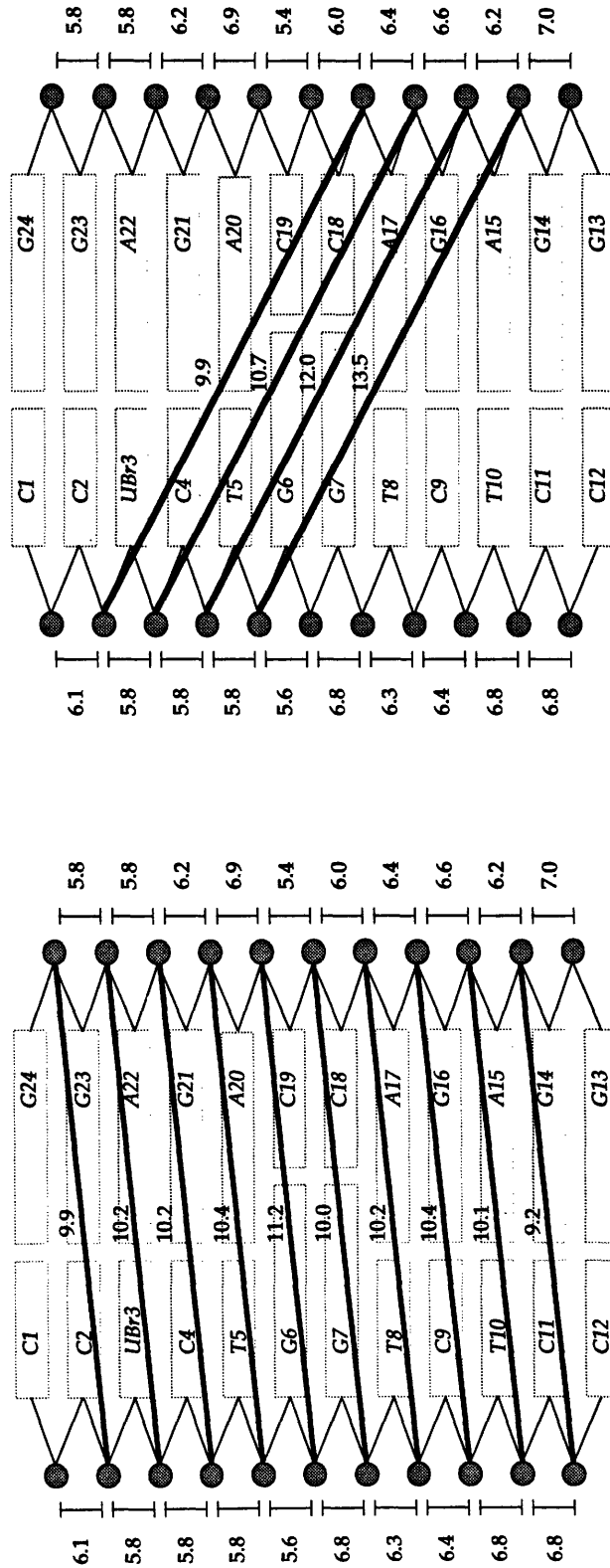


for a C3'-endo (A-DNA) sugar pucker and 6.5 Å for a C2'-endo (B-DNA) sugar pucker. Phosphate distances along the double helix backbone are shown schematically in Figure 44 and graphically in Figure 45. Base pair parameters and base step parameters are presented in Figures 42 and 43, respectively, and backbone torsion angles are listed in Table 11.

Base step stacking interactions are another feature of DNA which can be used to classify the double helix as A-form or B-form. Examples of canonical A-DNA and B-DNA stacking patterns are shown in Figure 46 and the base step stacking interactions for helix A are presented in parts a and b of Figures 47-57. The stacking of the first two base steps (Figures 47 and 48) resembles typical A-DNA stacking; purine-purine sequences have the 5 membered ring of one purine positioned over the 6 membered ring of the next. Base steps 3 and 4 (Figures 49 and 50) are A-like in terms of their ring conformations fall between A-DNA and B-DNA in their stacking interactions. In comparison to base steps 1 and 2, base steps 3 and 4 have slightly more pyrimidine ring overlap and less overlap between the five membered ring of one purine base and the six membered ring of the next in the sequence.

The fifth base step (Figure 51), which occurs between base pairs T5-A20 and G6-C19, is distorted because the N7 atom of G6 is coordinated to the platinum atom. Platinum coordination causes a -1.7 Å shift at this base step and moves base pair G6-C19 toward the major groove. The shift positions A20 to span base pair G6-C19, which has a +13° buckle (Table 9). The position of A20 and the non-planarity of base pair G6-C19 allows stacking to be maintained between base pairs five and six despite the platinum lesion. T5 of base pair five is pushed out into the major groove and does not participate in stacking with base pair G6-C19, but stacking of T5 with base pair C4-G21 and

Figure 44. (a) Schematic diagram of phosphorus atom distances ( $\text{\AA}$ ) along the backbone of cisplatin-modified DNA and phosphate-phosphate distances ( $\text{\AA}$ ) showing the width of the minor groove of cisplatin-modified DNA. (b) The phosphate-phosphate distances across the major groove of cisplatin-modified DNA. The phosphate-phosphate distances across the grooves of the helix are the distances between the phosphorus atoms minus  $5.8 \text{ \AA}$  for the van der Waals diameter of a phosphate group.



(a)

(b)



**Table 11a.** Pseudorotation angles, sugar puckers, and torsion angles for molecule A.  
 Torsion angles are defined as Phos- $\alpha$ -O5'- $\beta$ -C5'- $\gamma$ -C4'- $\delta$ -C3'- $\epsilon$ -O3'- $\zeta$ -Phos.  
 $\chi$  is the glycosyl torsion angle and P is the pseudorotation angle (Figure 21).

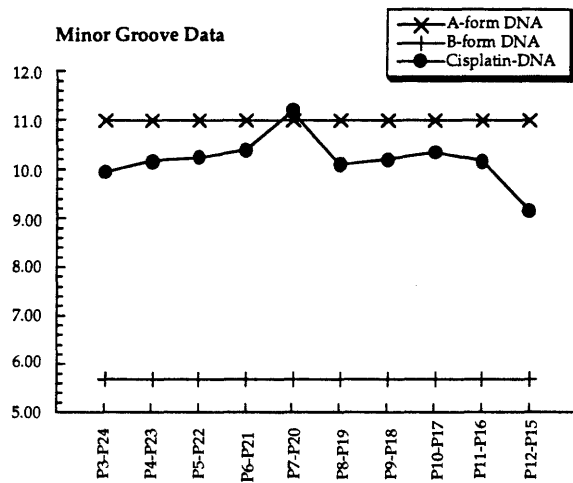
base	P	pucker	$\alpha$	$\beta$	$\gamma$	$\delta$	$\epsilon$	$\zeta$	$\chi$
CYT 1	31	C3'-endo	-71	172	.....	85	-164	-73	-164
CYT 2	20	C3'-endo	-85	179	59	84	-161	-67	-168
UBR 3	24	C3'-endo	-73	174	55	76	-168	-63	-161
CYT 4	19	C3'-endo	-62	162	61	83	-153	-77	-163
THY 5	15	C3'-endo	-69	-178	57	78	-169	-85	-155
GUA 6*	4	C3'-endo	-75	165	46	91	-149	-54	-144
GUA 7*	61	C4'-exo	-73	154	75	84	-164	-80	-167
THY 8	10	C3'-endo	-77	169	65	89	-165	-81	-135
CYT 9	26	C3'-endo	-66	177	64	90	-168	-68	-154
THY 10	162	C2'-endo	-68	178	65	136	-170	-94	-118
CYT 11	149	C2'-endo	-74	-179	55	134	-177	-97	-104
CYT 12	154	C2'-endo	.....	.....	59	144	.....	.....	-108
GUA 24	178	C2'-endo	.....	.....	-151	159	.....	.....	-164
GUA 23	27	C3'-endo	126	-107	55	79	-166	-116	-163
ADE 22	21	C3'-endo	-75	179	59	83	-156	-69	-165
GUA 21	18	C3'-endo	-80	179	66	81	-155	-68	-167
ADE 20	18	C3'-endo	-69	160	164	87	-155	-76	-165
CYT 19	24	C3'-endo	165	-178	59	83	-156	-64	-158
CYT 18	24	C3'-endo	-78	-174	56	82	-167	-78	-157
ADE 17	26	C3'-endo	-78	173	60	77	-167	-60	-156
CUA 16	152	C2'-endo	-79	138	52	145	-148	-146	-93
ADE 15	174	C2'-endo	-65	175	52	144	178	-95	-95
GUA 14	145	C2'-endo	-84	-142	55	135	174	-91	-122
GUA 13	168	C2'-endo	-66	165	.....	146	-163	-110	-123

Table 11b. Pseudorotation angles, sugar puckers, and torsion angles for molecule B.

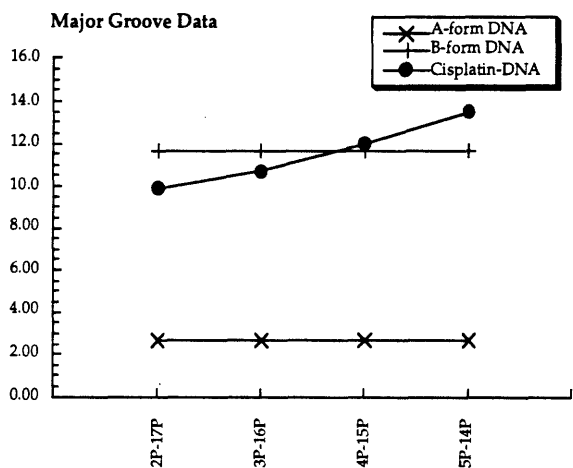
base	P	pucker	$\alpha$	$\beta$	$\gamma$	$\delta$	$\epsilon$	$\zeta$	$\chi$
CYT 1	27	C3'-endo	-72	173	.....	80	-171	-71	-163
CYT 2	19	C3'-endo	-87	-177	61	83	-159	-70	-171
UBR 3	24	C3'-endo	-74	171	61	80	-161	-61	-155
CYT 4	24	C3'-endo	-81	-177	62	80	-165	-68	-164
THY 5	20	C3'-endo	-71	174	56	81	-169	-77	-155
GUA 6*	13	C3'-endo	-79	161	59	85	-139	-51	-153
GUA 7*	47	C4'-exo	-77	162	75	75	-162	-80	-168
THY 8	19	C3'-endo	-72	172	67	91	-164	-67	-153
CYT 9	39	C4'-exo	-66	-178	61	88	-173	-71	-149
THY 10	179	C2'-endo	-70	-177	63	146	-180	-98	-98
CYT 11	154	C2'-endo	-72	-180	53	140	-171	-102	-105
CYT 12	164	C2'-endo	.....	.....	55	146	.....	.....	-103
GUA 24	162	C2'-endo	.....	.....	-170	151	.....	.....	-172
GUA 23	22	C3'-endo	146	-112	54	76	-177	-107	-161
ADE 22	20	C3'-endo	-76	171	59	83	-150	-67	-164
GUA 21	12	C3'-endo	-78	174	58	85	-163	-60	-159
ADE 20	23	C3'-endo	-67	168	175	80	-151	-77	-173
CYT 19	26	C3'-endo	143	-153	54	81	-157	-76	-163
CYT 18	17	C3'-endo	-91	-170	64	89	-156	-76	-164
ADE 17	14	C3'-endo	-72	170	56	84	-152	-69	-157
CUA 16	146	C2'-endo	-70	137	53	145	-158	-158	-97
ADE 15	155	C2'-endo	-78	176	57	138	-167	-94	-110
GUA 14	159	C2'-endo	-71	-179	50	143	-170	-104	-117
GUA 13	166	C2'-endo	-71	176	.....	142	-167	-121	-103

**Figure 45.** (a) Graph of the phosphorus atoms distances along the backbones of the platinated and unplatinated strands of cisplatin-modified DNA. The distances are compared to those for canonical A-DNA and B-DNA. Graphs of the phosphate group distances across the (b) minor groove and (c) major groove of cisplatin-modified DNA. The distances across the grooves are the phosphorus atom distances minus the diameter of a phosphate group, 5.8 Å. Distances are compared to those of canonical A-DNA and B-DNA.

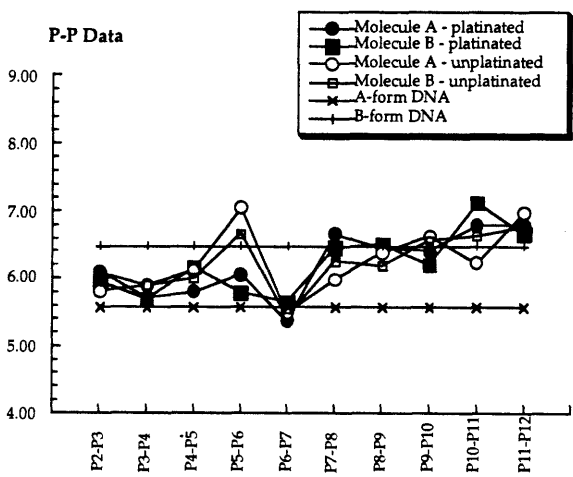
(a)



(b)



(c)



Watson-Crick hydrogen bonding between T5 and A20 are still maintained. The negative shift at this step is also stabilized by hydrogen bonding and end-groove packing interactions between G6-C19 and C1-G24 of a neighboring molecule, discussed previously.

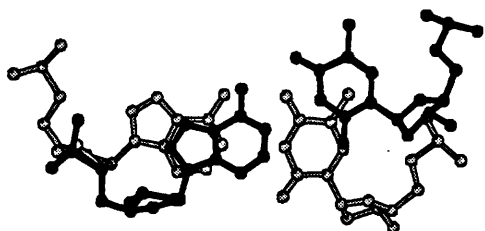
The sixth base step (Figure 52) occurs between base pairs G6-C19 and G7-C18 and both guanine residues have are bound to platinum at their N7 atoms. The coordination of platinum causes roll of  $26^\circ$  toward the major groove with a concomitant opening of the minor groove. The roll at this base step is the main cause of the overall bend in the structure and probably facilitates the fusion of A-like and B-like segments of DNA. This configuration supports modeling studies which had predicted that a bend was necessary at a junction between canonical A- and B-DNA helices (Selsing et al., 1979). Platinum coordination also causes a positive shift at the sixth base step. Base pair G7-C18 is forced toward the minor groove as base pair G6-C19 is pulled toward the major groove in order to accommodate platinum binding. The five membered ring of G7 stacks under the six membered ring of G6, a situation which is the reverse of A-type stacking where the five membered ring of the 5' purine stacks over the six membered ring of the 3' purine. The cytosine residues which are paired with G6 and G7, C19 and C18, respectively, do not stack on one another but maintain base pairing while accommodating the guanine-guanine unstacking at the platinum binding site. At this base step, there is also a change from negative slide to a slide of about zero, which demarcates the junction between A-like DNA and B-like DNA.

The seventh base step (Figures 53 and 58) comprises base pairs G7-C18 and T8-A17 and the locus where most of the disruption caused by platinum binding occurs. Watson-Crick hydrogen bonding interaction within base pair

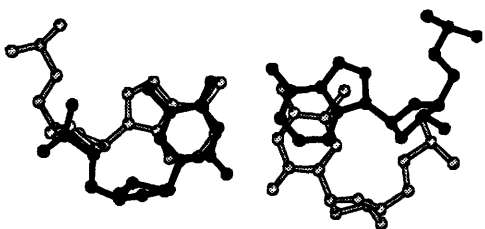


**Figure 46.** Base stacking patterns for the different types of steps of A-DNA and B-DNA as viewed down their helical axes. The base in front is in dark gray and the base below it is in light gray.

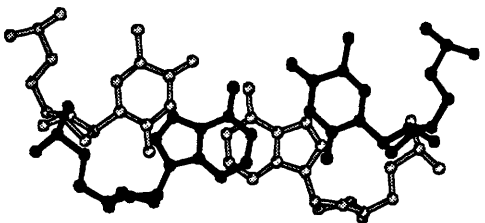
A-DNA



purine - pyrimidine (dark)  
purine - pyrimidine (light)

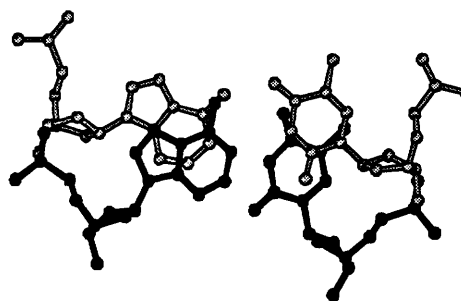


pyrimidine - purine (dark)  
purine - pyrimidine (light)

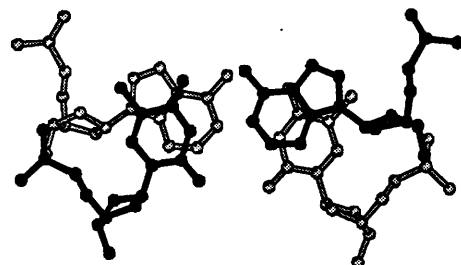


purine - pyrimidine (dark)  
pyrimidine - purine (light)

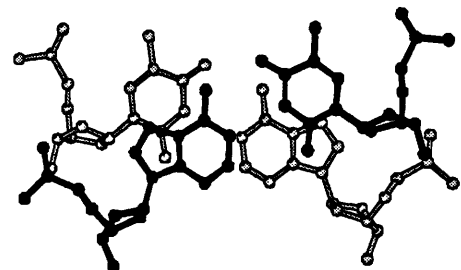
B-DNA



purine - pyrimidine (dark)  
purine - pyrimidine (light)



pyrimidine - purine (dark)  
purine - pyrimidine (light)



purine - pyrimidine (dark)  
pyrimidine - purine (light)

**Figure 47.** Stacking arrangement in base step 1, C1-G24/C2-G23. (a) Base step in molecule A viewed down the helix axis and (b) viewed perpendicular to the estimated helix axis. (c) Base step in molecule B viewed down the helix axis and (d) viewed perpendicular to the estimated helix axis.

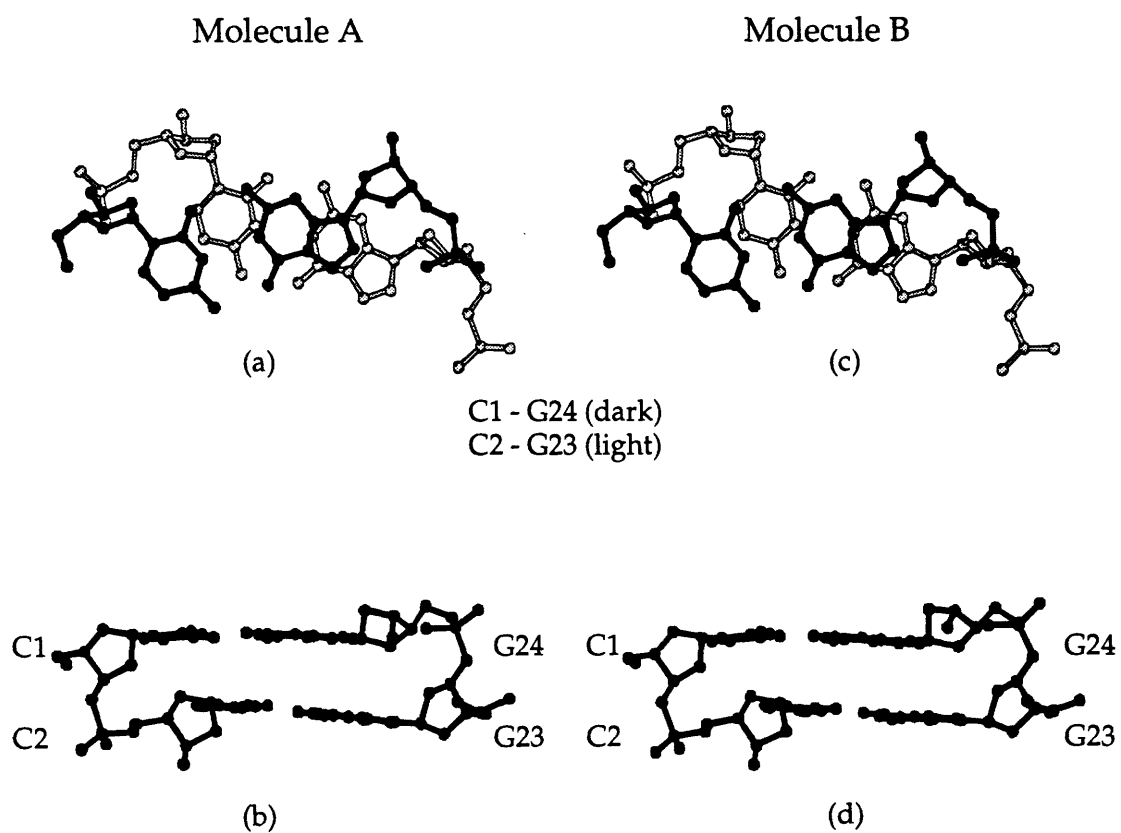


**Figure 48.** Stacking arrangement in base step 2, C2-G23/UBr3-A22. (a) Base step in molecule A viewed down the helix axis and (b) viewed perpendicular to the estimated helix axis. (c) Base step in molecule B viewed down the helix axis and (d) viewed perpendicular to the estimated helix axis.

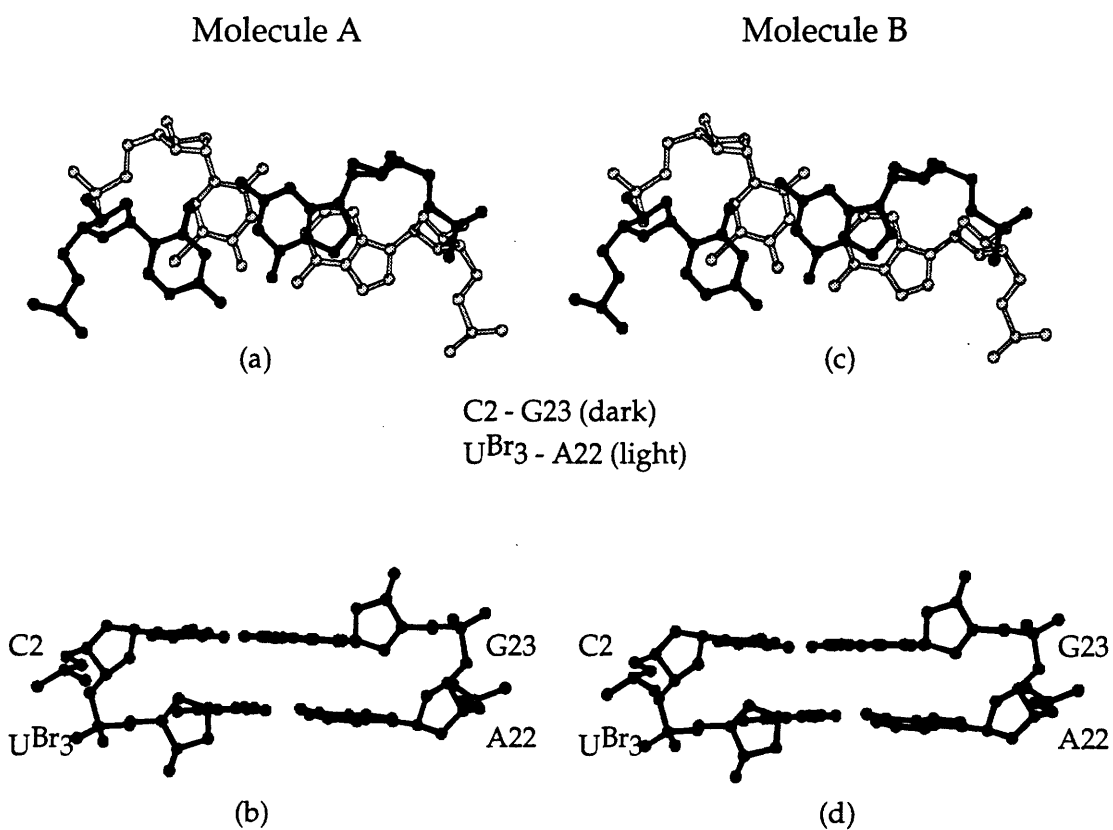


**Figure 49.** Stacking arrangement in base step 3, UBr3-A22/C4-G21. (a) Base step in molecule A viewed down the helix axis and (b) viewed perpendicular to the estimated helix axis. (c) Base step in molecule B viewed down the helix axis and (d) viewed perpendicular to the estimated helix axis.

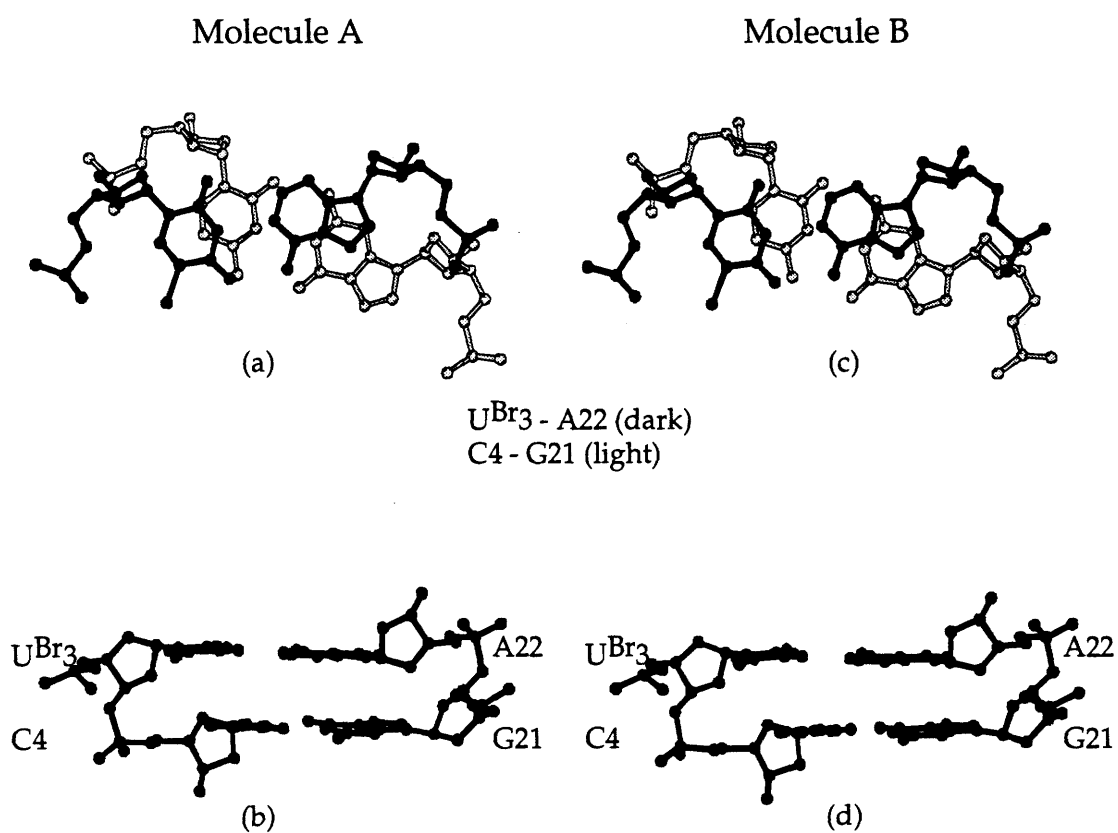


**Figure 50.** Stacking arrangement in base step 4, C4-G21/T5-A20. (a) Base step in molecule A viewed down the helix axis and (b) viewed perpendicular to the estimated helix axis. (c) Base step in molecule B viewed down the helix axis and (d) viewed perpendicular to the estimated helix axis.

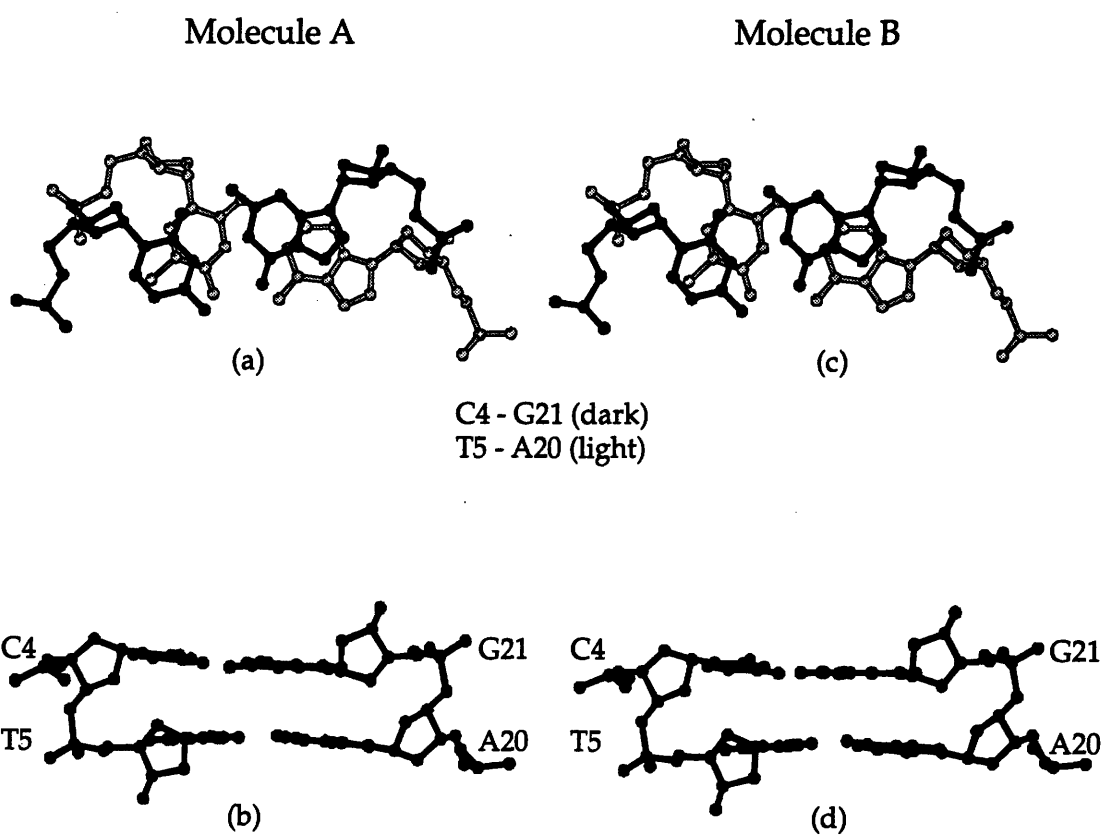


**Figure 51.** Stacking arrangement in base step 5, T5-A20/G6-C19. (a) Base step in molecule A viewed down the helix axis and (b) viewed perpendicular to the estimated helix axis. (c) Base step in molecule B viewed down the helix axis and (d) viewed perpendicular to the estimated helix axis.

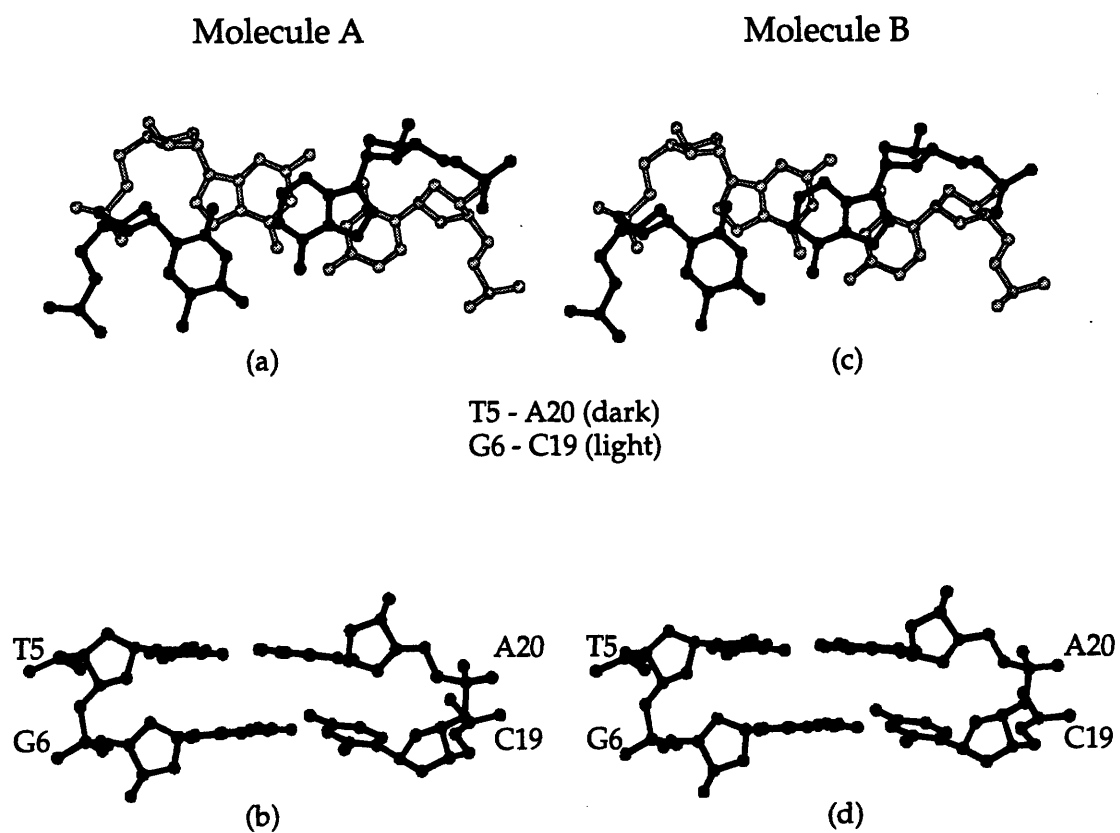


**Figure 52.** Stacking arrangement in base step 6, G\*6-C19/G\*7-C18. (a) Base step in molecule A viewed down the helix axis and (b) viewed perpendicular to the estimated helix axis. (c) Base step in molecule B viewed down the helix axis and (d) viewed perpendicular to the estimated helix axis. G\*6 and G\*7 are coordinated to cis-[Pt(NH<sub>3</sub>)<sub>2</sub>]<sup>2+</sup>.

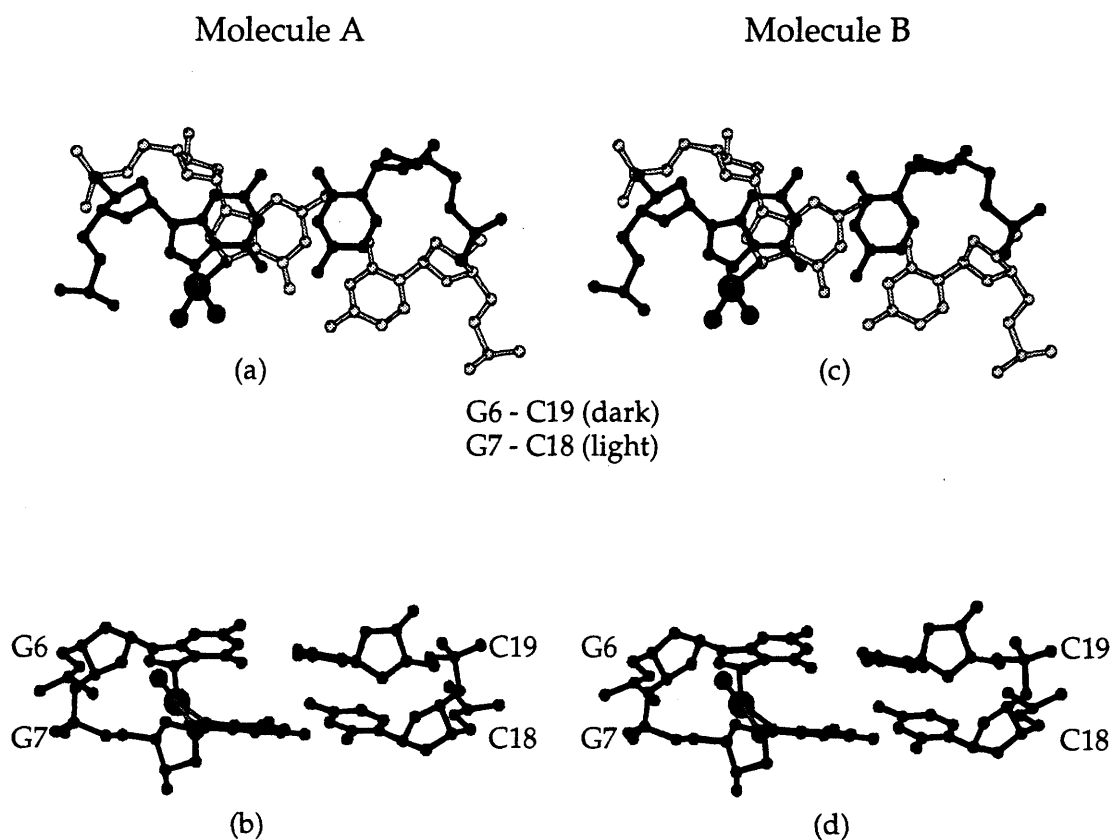


**Figure 53.** Stacking arrangement in base step 7, G7-C18/T8-A17. (a) Base step in molecule A viewed down the helix axis and (b) viewed perpendicular to the estimated helix axis. (c) Base step in molecule B viewed down the helix axis and (d) viewed perpendicular to the estimated helix axis.

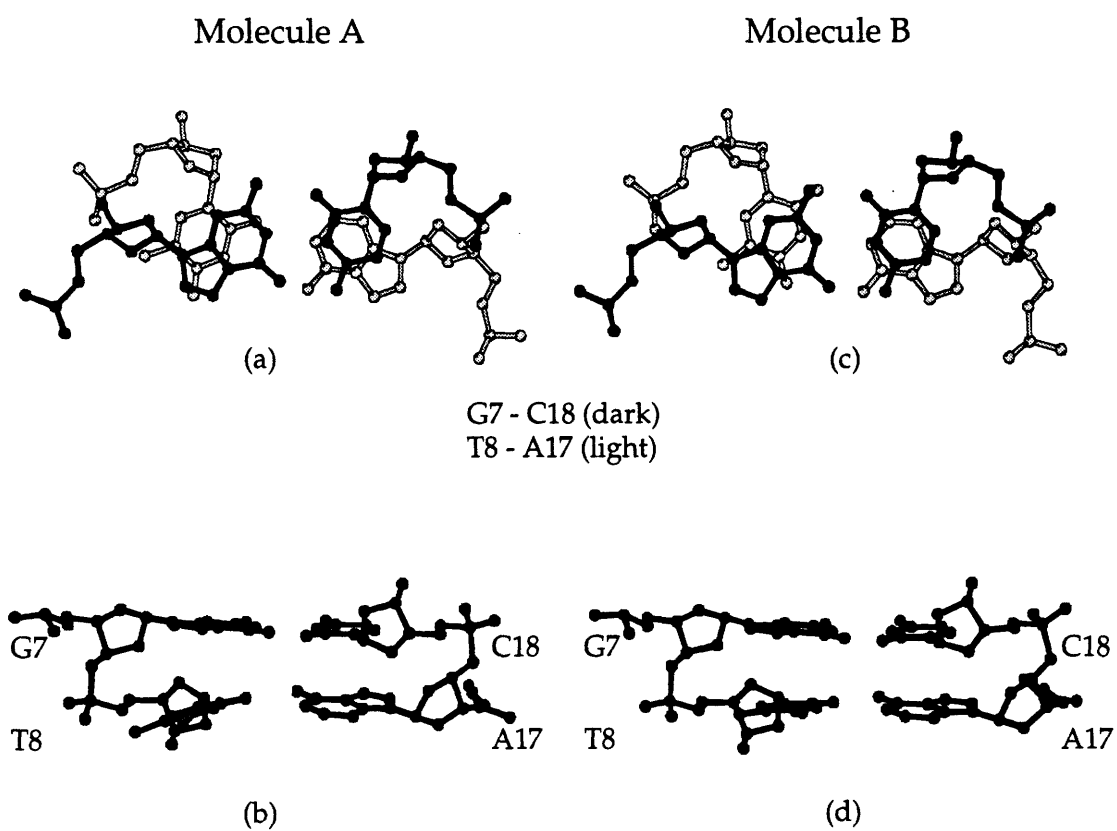




**Figure 54.** Stacking arrangement in base step 8, T8-A17/C9-G16. (a) Base step in molecule A viewed down the helix axis and (b) viewed perpendicular to the estimated helix axis. (c) Base step in molecule B viewed down the helix axis and (d) viewed perpendicular to the estimated helix axis.

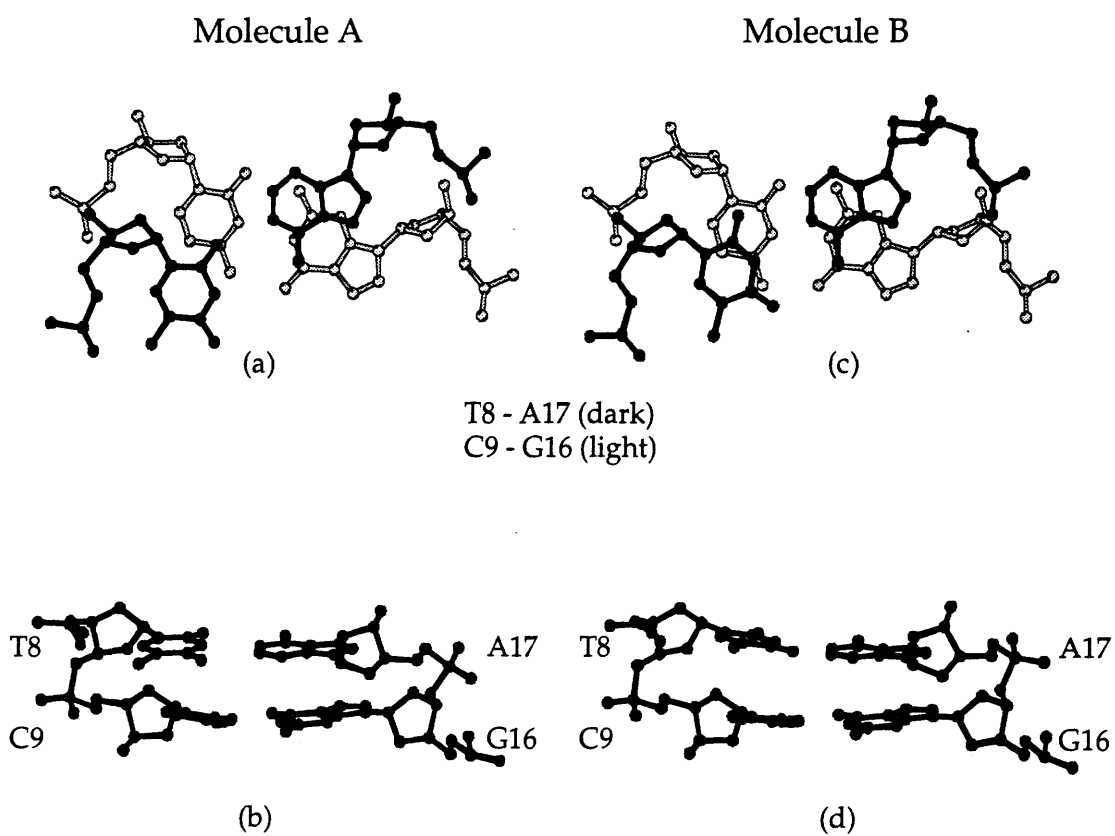


**Figure 55.** Stacking arrangement in base step 9, C9-G16/T10-A15. (a) Base step in molecule A viewed down the helix axis and (b) viewed perpendicular to the estimated helix axis. (c) Base step in molecule B viewed down the helix axis and (d) viewed perpendicular to the estimated helix axis.

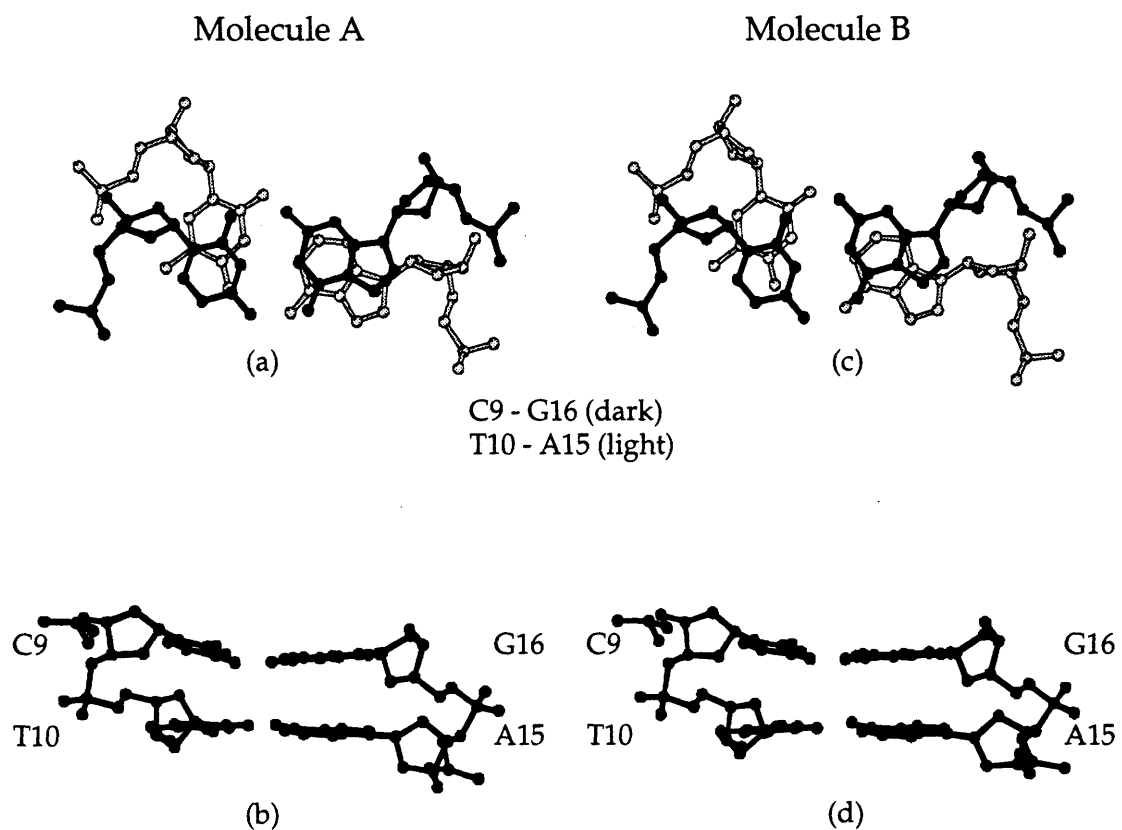


**Figure 56.** Stacking arrangement in base step 10, T10-A15/C11-G14. (a) Base step in molecule A viewed down the helix axis and (b) viewed perpendicular to the estimated helix axis. (c) Base step in molecule B viewed down the helix axis and (d) viewed perpendicular to the estimated helix axis.

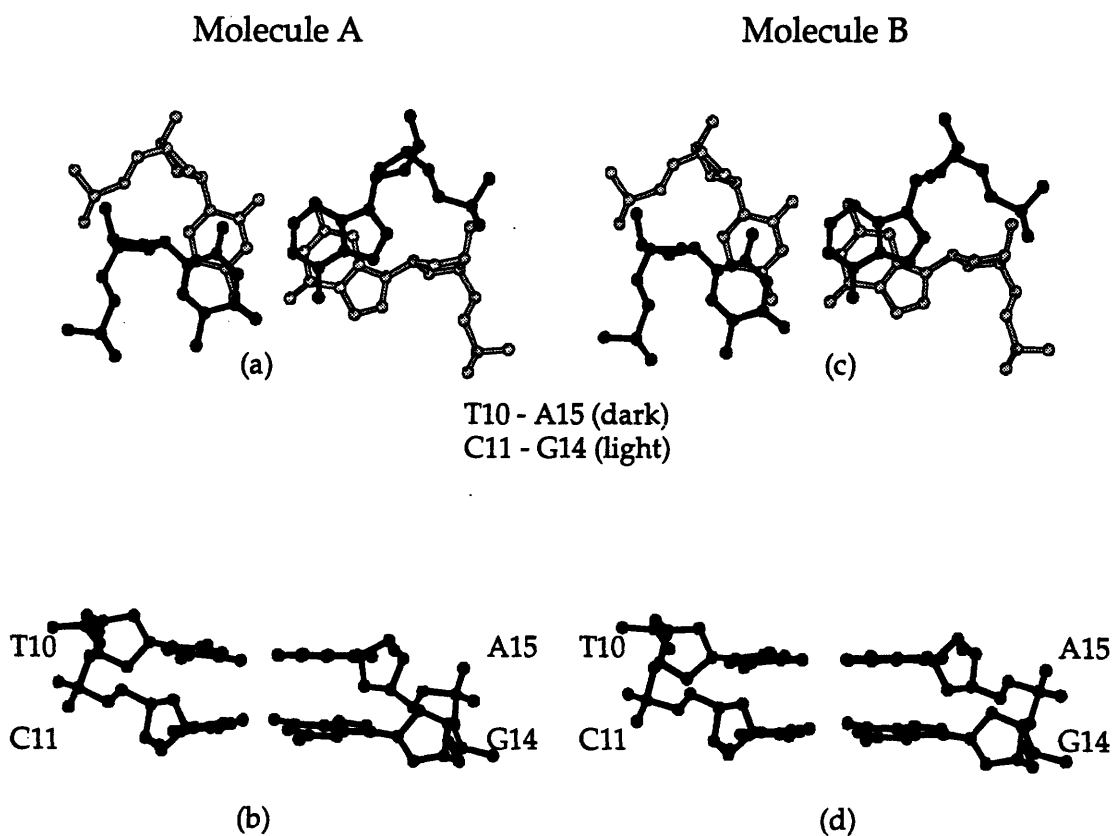


**Figure 57.** Stacking arrangement in base step 11, C11-G14/C12-G13. (a) Base step in molecule A viewed down the helix axis and (b) viewed perpendicular to the estimated helix axis. (c) Base step in molecule B viewed down the helix axis and (d) viewed perpendicular to the estimated helix axis.

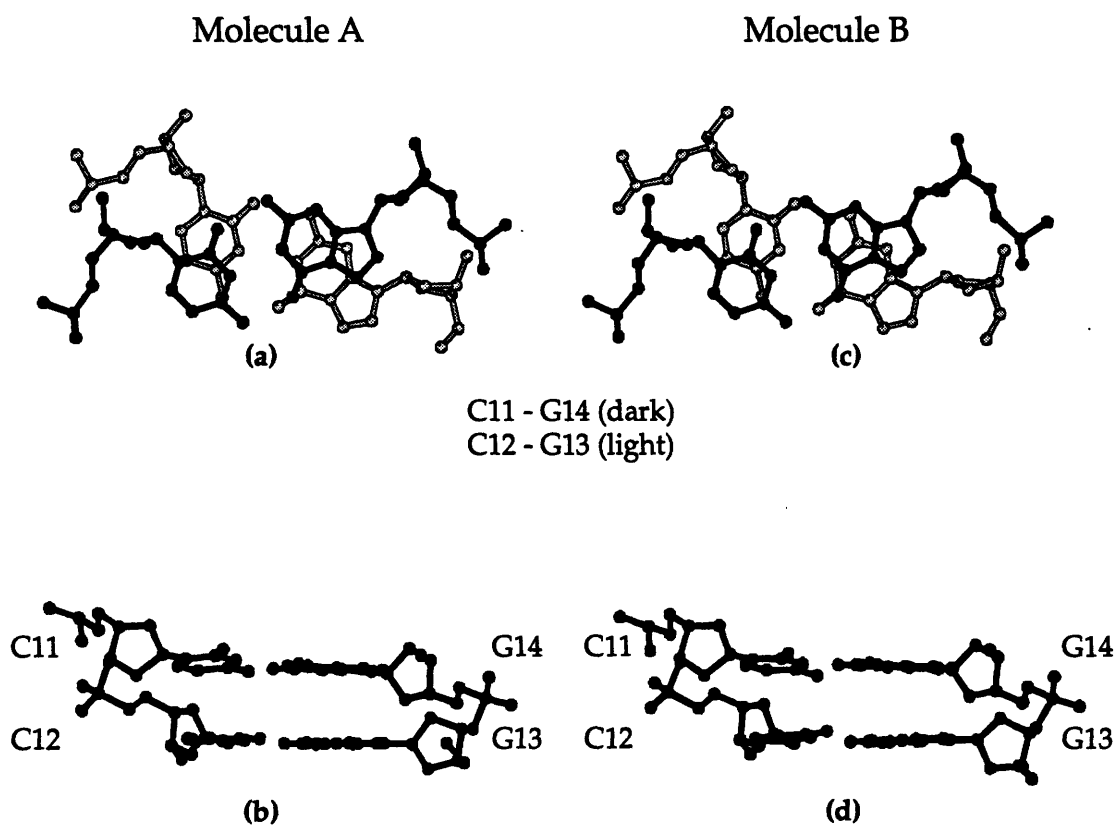
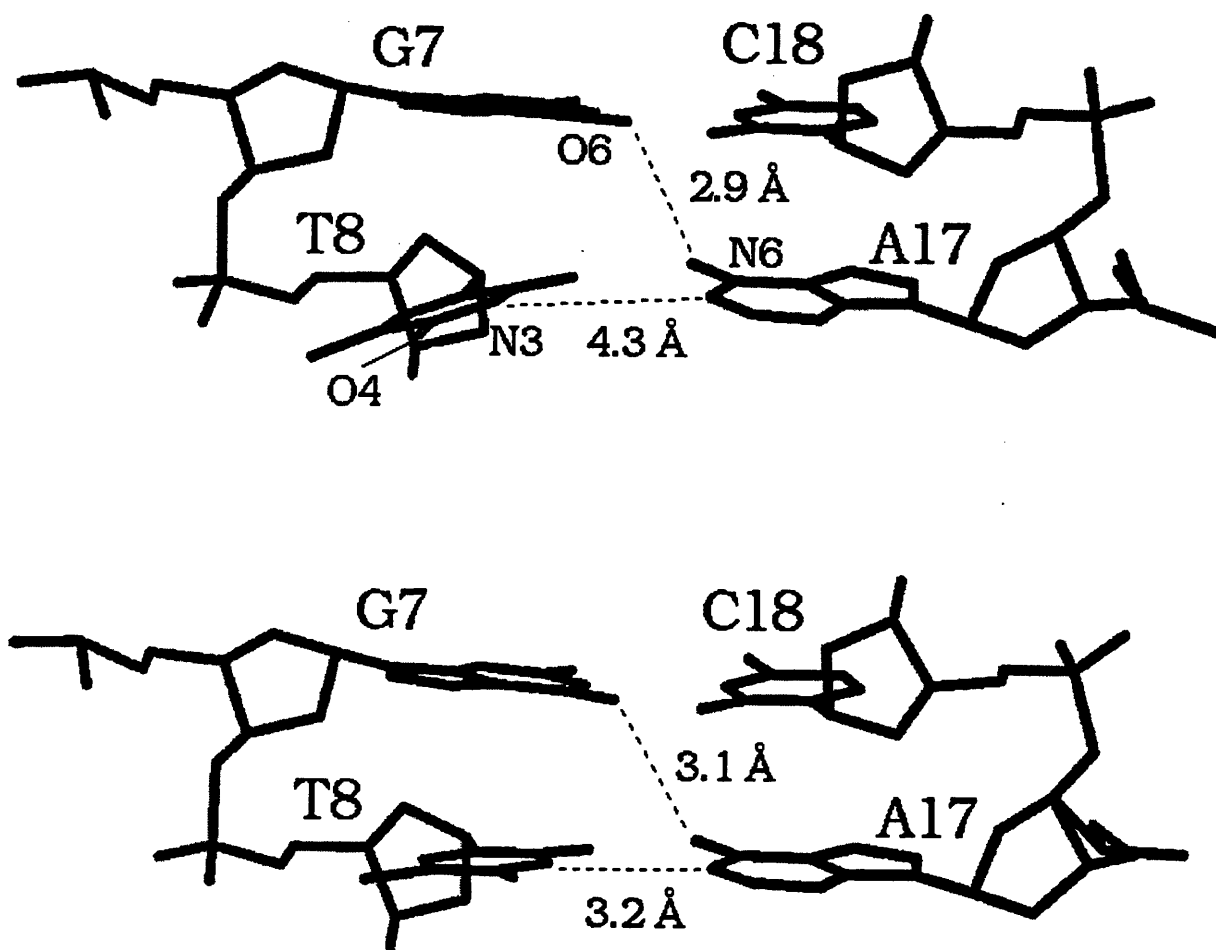


Figure 58. Hydrogen bonding in base step 7, G7-C18/T8-A17. (a) Molecule A and (b) Molecule B.



T8-A17 is diminished but not totally abolished. N6 of A17 is hydrogen bonded to O6 of G7 rather than to O4 of T8, but N1 of A17 remains hydrogen bonded to N3 of T8. The unusual hydrogen bonding is apparent from the positive shear, stretch, opening, and buckle and by the negative stagger and propeller twist within this base pair (Tables 9 and 10). The distortion is compensated for by a highly twisted stacking interaction between T8-A17 and G7-C18. In base step seven, G7 is stacked directly on top of T8 while C18 sits directly over A17. This type of stacking is unusual and does not resemble either A- or B-DNA, and it is the origin of the large positive twist and the positive tilt at this step. Further compensation for the large helical disruption at the seventh base step comes from a negative buckle at base pair C9-G16 and a negative stagger at base pair C11-G14, both of which keep the bases of the double helix stacked in an energetically favorable manner.

The negative buckle at C9-G16 and the negative stagger at C11-G14 are minor local base pair adjustments and do not affect the overall helical structure of the last four base steps on helix A. Steps eight through eleven (Figures 54-57) which include base pairs T8-A17 to C12-G13, are fairly uniform in structure and most closely resemble B-DNA. This similarity is most obvious from the distances between adjacent phosphates on both the platinated and unplatinated strands, all of which are closer to the 6.5 Å value of B-DNA than the 5.6 Å value of A-DNA (Saenger, 1984). Furthermore, the base stacking pattern of each step is very similar to that in B-DNA.

### *Structure of Molecule B*

As previously stated, helix B has the same overall shape as helix A. The sugar puckers and base stacking patterns are the same as for helix A and

show a transition from A-like DNA on the 5' side of the platinum lesion to B-like DNA on the 3' side. The base pair and base step parameters are the same for helices A and B from the first base pair, C1-G24, to the seventh, G7-C18 (Figures 47-52). Differences between the two independent molecules are subtle and become most evident at base step seven (Figure 53), between G7-C18 and T8-A17. For molecule B, all base steps are shown in Figures 47-57, sections c and d.

In helix A, disruption at the seventh base step comprises a positive twist and positive tilt, but these parameters are more normal in helix B. The base pair parameters at this step also differ slightly. Helix B has only positive stretch and negative propeller twist at base pair eight, T8-A17, and does not have unusual shear, opening, stagger or buckle observed in pair eight in helix A (Tables 9 and 10). N6 of A17 is hydrogen bonded to O6 of G7 in helices A and B, but the base complementary base, T8, is propeller twisted differently in helices A and B. Loss of a hydrogen bond within the T8-A17 base pair makes it much more flexible than the other base pairs and is presumably the reason it can adopt different orientations in the two independent molecules.

In molecule B the positive tilt occurs farther down the helix, at base step nine (Figure 55), between C9-G16 and T10-A15. Several base pair parameters are also subtly different in this region. Base pair nine has negative buckle in both helices, but base pair ten, which appears normal in helix A, has a positive stretch and a negative stagger in helix B. Helix B also has a negative stagger farther down the helix at base pair twelve instead of at base pair eleven as was seen in helix A. These base pairs and their stacking interactions are shown in Figures 55 through 57.

The base pair disruptions in molecules A and B differ, but the overall shape of the two independent helices remains generally the same and the

molecules can easily be superimposed on one another, as indicated in Figure 29. The overall shape is approximately the same within experimental error for molecules A and B and is mainly the results of a significant bend in the DNA, discussed next.

### *Bending*

Helix axes for molecules A and B as calculated with the program CURVES (Lavery & Sklenar, 1988; Lavery & Sklenar, 1989) are depicted in Figure 59 viewed perpendicular to the plane formed by the platinum atom and its two ammine ligands in each molecule. For reference, the solution structure of a cisplatin-modified duplex octamer with a reported bend of  $58^\circ$  is also shown in Figure 59 (Yang et al., 1995). Molecules A and B have slightly different bend angles and helical axes because they have slightly different parameters for the eighth through eleventh base steps. The overall bend for both helices appears to be  $\sim 35\text{-}40^\circ$  and is distributed over several base pairs around the site of platinum coordination with the major component of the bend arising from the  $+26^\circ$  roll between the platinated guanosines. A more exact bend angle can be calculated for each helix by using the helix axis of the three terminal base pairs of the B-type segment and the helix axis of the five terminal base pairs of the A-DNA segment. One axis is translated such that its endpoint superimposes onto that of the other axis and, in this orientation, a  $39^\circ$  bend is obtained for helix A and a  $55^\circ$  bend is calculated for helix B. The bend calculated in this manner from coordinates of the NMR solution structure is  $34^\circ$ , far less than the reported value of  $58^\circ$ . The difference between the bends for molecules A and B in the crystal structure reflects the lack of a point of intersection for the axes and our inability to determine an



exact helix axis with only three base pairs in the B-type fragment. Furthermore, when the crystal structure bends are compared with the calculated bend and pictured NMR model, it is quite clear that it is difficult to calculate rigorously and assign bend angles to the helices presented in Figure 59, but it is obvious that the intrastrand *cis*-{Pt(NH<sub>3</sub>)<sub>2</sub>}<sup>2+</sup> cross-link bends the duplex substantially.

#### *Details of the Platinum Binding Site*

A view of the metal binding interaction (Figure 60) illustrates the large positive roll caused by coordination of platinum to the N7 atoms of adjacent guanosine residues. The dihedral angle between the two guanine rings is approximately 26°, far less than the ~80° angle found in the crystal structure of the *cis*-{Pt(NH<sub>3</sub>)<sub>2</sub>}<sup>2+</sup>-dinucleotide complex (Sherman et al., 1988). As was observed in the latter structure, one of the amines in the present structure appears to be within hydrogen bonding distance of a phosphate oxygen atom, the NH<sub>3</sub>...O distance being 3.3 Å for duplex A and 3.7 Å for duplex B.

The platinum atom is coordinated to N7 of G6 and N7 of G7 and all platinum-nitrogen distances are about 2.0 Å. The {Pt(NH<sub>3</sub>)<sub>2</sub>}<sup>2+</sup> moiety, the individual platinum atoms and NH<sub>3</sub> groups of which are not resolved at 2.6 Å resolution, and the guanine bases have very well defined positions and the final model nicely fits the data (Figure 61). All four platinum-nitrogen bonds were left unrestrained during the final stages of refinement and converged to the expected distances of 2.0 Å. The platinum atom is not perfectly square-planar, however. The metal atom sits out of the plane of the G6 and G7 rings by 1.2 and 0.8 Å, respectively. The platinum centers have the same structures

in molecules A and B, with an rmsd for all atoms in base pairs six and seven being 0.10 Å.

**Figure 59.** Helical axes calculated with the program CURVES for (a) molecule A, (b) molecule B, and (c) the NMR solution structure.

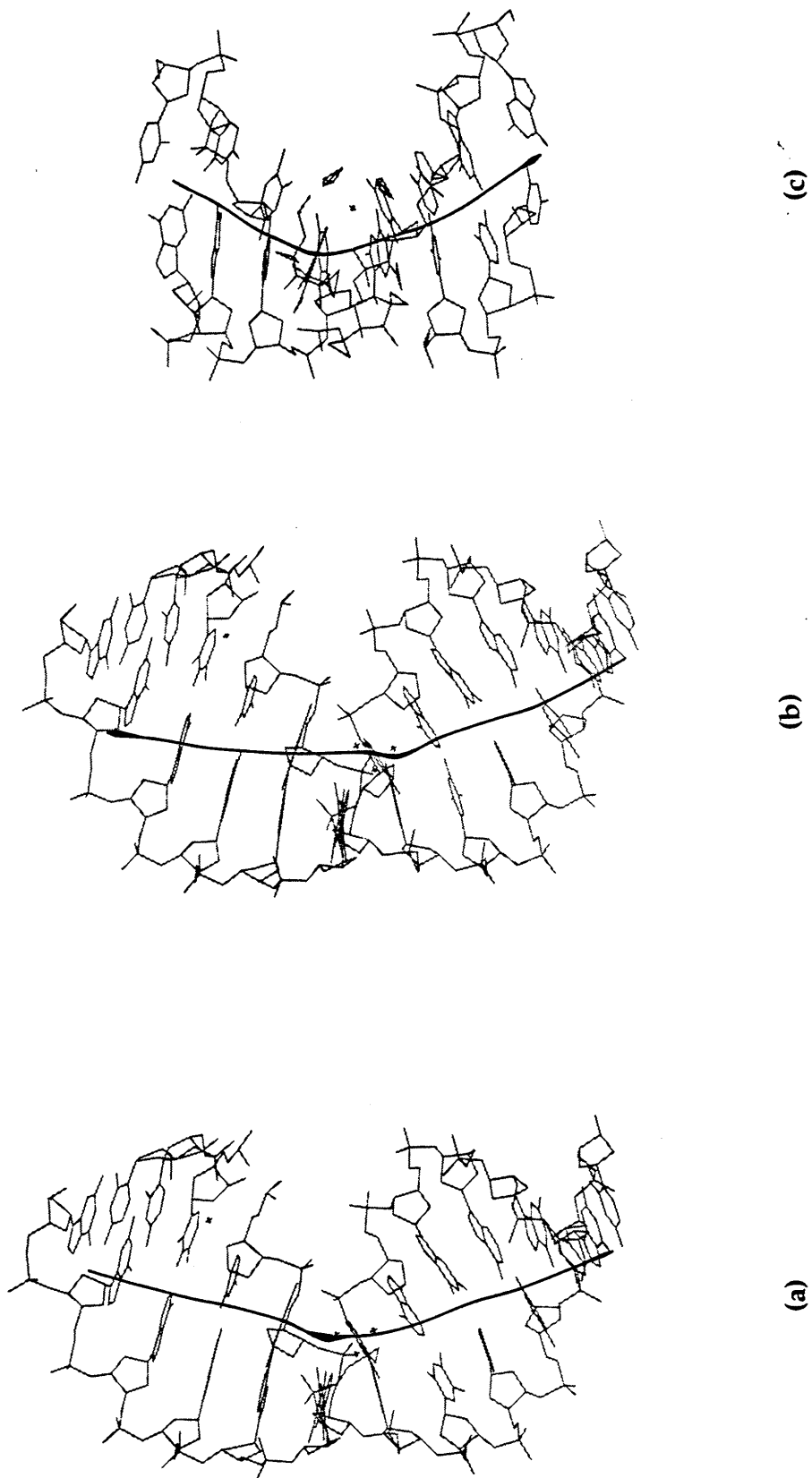


**Figure 60.** The -G\*G\*- platination site. The base pairs are propeller twisted but retain their hydrogen bonds. One of the ammine ligands on platinum is hydrogen bonded to phosphate group on the backbone of the platinated deoxyoligonucleotide strand.

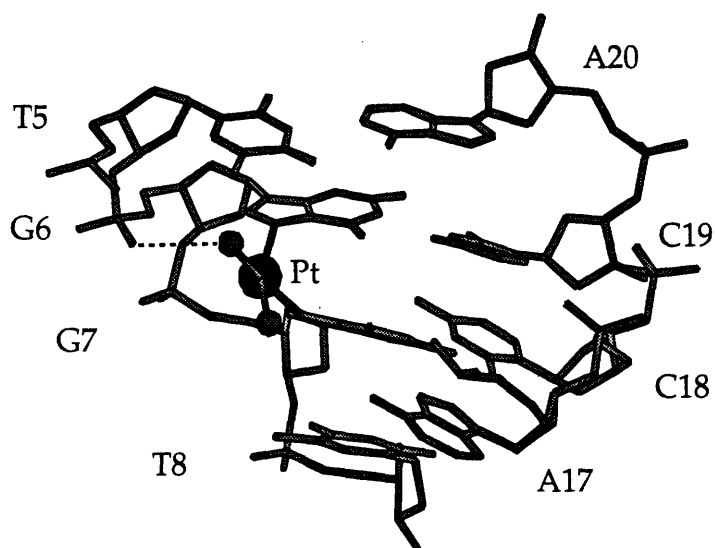
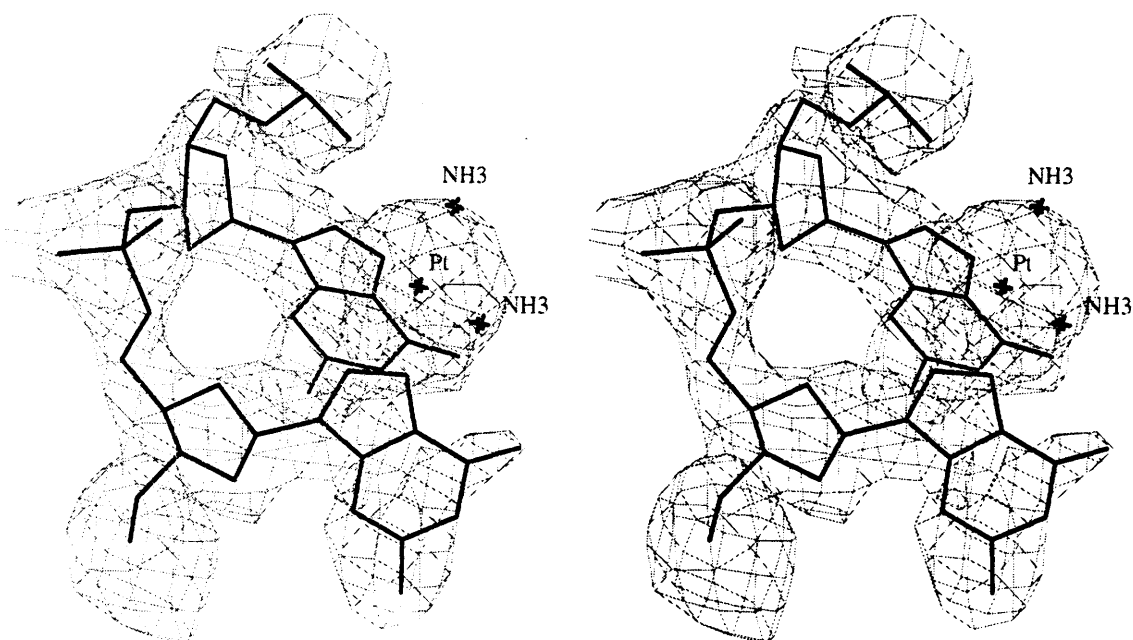


**Figure 61.** Stereo image of *cis*-[Pt(NH<sub>3</sub>)<sub>2</sub>]<sup>2+</sup> bound to a d(GpG) site on duplex DNA. The 2Fo-Fc electron density map is shown in light gray and is contoured at 1σ. The platinum atom is shown coordinated to two ammines and the N7 atoms of adjacent guanine rings.





**CHAPTER 4**  
**DISCUSSION**

*Crystal Structure of Cisplatin-modified DNA*

The crystal structure described in this thesis is the first X-ray determination of a segment of duplex DNA containing the major adduct of the anticancer drug cisplatin. The data reveal that, when *cis*-{Pt(NH<sub>3</sub>)<sub>2</sub>}<sup>2+</sup> binds to adjacent guanosine residues on duplex DNA, it severely distorts the double helix by causing a bend toward the major groove and a widening and flattening of the minor groove. The shape of the cisplatin-modified DNA double helix probably accounts for the difficulty in crystallizing it. The structure of the double helix modified by cisplatin contains a junction of A-like and B-like DNA segments and is accommodated in the crystal lattice by a combination of A-DNA and B-DNA type packing motifs.

The crystals used in this study afford two crystallographically independent views of the structure. Two slightly different ways in which a segment of duplex DNA can accommodate a *cis*-{Pt(NH<sub>3</sub>)<sub>2</sub>}<sup>2+</sup> lesion are manifested. Despite these minor differences the two molecules have nearly identical global features indicating that the structure obtained is probably not just an artifact of crystal packing forces.

When *cis*-{Pt(NH<sub>3</sub>)<sub>2</sub>}<sup>2+</sup> forms an intrastrand cross-link between adjacent guanine residues on duplex DNA, it causes a large positive roll between bases. This roll compresses the major groove while concomitantly opening up the minor groove and causing a bend to build up over the base pairs near the platination site. The overall structure of the double helix remains intact and most of the distortion is absorbed by conformational changes in the sugar-phosphate backbone and base pair parameters for those residues near the platinum lesion. The backbone of DNA is relatively flexible and its torsion angles are correlated so as to allow local fluctuations in the



structure of a segment of DNA while maintaining the overall geometry of the double helix (Kennard & Salisbury, 1993). In the case of cisplatin-modified DNA, the phosphate groups on the backbone move closer together at the site of platinum coordination in order to accommodate the positive charge and the widening of the minor groove. Compression of the phosphate backbone causes the sugar puckers of the residues to the 5' side of the platinum lesion to adopt a C3'-endo conformation while the deoxyribose rings of the T10-C12 segment at the 3' end of the helix remain in the C2'-endo conformation.

The A-type conformation to the 5' side of the platinum lesion is propagated all the way to the 5' end of the helix because the minor groove adopts a wide and flat conformation to accommodate the groove packing interaction of the C1-G24 base pair of a neighboring molecule. The 3' end of the helix remains in a conformation closely resembling that of B-DNA. Previous study revealed that DNA having an A/B junction would display an overall bend of about  $26^\circ$ , which happens to be the roll angle between the bases coordinated to *cis*-{Pt(NH<sub>3</sub>)<sub>2</sub>}<sup>2+</sup> (Selsing et al., 1979). Platination is likely the cause of the structure observed, and the presence of A-like and B-like DNA conformations would appear to be stabilized by the crystallization conditions employed. [Co(NH<sub>3</sub>)<sub>6</sub>]Cl<sub>3</sub>, used in place of a spermine to stabilize the negative phosphate backbone during crystallization, is routinely used for DNA crystallizations and known to facilitate conversion of B-form DNA to A-form DNA in solution (Gao et al., 1995; Robinson & Wang, 1996) and to stabilize unusual DNA structures such as cruciforms (Duckett et al., 1990). The effect of [Co(NH<sub>3</sub>)<sub>6</sub>]Cl<sub>3</sub> on the crystal structure of cisplatin-modified DNA presented here cannot be evaluated because no cobalt atoms were located during the structure refinement, although it was necessary for crystal formation. The junction of A-like and B-like DNA seen in the platinated

DNA structure proves that the conditions under which these crystals grow can support the coexistence of A- and B- DNA segments and that these conformations are probably quite similar in energy (Doucet et al., 1989).

The structure of cisplatin-modified DNA also revealed extended contacts between the backbones of the two crystallographically independent helices. The backbone interactions appear to be stabilized by C-H...O hydrogen bonds. This type of hydrogen bond has been observed in biologically significant structures (Desiraju, 1991) and, in particular, has been suggested as a stabilizing interaction in non-Watson-Crick base pairs (Leonard et al., 1995). The six sequential C-H...O interactions we observe appear to be a feature unique to our structure, however. The series of hydrogen bonds between the backbones is probably critical for stabilization of the observed structure and crystal formation.

#### *Comparison with the NMR Solution Structure*

Recently an NMR solution structure of d(CCTG\*G\*TCC)·d(GGACCAGG), where -G\*G\*- denotes the site of *cis*-{Pt(NH<sub>3</sub>)<sub>2</sub>}<sup>2+</sup> coordination, was reported (Yang et al., 1995). This work confirmed the conversion of the 5' platinated guanosine from C2'-endo to C3'-endo found in numerous earlier NMR studies of the *cis*-{Pt(NH<sub>3</sub>)<sub>2</sub>}<sup>2+</sup> 1,2-intrastrand d(GpG) cross-link (Sherman & Lippard, 1987). The bend angle was 58°, in agreement with molecular mechanics studies (Kozelka & Chottard, 1990), but considerably larger than the 32°-40° angle estimated by gel electrophoresis studies (Bellon & Lippard, 1990; Rice et al., 1988) and the 2.6 Å crystal structure (Takahara et al., 1995). The NMR solution structure has many features in common with the present crystal structure determination,

including a similar dihedral angle of  $23^\circ$  between guanine rings coordinated to platinum, minimal disruption of base pairing at the platination site (Figure 62), and a wide, flat minor groove opposite the site of platinum coordination (Figure 63).

There are also some significant differences between the solution and crystal structures. The probable hydrogen bond observed between one of the ammine ligands on platinum and a phosphate oxygen in the crystal structure is not observed in the solution structure, possibly due to the different buffer and salt environments used for the X-ray and NMR experiments. In the solution structure, the sugar ring on the 5' side of the platinum lesion adopts the C3'-endo conformation but the rest of the double helix is similar to B-DNA, whereas the crystal structure shows a combination of A-like and B-like helices. Because the structures are so different with respect to helical axes, the bend angles cannot be precisely compared. It is obvious, however, that platinum binding severely distorts and bends duplex DNA and that the magnitude of the bend is in general agreement with gel electrophoresis bending studies of the platinated duplex.

Structural information obtained from solution NMR studies and X-ray crystallographic studies of cisplatin-modified DNA complement each other and together provide a detailed picture of the distortions caused by platinum coordination. NMR measurements can afford very good information about short range distances, especially base pairing patterns and deoxyribose ring conformations. Limitations in the method make it difficult to determine long range distances and a reliable model for groove shapes. This problem may be overcome by the use of paramagnetic spin labels to obtain long range distance constraints in NMR structure determinations (Dunham & Lippard, 1995). X-ray crystallography, on the other hand, is limited by crystal quality

**Figure 62.** The platination sites of cisplatin-modified DNA from (a) the crystal structure and (b) the NMR solution structure.

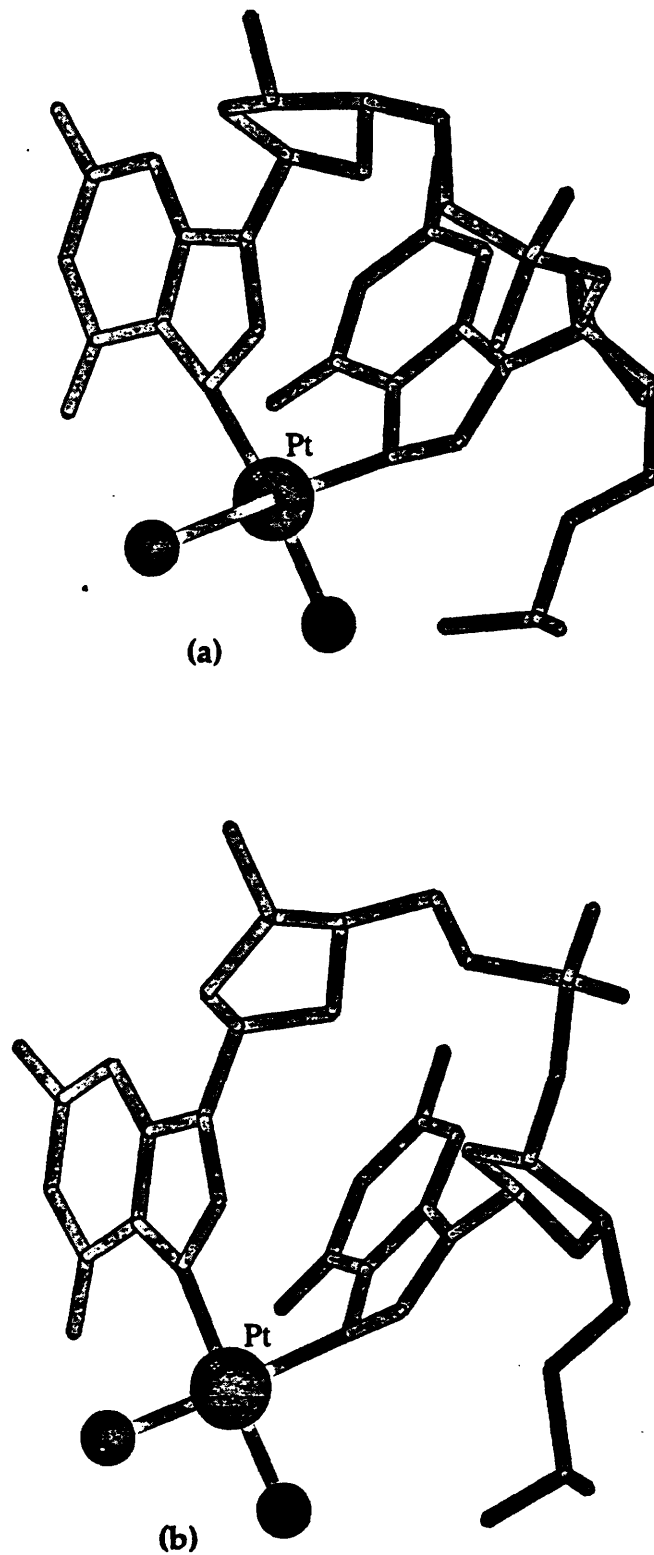
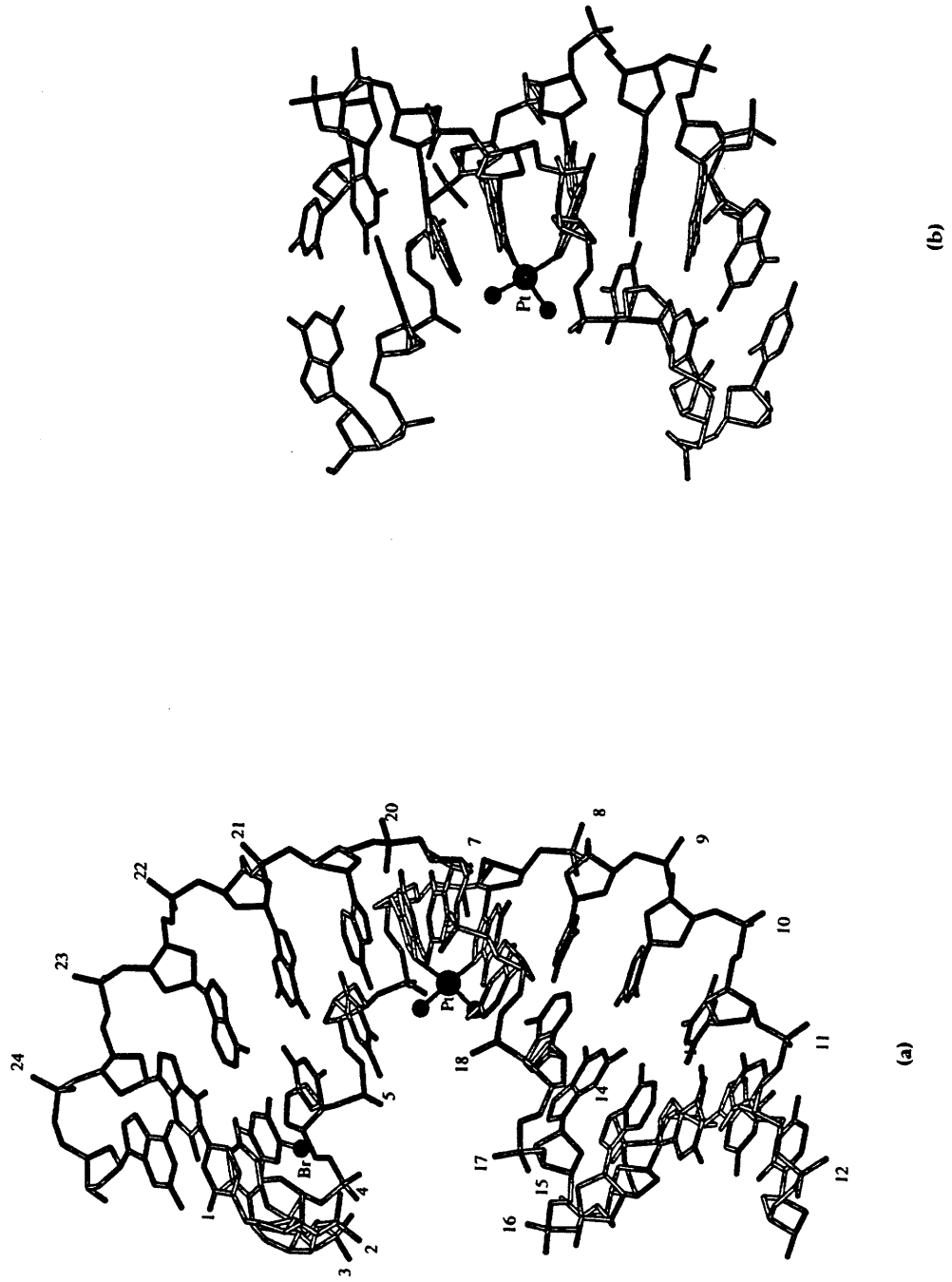


**Figure 63.** The structures of cisplatin-modified DNA determined (a) by X-ray crystallography and (b) by NMR. The minor grooves in both structures are widened opposite the intrastrand platinum cross-link.



which controls the resolution of the diffraction data collected. At the resolution of the structure reported in the paper, 2.6 Å, electron density maps do not reveal the sugar pucker. The electron density maps do, however, clearly show the positions of phosphorus atoms and platinum atoms as well as the planes of the bases. From the phosphate distances along the backbone, sugar pucker can be determined and groove widths measured. Packing interactions in crystals may influence the structure observed. The latter concern, however, is partially obviated by the extremely high solvent content (~60%) of the crystals used in this investigation. The packing interactions we observe reveal interesting contacts between neighboring nucleic acid helices and may indicate how DNA-DNA or protein-DNA contacts might involving platinated nucleic acids take place in vivo.

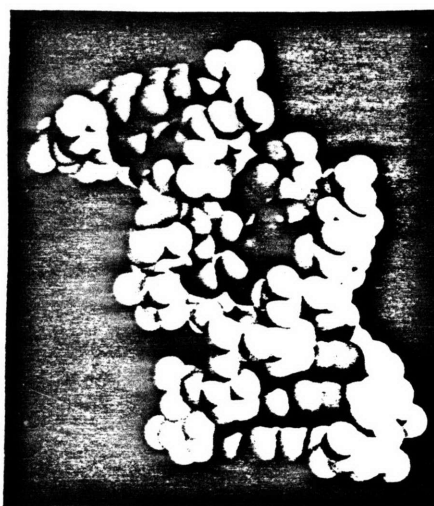
In both the solution and crystal structures of the d(GpG) intrastrand cross-link of *cis*-[Pt(NH<sub>3</sub>)<sub>2</sub>]<sup>2+</sup> on DNA, the bend occurs over several base pairs and the major component is a large positive roll between coordinated guanosines. The roll results in a wide minor groove with a large hydrophobic surface which might be a good target for protein binding. This hydrophobic groove was a key feature in the crystal packing where the end base pair of one helix was able to lodge tightly in the minor groove of its neighbor.

The crystal structure also reveals a potential for drug design with this complex. The major groove, which contains the platinum atoms has many functional groups which might interact favorably with ligands other than simple amines. Octahedral metal complexes are currently in clinical use as chemotherapeutic agents (Esposito et al., 1992). An octahedral metal complex such as [M(L)<sub>4</sub>]<sup>2+</sup>, where M is a metal such as ruthenium and L is a small ligand such as ammine, fits into the structure and binds two guanine residues

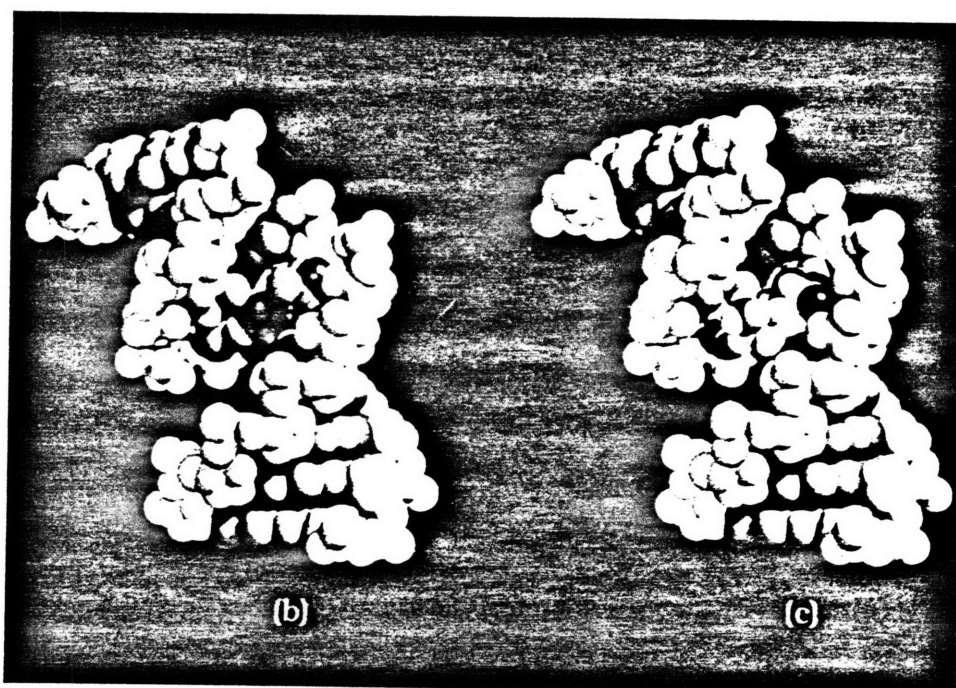
in place of *cis*-{Pt(NH<sub>3</sub>)<sub>2</sub>}<sup>2+</sup> and shows that the major groove is large enough to accommodate moieties larger than the *cis*-{Pt(NH<sub>3</sub>)<sub>2</sub>}<sup>2+</sup> fragment (Figure 64 b). A similar exercise with the dinucleotide structure, *cis*-[Pt(NH<sub>3</sub>)<sub>2</sub>{d(pGpG)-N7(G<sub>1</sub>),-N7(G<sub>2</sub>)}], showed some unacceptably close contacts between the ligands and the guanine rings (Sherman et al., 1988). These were not apparent in the cisplatin-duplex crystal structure due to the smaller roll between the guanine ring planes.

A platinum-lysine complex also fits easily into the major groove (Figure 64 c) (Sandman & Lippard, 1996). Initial experiments have shown that platinum-lysine and perhaps platinum-peptide complexes might be useful for future anticancer drug design.

**Figure 64.** (a) Space-filling picture of cisplatin-modified DNA. The platinum atom is yellow and the ammine ligands are blue. (b) Model of an octahedral metal complex docked in the major groove at the site of *cis*-{Pt(NH<sub>3</sub>)<sub>2</sub>}<sup>2+</sup> binding. (c) Representation of a platinum-lysine complex docked in place of *cis*-{Pt(NH<sub>3</sub>)<sub>2</sub>}<sup>2+</sup>. The structures shown are only to show the size of the moieties that the major groove can accommodate and are not meant to represent true structures.



(a)



(b)

(c)



*Stabilization of the Cisplatin Lesion by Further Bending*

In order to accommodate a shallow dihedral angle of  $\sim 26^\circ$  between the planes of G6 and G7, the platinum atom lies out of the guanine planes by 1.3 Å and 0.8 Å respectively. This result contrasts with that of X-ray crystal structure of *cis*-{Pt(NH<sub>3</sub>)<sub>2</sub>}<sup>2+</sup> coordinated to d(pGpG) in which the corresponding dihedral angle is  $\sim 80^\circ$  and platinum deviates by no more than 0.4 Å from the purine ring planes. The model derived to account for the NMR data also did not show a large deviation of platinum from the planes of the coordinated guanines, but the structure refinement was based on the platinated d(GpG) crystal structure results and on constraints applied in earlier modeling studies, none of which allowed metal-N7 bond bendability (Yang et al., 1995).

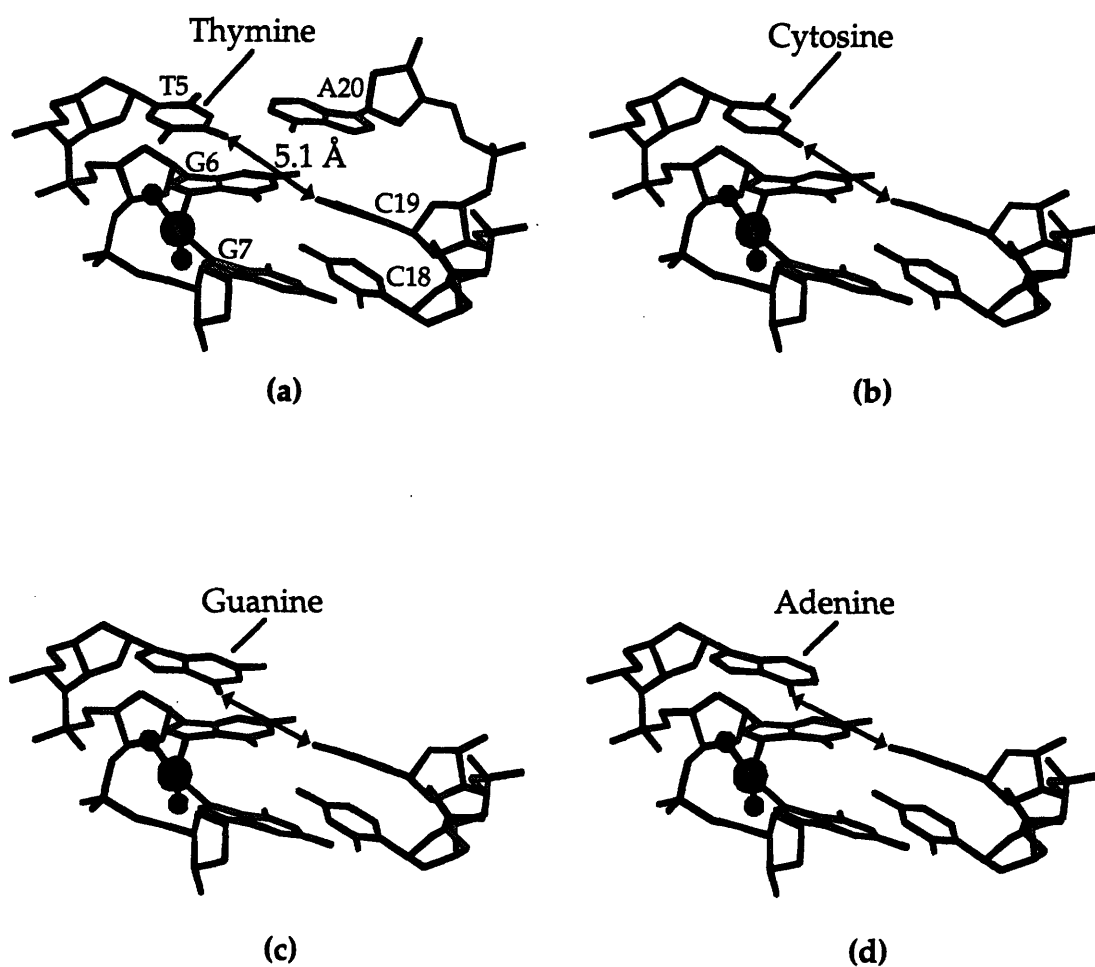
A modeling study of cisplatin bound to duplex DNA was conducted with data from the X-ray structure of cyclic diguanylic acid crystallized with CoCl<sub>2</sub> (Guan et al., 1993). In this structure, the cobalt binds to the N7 atoms of adjacent guanine residues and results in a roll of  $33^\circ$  between the guanine base planes. These results were used to model cisplatin bound to a duplex decamer, d(CAATG\*G\*ATTG)-d(CAATCCATTG), with platinum at the -G\*G\*- site. The structure was minimized and the resulting duplex had an overall bend of  $\sim 34^\circ$ , much less than was predicted by earlier molecular mechanics calculations but in agreement with gel electrophoresis studies (Bellon & Lippard, 1990; Rice et al., 1988). The diminished bend in the cobalt-derived model and in the present crystal structure of cisplatin bound to duplex DNA reveal the ability of the latter to induce strain at the metal center and indicates that metal-N7 bonds have some flexibility. This feature might play an important role in the anticancer activity of the drug because protein

binding can further bend platinated DNA, and perhaps be energetically driven by release of strain at platinum owing to the 1,2-intrastrand cross-link.

The idea that proteins might bind to bent cisplatin/DNA lesions and further distort them to provide an energetically more favorable state might result in sequence specificity and possibly result in lethal adducts of the drug. Previous modeling studies suggested that the sequence d(-TG\*G\*-) would be favored over d(-CG\*G\*-) for cisplatin binding (Kozelka et al., 1987). Although this preference has not been proved, it is interesting to consider, especially if a protein were to bind the platinated DNA and further bend the double helix toward the major groove. In the present crystal structure of *cis*-[Pt(NH<sub>3</sub>)<sub>2</sub>]<sup>2+</sup> bound to duplex DNA, O4 of T5 is about 5.1 Å from N4 of C19, which is base paired to the platinated residue G6 (Figure 65 a). If the helix were more significantly bent, these atoms would move closer together and be positioned for a hydrogen bonding interaction. If T5 were replaced by a cytosine then position 4 of the pyrimidine ring would be occupied by an exocyclic amino group, and there would be a steric clash when the DNA is further bent upon protein binding (Figure 65 b). Such an interaction does not occur on the 3' side of the platinum lesion. The sequence -G\*G\*T- would not be preferred over -G\*G\*C- because the cytosine complementary to the platinated guanine, C18, is pushed up and away from T8 so that it can maintain good stacking interactions with A17 and C19.

A comparison of the sequences -GG\*G\*- and -AG\*G\*- affords a similar conclusion. Replacement of T5 by guanosine would provide an oxygen atom, O6, which is 5.1 Å from N4 of C19 and might form a hydrogen bond if the helix were more bent (Figure 65 c). An adenine substituted for T5 would place an exocyclic amine group, N6, in the major groove, which would cause a steric clash with N4 of C19 if the DNA were bent further (Figure 65 d).

**Figure 65.** (a) -TG\*G\*- segment from the crystal structure of cisplatin-modified DNA. The O4 atom of residue T5 is 5.1 Å from the N4 atom of residue C19 in the current structure. Model with -TG\*G\*- replaced by (b) -CG\*G\*-, (c) -AG\*G\*-, and (d) -GG\*G\*-.



Coordination of ligands other than cis-ammine moieties to the platinum atom could also influence bending. In the case of a square-planar metal complex with an amino acid such as lysine or peptide in place of cis-ammine ligands, favorable interactions between major groove functional groups and the ligand on the metal might stabilize a more bent structure. It is likely that replacement of the square-planar complex with an octahedral complex would probably prevent further bending of the duplex for steric reasons, however. This observation suggests that perhaps octahedral metal complexes would have a different mechanism of action from that of cisplatin.

#### *HMG Domain Protein Binding to Cisplatin-modified DNA*

Proteins that recognize, bind to, and further bend cisplatin lesions on DNA all contain a stretch of about 80 amino acids known as the high mobility group (HMG) domain (Whitehead & Lippard, 1995). HMG proteins are involved in transcription and bind to specific sequences or unusual structures such as bent DNA or cruciforms. These proteins can bind specifically to and prevent repair of the major cisplatin intrastrand adducts, Pt-GG and the presumably closely related Pt-AG (Huang et al., 1994). Gel electrophoresis studies reveal that HMG protein binding to these lesions increases the overall bend of the DNA from  $\sim 33^\circ$  to  $\sim 80^\circ$  (Chow et al., 1994). This change in bend angle supports the hypothesis that protein binding might relieve strain at the platinum site by allowing the metal atom to return to a more favorable position in the planes of the guanine bases.

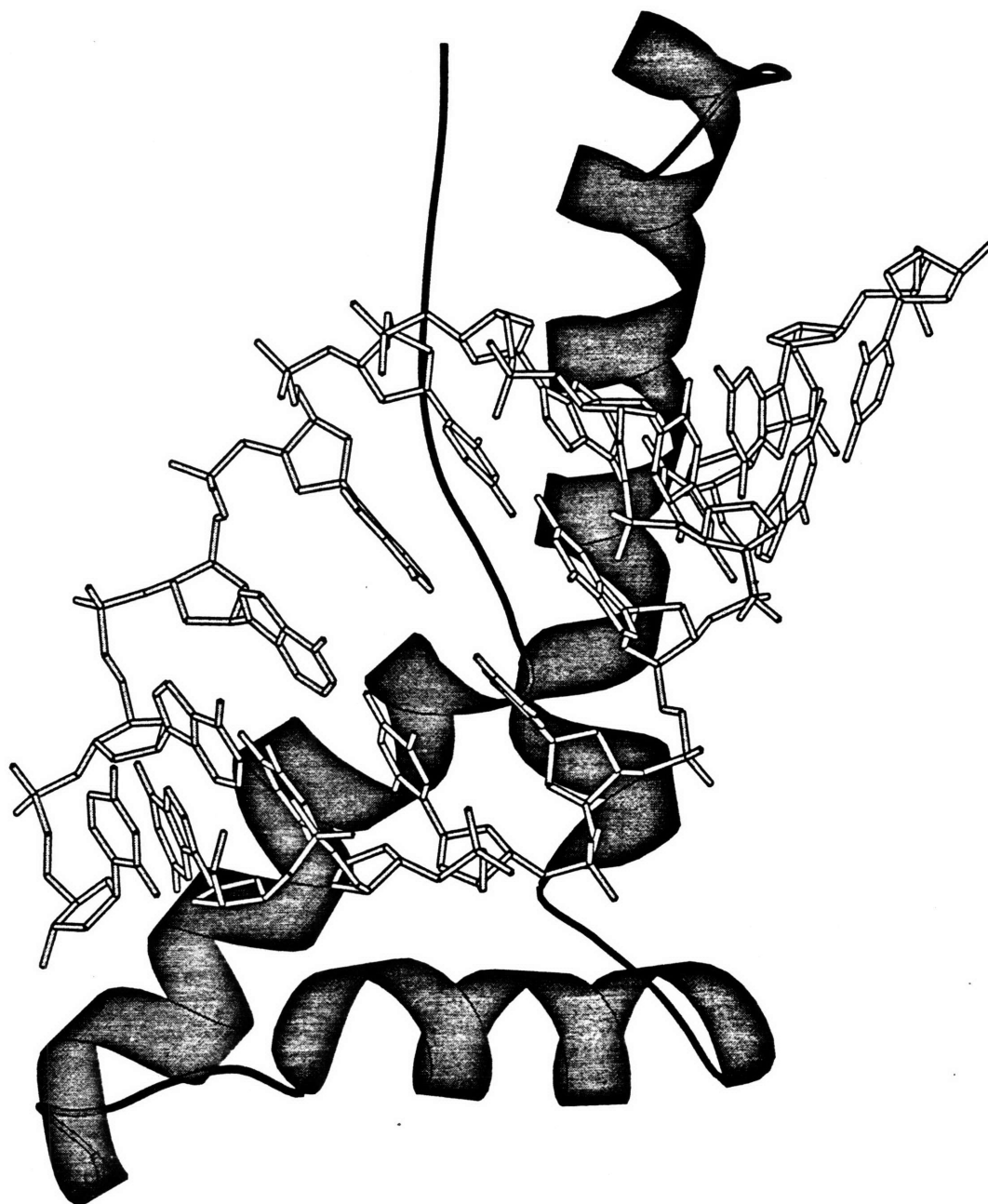
Recently, the solution structures of HMG domains from two proteins, the human testis determining factor (SRY) (Figure 66) (Werner et al., 1995) and the lymphoid enhancer binding factor (LEF-1) (Love et al., 1995), bound to

their target DNA sequences have solved by NMR spectroscopic analysis. The HMG domains from SRY and LEF-1 bind to the minor grooves of their target DNA sequences. In each case, the protein intercalates a hydrophobic residue between two adjacent adenine bases on the target DNA. SRY intercalates an isoleucine (Ile) and LEF-1 inserts a methionine (Met). For both, the protein causes a wedge in the base stack at an -AA- site from the minor groove side of the helix and causes a positive roll. The positive roll is accompanied by the widening of the minor groove and duplex underwinding. In the case of the DNA in the SRY structure, the groove opposite the site of Ile intercalation is 9.4 Å wide, the dihedral angle between the adjacent adenine residues involved in the intercalation is about 25°, and the twist at this step is about 26°. The DNA in the LEF-1 structure has a minor groove width of 11.0 Å and a twist of 19-24° at the site of Met intercalation. The disruption in the double helix caused by intercalation of a side chain from an HMG protein looks similar to that caused by binding of *cis*-{Pt(NH<sub>3</sub>)<sub>2</sub>}<sup>2+</sup> to adjacent guanine residues on DNA, but a detailed comparison is not possible because the LEF-1 NMR structure coordinates have not been released. In the cisplatin-DNA structure, the minor groove opens to a width of about 11.0 Å while the dihedral angle between the planes of the adjacent purines is about 26°. Some details of the structures of DNA bound to cisplatin and to the HMG domains of SRY and LEF-1 are listed for comparison in Table 12.

#### *Other DNA-binding Proteins and Bent DNA*

DNA binding and bending by proteins have been implicated in biological processes such as transcription. The structure of the TATA binding protein (TBP) complexed with the TATA box shows the distinct bend that a

**Figure 66.** NMR solution structure of SRY bound to its DNA sequence. The N-terminus of the protein has an irregular structure and the C-terminus is an  $\alpha$ -helix. The DNA in this structure has many features in common with cisplatin-modified DNA.



protein can induce in a segment of double helical DNA (Kim et al., 1993a; Kim et al., 1993b). The DNA bend seen the TBP/TATA box structure was  $\sim 100^\circ$  and occurred over four base pairs. Interestingly, the bend did not disrupt base pairing but severely unwound the helix. Another protein which has been shown to bind to and bend DNA is HIV reverse transcriptase (Jacobo-Molina et al., 1993). In the crystal structure, the DNA appeared to be a junction of A-form and B-form DNA with an overall bend of  $\sim 40\text{-}45^\circ$ . This value is very similar to that in the structure of cisplatin-modified DNA and indicates that bent DNA or DNA composed of an A/B junction can be a signal for biological processes.

### *Interstrand Adducts*

One of the less abundant adducts to which HMG proteins also bind and may play a role in the cytotoxicity of the drug has also been structurally characterized. The sequence d(CATAG\*CTATG)·(CATAG\*CTATG), where the G\* residues are linked by a *cis*-{Pt(NH<sub>3</sub>)<sub>2</sub>}<sup>2+</sup> interstrand cross-link has been studied by NMR and its solution structure has been determined (Huang et al., 1995). The structure formed is extremely unusual with the bound platinum atom sitting in the minor groove of the helix and the cytosine residues complementary to the guanines bound to platinum in an extrahelical conformation (Figure 67). The overall bend of the helix with an interstrand cross-link is about  $45^\circ$ , of the same magnitude as the angle observed in solution and crystallographic studies of the major intrastrand cross-link. The similar bend angle probably explains why interstrand cross-links are recognized by HMG domain proteins.

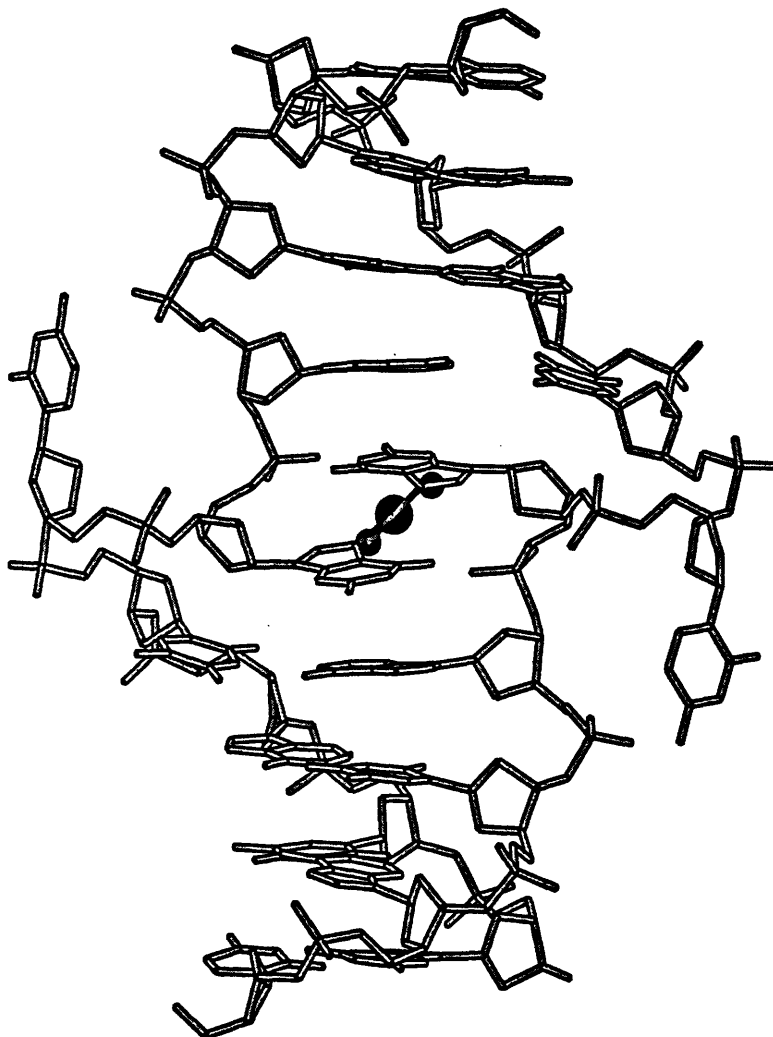
**Table 12.** Comparison of hSRY/DNA, LEF-1/DNA, and the cisplatin/DNA crystal structure.

Complex	hSRY/DNA	LEF-1/DNA	Cisplatin/DNA crystal structure
DNA form	intermediate A/B	intermediate A/B	junction of A/B
Minor groove width	9.4 Å	11.0 Å in protein binding region	9.5-11.0 Å
P-P distance	5.4 Å Ile intercalation	* Pt coordination	5.5 Å
Roll	19° Ile intercalation	52° Met intercalation	26° Pt coordination
Average helical twist	26°	*	32°
Bend: Protein/DNA complex	~70-80°	~117°	~80°

\* The coordinates for the LEF-1/DNA complex are not available so these parameters could not be compared.



**Figure 67.** NMR solution structure of an interstrand cross-link of  $\text{cis-}\{\text{Pt}(\text{NH}_3)_2\}^{2+}$  on duplex DNA. The self-complementary sequence is  $\text{d}(\text{CATAG}^*\text{CTATG})$  where a  $\text{G}^*$  residue on each strand is coordinated to platinum by N7.



*Concluding Remarks*

The crystal structure of the major adduct of cisplatin bound to DNA is an important advancement toward understanding how this incredible antitumor drug works. The structure reveals that, because DNA is a remarkably flexible molecule, it can accommodate an intrastrand cisplatin cross-link by adopting an unusual structure. The coordination requirement of the metal ion affords a bend in the DNA duplex and sets up a structure which is recognized by proteins which contain the HMG domain. Such recognition may be involved in potentiation of the anticancer activity of the drug. In order to understand details of the interactions between HMG proteins and cisplatin-modified DNA, the structures of other adducts of the drug on duplex DNA and protein/platinated-DNA complexes must be solved by X-ray crystallography and NMR. After the basic interactions between HMG proteins and platinated duplex DNA are understood, strategies might be developed to afford more specific protein binding and thereby increase the potency of the drug.

*Note*

The data for the structure described in this thesis are available on 4mm DAT tape. The coordinates for the crystal structure have been deposited with the Protein Data Bank and are available under the PDB access code 1GPG.

## REFERENCES

- Admiraal, G., van der Veer, J. L., de Graaff, R. A. G., den Hartog, J. H. J. & Reedijk, J. (1987) *J. Am. Chem. Soc.* 109, 592-594.
- Bellon, S. F. (1992) Structural Investigations of Platinum Anticancer Drugs with DNA. Physical Chemistry, Massachusetts Institute of Technology.
- Bellon, S. F., Coleman, J. H. & Lippard, S. J. (1991) *Biochemistry* 30, 8026-8035.
- Bellon, S. F. & Lippard, S. J. (1990) *Biophys. Chem.* 35, 179-188.
- Borer, P. N. (1975) in *Handbook of Biochemistry and Molecular Biology* (Fasman, G. D., Ed.) CRC Press, Boca Raton.
- Bruhn, S. L., Toney, J. H. & Lippard, S. J. (1990) *Prog. Inorg. Chem.* 477-516.
- Brünger, A. T. (1992a) *Nature* 355, 472-475.
- Brünger, A. T. (1992b). *X-PLOR Version 3.1. A System for X-ray Crystallography and NMR* Yale University Press, New Haven, CT.
- Brünger, A. T. (1993) *Acta Cryst. D*49, 24-36.
- Brünger, A. T., Kuriyan, J. & Karplus, M. (1987) *Science* 235, 458-460.
- Chow, C. S., Whitehead, J. P. & Lippard, S. J. (1994) *Biochemistry* 33, 15124-15130.
- Collaborative Computing Project Number 4 (1994) *Acta Cryst. D*50, 760-763.
- Comess, K. M. & Lippard, S. J. (1993) in *Molecular Aspects of Anticancer Drug-DNA Interactions* (Neidle, S. & Waring, M., Eds.) pp 134-168, MacMillan, London.
- den Hartog, J. H. J., Altona, C., van Boom, J. H., van der Marel, G. A., Haasnoot, C. A. G. & Reedijk, J. (1985) *J. Biomol. Struct. Dyn.* 2, 1137-1155.
- Derewenda, Z. S., Lee, L. & Derewenda, U. (1995) *J. Mol. Biol.* 252, 248-262.
- Desiraju, G. R. (1991) *Acc. Chem. Res.* 24, 290-296.
- Dickerson, R. E. (1989) *J. Biomol. Struct. Dyn.* 6, 627-634.

- Doucet, J., Benoit, J.-P., Cruse, W. B. T., Prange, T. & Kennard, O. (1989) *Nature* 337, 190-192.
- Drenth, J. (1994). *Principles of Protein X-ray Crystallography* Springer-Verlag, New York.
- Duckett, D. R., Murchie, A. I. H. & Lilley, D. M. J. (1990) *EMBO J.* 9, 583-590.
- Dunham, S. U. & Lippard, S. J. (1995) *J. Am. Chem. Soc.* 117, 10702-10712.
- Eastman, A. (1986) *Biochemistry* 25, 3912-3915.
- Esposito, G., Cauci, S., Fogolari, F., Alessio, E., Scocchi, M., Quadrifoglio, F. & Viglino, P. (1992) *Biochemistry* 31, 7094-7103.
- Fichtinger-Schepman, A. M. J., van der Veer, J. L., den Hartog, J. H. J., Lohman, P. H. M. & Reedijk, J. (1985) *Biochemistry* 24, 707-713.
- Frederick, C. A., Quigley, G. J., Teng, M.-K., Coll, M., van der Marel, G., van Boom, J., Rich, A. & Wang, A. H.-J. (1989) *Eur. J. Biochem.* 181, 295-307.
- Gao, Y.-G., Robinson, H., van Boom, J. H. & Wang, A. H.-J. (1995) *Biophysical Journal* 69, 559-568.
- Guan, Y., Gao, Y.-G., Liaw, Y.-C., Robinson, H. & Wang, A. H.-J. (1993) *J. Biomol. Struct. Dyn.* 11, 253-276.
- Huang, H., Zhu, L., Reid, B. R., Drobny, G. P. & Hopkins, P. B. (1995) *Science* 270, 1842-1845.
- Huang, J.-C., Zamble, D. B., Reardon, J. T., Lippard, S. J. & Sancar, A. (1994) *Proc. Natl. Acad. Sci.* 91, 10394-10398.
- Jacobo-Molina, A., Ding, J., Nanni, R. G., Clark, A. D., Lu, X., Tantillo, C., Williams, R. L., Kamer, G., Ferris, A. L., Clark, P., Hizi, A., Hughes, S. H. & Arnold, E. (1993) *Proc. Natl. Acad. Sci.* 90, 6320-6324.
- Jennerwein, M. & Andrews, P. A. (1995) *Drug Metabolism and Disposition* 23, 178-184.
- Jones, T. A., Bergdoll, M. & Kjeldgaard, M. (1989) in *Crystallographic Computing and Modeling Methods in Molecular Design* (Bugg, C. & Ealick, S., Eds.) Springer-Verlag, New York.

- Kennard, O. & Hunter, W. N. (1989) *Quar. Rev. Biophys.* 22, 327-379.
- Kennard, O. & Salisbury, S. A. (1993) *J. Biol. Chem.* 268, 10701-10704.
- Kim, J. L., Nikolov, D. B. & Burley, S. K. (1993a) *Nature* 365, 520-527.
- Kim, Y., Geiger, J. H., Hahn, S. & Sigler, P. B. (1993b) *Nature* 365, 512-520.
- Kozelka, J., Archer, S., Petsko, G. A. & Lippard, S. J. (1987) *Biopolymers* 26, 1245-1271.
- Kozelka, J. & Chottard, J.-C. (1990) *Biophys. Chem.* 165-178.
- Kozelka, J., Petsko, G. A. & Lippard, S. J. (1985) *J. Am. Chem. Soc.* 107, 4079-4081.
- Lavery, R. & Sklenar, H. (1988) *J. Biomol. Struct. Dyn.* 6, 63-91.
- Lavery, R. & Sklenar, H. (1989) *J. Biomol. Struct. Dyn.* 6, 655-667.
- Leonard, G. A., McAuley-Hecht, K., Brown, T. & Hunter, W. N. (1995) *Acta Cryst. D51*, 136-139.
- Love, J. J., Li, X., Case, D. A., Giese, K., Grosschedl, R. & Wright, P. E. (1995) *Nature* 376, 791-795.
- McA'Nulty, M. M. & Lippard, S. J. (1995) in *Nucleic Acids and Molecular Biology* (Eckstein, F. & Lilley, D. M. J., Eds.) pp 264-284, Springer-Verlag, Berlin.
- Pil, P. M. & Lippard, S. J. (1992) *Science* 256, 234-237.
- Read, R. J. (1986) *Acta Cryst. A42*, 140-149.
- Rice, J. A., Crothers, D. M., Pinto, A. L. & Lippard, S. J. (1988) *Proc. Natl. Acad. Sci.* 85, 4158-4161.
- Robinson, H. & Wang, A. H.-J. (1996) *Nuc. Acids Res.* 24, 676-682.
- Saenger, W. (1984). *Principles of Nucleic Acid Structure* Springer-Verlag, New York.
- Sandman, K. E. & Lippard, S. J. (1996) *submitted for publication*

- Selsing, E., Wells, R. D., Alden, C. J. & Arnott, S. (1979) *J. Biol. Chem.* 254, 5417-5422.
- Sherman, S. E., Gibson, D., Wang, A. H.-J. & Lippard, S. J. (1985) *Science* 230, 412-417.
- Sherman, S. E., Gibson, D., Wang, A. H.-J. & Lippard, S. J. (1988) *J. Am. Chem. Soc.* 110, 7368-7381.
- Sherman, S. E. & Lippard, S. J. (1987) *Chem. Rev.* 87, 1153-1181.
- Sriram, M. & Wang, A. H.-J. (1996) in *Bioorganic Chemistry: Nucleic Acids* (Hecht, S. M., Ed.) Oxford University Press, New York.
- Takahara, P. M., Rosenzweig, A. C., Frederick, C. A. & Lippard, S. J. (1995) *Nature* 377, 649-652.
- Wang, A. H.-J., Fujii, S., van Boom, J. H. & Rich, A. (1982) *Proc. Natl. Acad. Sci.* 79, 3968-3972.
- Wang, A. H.-J. & Teng, M.-K. (1987) *J. Cryst. Growth* 90, 295-310.
- Werner, M. H., Huth, J. R., Gronenborn, A. M. & Clore, G. M. (1995) *Cell* 81, 705-714.
- Whitehead, J. P. & Lippard, S. J. (1995) in *Metal Ions in Biological Systems* (Sigel, H. & Sigel, A., Eds.) Marcel Dekker, New York.
- Wing, R. M., Pjura, P., Drew, H. R. & Dickerson, R. E. (1984) *EMBO J.* 3, 1201-1206.
- Yang, D., van Boom, S. S. G. E., Reedijk, J., van Boom, J. H. & Wang, A. H.-J. (1995) *Biochemistry* 34, 12912-12290.

**BIOGRAPHICAL NOTE**

The author is the daughter of Lt. Col. Edmund W. Takahara (USAF, Ret.) and Patricia L. Takahara and was born at Hill Air Force Base, Utah. After attending eight different schools in California, Saudi Arabia, Virginia, Ohio, and Hawaii, she graduated from Fountain Valley High School in Fountain Valley, California in June 1987. She began her undergraduate studies in chemistry at the University of California at Berkeley in August 1987, conducted research with Professor Steven F. Pedersen from May, 1988 until December, 1990, and graduated with a Bachelor of Science degree in December 1990. During the winter and spring terms of 1991, she worked as a chemistry teaching assistant at the University of California at Irvine. In the fall of 1991, she began her graduate studies with Professor Stephen J. Lippard at the Massachusetts Institute of Technology. On August 8, 1992, she was married to Mark M. Hasegawa. She is the recipient of a National Science Foundation postdoctoral fellowship and will continue her studies in the fields of macromolecular crystallography and bioinorganic chemistry with Professor Douglas C. Rees at the California Institute of Technology.